UC Berkeley
UC Berkeley Electronic Theses and Dissertations

Title

Modeling Adaptive Cruise Control (ACC) on Internal Combustion and Fully Electric Vehicles in Microscopic Simulation

Permalink

https://escholarship.org/uc/item/82d4v1rf

Author

Yang, Mingyuan

Publication Date

2024

Peer reviewed|Thesis/dissertation

Modeling Adaptive Cruise Control (ACC) on Internal Combustion and Fully Electric Vehicles in

Microscopic Simulation

By

Mingyuan Yang

A dissertation submitted in partial satisfaction of the

requirements for the degree of

Doctor of Philosophy

in

Engineering - Civil and Environmental Engineering

in the

Graduate Division

of the

University of California, Berkeley

Committee in Charge:

Professor Raja Sengupta, Chair
Professor Alexander Skabardonis
Professor John Radke

Spring 2024

Abstract

Modeling Adaptive Cruise Control (ACC) on Internal Combustion and Fully Electric Vehicles in

Microscopic Simulation

by

Mingyuan Yang

Doctor of Philosophy in Engineering - Civil and Environmental Engineering

University of California, Berkeley

Professor Raja Sengupta, Chair

Commercial availability of vehicle automation has become mainstream. Most of today's new vehicles can perform longitudinal car following autonomously via Adaptive Cruise Control (ACC). Understanding ACC car following behaviors has become crucial to modeling traffic flow at the microscopic level as market penetration increases. Besides, autonomous vehicles at any Society of Automotive Engineers (SAE) level use ACC for longitudinal control. Thus, ACC vehicle behavior will significantly impact traffic over a long period.

Field experiments demonstrated that today's commercially available ACC vehicles provide similar headways and capacities as human-driven vehicles on freeways under steady-state and free-flow conditions. However, field tests also showed that combustion-based vehicles paired with ACC could lead to further capacity reduction when operating in non-steady state conditions where queues are present, and speeds frequently fluctuate. Electric vehicles (EVs), on the other hand, have been verified to allow ACC to adopt shorter headways and accelerate more swiftly to maintain shorter headways during queue discharge due to their unique powertrain characteristics such as instantaneous torque and regenerative braking, and therefore reverse the negative impact on capacity. These experiments generated MicroSIMACC, a comprehensive field data set that encompasses full-speed range car following with interruptions from lane change maneuvers.

This study developed full-speed range car-following models for both internal combustion engine vehicles (ICE vehicle) and electric vehicles (EV) equipped with ACC, capturing the variable gaps under large speed oscillation and heterogeneous car-following behaviors across different speed levels, gap settings, and powertrains. New ACC trajectory data from MicroSIMACC were utilized to help identify the limitations of the well-established constant gap ACC car-following model and propose changes. More importantly, this study clarified the logistics of implementing and incorporating the new ACC models with other models in microscopic simulation and provided novel insights about the impact of increasing market penetration of ACC with different powertrains via sensitivity analysis. The simulation results indicated that the higher the market penetration rates of EVs are, the larger discharge flow and longer total travel distance can be achieved on a freeway corridor. This was consistent with filed observations and proved that EVs with ACC provided better traffic performance than ICE vehicles with ACC.

TABLE OF CONTENTS

LIST OF FIGURES

LIST OF TABLES

GLOSSARY OF TERMS, ABBREVIATIONS, AND ACRONYMS

AV	Automated Vehicle
ADAS	Advanced Driver Assistance System
ACC	Adaptive Cruise Control
SAE	Society of Automotive Engineers
ICE	Internal Combustion Engine
EV	Electric Vehicle
OVRV	Optimal Velocity micro-model with a Relative Velocity term
IDM	Intelligent Driver Model
PATH	California Partners for Advanced Transit and Highways
OBD	On-Board Diagnostics
GPS	Global Positioning System
CF	Car Following
LC	Lane Changing
CCF	Congested Car Following
RCF	Receiving-lane-change Car Following
SCG	Symmetric Constant Gap
ASCG	Asymmetric Constant Gap
ASVG	Asymmetric Variable Gap
RMSE	Root Mean Squared Error
MPR	Market Penetration Rate
SDK	Software Development Kit

ACKNOWLEDGEMENTS

CHAPTER 1: INTRODUCTION

1.1 Motivation

Automated Vehicles (AVs) have been highly anticipated as they promise to potentially reduce congestion by improving capacity. While fully automated vehicles may take decades to become commercially available and eventually reach a mass market adoption, most mainstream new vehicles sold today (many for $20,000 or less) are partially automated via an advanced driver assistance systems (ADAS) feature known as adaptive cruise control (ACC). ACC automatically maintains a desired speed and safe following distance with the preceding vehicle based on measurements from on-board sensors. Currently, all of the 25 best selling cars in the United States have ACC capability. In the past year, an increasing number of vehicle manufacturers have expanded the operational speed of ACC' from higher ranges to speeds lower than 25 mph. This new generation of ACC is commonly known as the full-speed range ACC, which enables vehicles to operate autonomously not only on freeways under free flow speeds but also in stop-and-go conditions of both congested freeways and signalized arterials. Full-speed range ACC has become widely available on today's new vehicles, and its market penetration is expected to increase in the coming years. Besides, ACC is the foundation of all the intelligent vehicle categories, and autonomous vehicles in any Society of Automotive Engineers (SAE) level are ACC for longitudinal control. Therefore, understanding the car following behavior of full-speed range ACC vehicles is crucial to modeling traffic flow at the macroscopic level in preparation for prospective analysis and developing traffic control strategies in scenarios such as freeway bottlenecks and arterials with signalized intersections.

Many researchers have paid significant attention to the traffic flow impact of ACC, primarily to ACC equipped vehicles powered by internal combustion engines (ICE). A plethora of research findings on the traffic flow impact of ACC have been negative or do not report significant benefits (Vander Werf et al, 2002; Alkim et al, 2007; Shladover et al, 2012; Mattas et al, 2018; James et al, 2019; Shang and Stern, 2021). Unfortunately, these research efforts have only concentrated on vehicles equipped with ICE and at most hybrid electric powertrain, and none has specifically addressed the car-following model of pairing ACC with EV's unique powertrain characteristics and investigated their impacts on roadway capacity. There is still a lack of knowledge about how low-level automated vehicles such as ACC equipped vehicles will affect capacity when paired with fully electric powertrain, which has significantly different power delivery, acceleration, and braking characteristics. Interestingly, electrification of vehicle powertrain has become increasingly ubiquitous and mainstream, and the combination of fully electric vehicles (EVs) with ADAS could present new opportunities that have not yet been discovered. This is an important area that deserves significant attention, especially considering the ever-increasing popularity and market penetration of EVs as stricter emissions regulations will incentivize greater EV adoption in the near future.

The combination of EVs and ADAS features such as ACC cannot be overlooked when modeling traffic flow because the unique powertrain characteristics of fully EVs could present significant opportunities to improve capacity and reduce congestion. ICE gradually increases its torque output as the engine speed increases. Since power is the product of torque and engine speed, higher power output on ICE would only be attainable after reaching higher engine speeds. However, alike human drivers, ACC seldom operate at high engine speeds but rather at low to

medium engine speeds (3500 revolutions per minute or lower) to maintain driver comfort, reasonable fuel economy, and long-term reliability of the vehicle powertrain, and thus, an ICE vehicle paired with ACC could not generate significant power and acceleration during normal operation conditions (i.e., at medium to low engine speeds). Conversely, EVs produce very high maximum torque almost instantaneously at relatively low engine speeds, when accelerating from both higher and lower speeds. Revisiting the concept that power is the product of torque and engine speed, EVs could produce relatively higher power at lower ranges of engine speeds as illustrated in Figure 1.1. As a result, the unique powertrain characteristics of EVs mean that EVs yield an immediate higher acceleration for a broad range of speeds under normal operating conditions, at low to medium engine speeds. This enhanced performance at a broad speed range also translates to higher energy efficiency in EVs when compared to ICE vehicles (Fiori et al, 2019), particularly in congested traffic. Moreover, the electric motors of EVs apply regenerative braking immediately upon releasing the throttle, and the regenerative braking alone could yield an instantaneous deceleration of as much as 2.5 m/s^2 on mainstream EVs. Combining the instantaneous torque with the strong braking performance from electric motor's regenerative braking, EVs paired with ACC could potentially adopt shorter headways and accelerate more swiftly to maintain shorter headways when speeds fluctuate and during queue discharge, thereby improve capacity and reverse the previously mentioned negative impact of ACC.
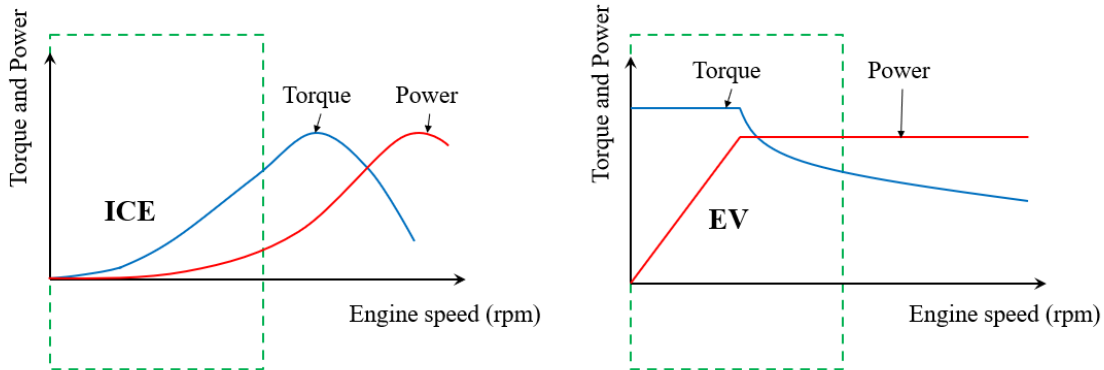
Figure 1.1. Torque and power vs. engine speed for ICE (left) vs. EVs (right).

The rest of this chapter presents the research question and the research contribution, followed by an overview of the dissertation organization.

1.2 Research Questions

Followed by the motivations, two major problems will be addressed in this research:

- Heterogenous ACC car-following behaviors are expected across different speed levels, gap settings, and powertrains. This study is intended to investigate how these different operating conditions and traffic scenarios can affect the ACC car-following behaviors qualitatively and quantitatively.
- Electric vehicles can potentially adopt shorter headways and accelerate more swiftly to maintain shorter headways when speeds fluctuate and during queue discharge, thereby improve capacity and reverse the negative impact of ACC paired with conventional internal combustion engine. This research is intended to verity that ACC-equipped EVs outperform

2

ACC-equipped ICE vehicles in terms of the potential capacity and congestion reduction benefits, under stop-and-go conditions at freeway bottlenecks and signalized intersections on arterial.

1.3 Research Contribution

The main contribution of this study is to develop a set of full-speed range ACC car-following models for both ICE vehicles and EVs under a wide variety of traffic scenarios. The new models can capture the non-linearity of ACC car-following behaviors under a wide variety of vehicle speed, as well as the heterogeneity of ACC car-following behaviors between acceleration and deceleration. This set of models should also be capable of covering comprehensive traffic scenarios that happen in real world, like how ACC will behave differently when the leading vehicle has a different desired speed, and how ACC will respond to the lane-changing vehicles (i.e., cut-in scenarios). Besides, this research will develop a comprehensive ACC car-following framework that clarifies the logistics on how to implement and incorporate the new models with other models in microscopic simulation and provide novel insights about the impact of increasing market penetration of ACC with different powertrains via sensitivity analysis. Furthermore, the new models can provide guidelines for more advanced automated vehicles and/or driver assist systems in the future when new technologies arrive.

1.4 Dissertation Organization

The remaining chapters are organized as follows. Chapter 2 provides an overview of the recent literature in the area of simulation-based ACC car-following models and existing commercial ACC field datasets. Chapter 3 describes the data collection efforts that contribute to a new ACC trajectory dataset, named MicroSIMACC. Chapter 4 discusses and compares the field observations of ACC car-following behaviors across a wide variety of traffic scenarios and between ICE vehicles and EVs. Chapter 5 details the development, calibration and implementation of a series of new simulation-based ACC car-following models under different traffic scenarios. Chapter 6 shows the traffic impacts of ACC-equipped ICE vehicles and EVs under varying market penetrations via microscopic simulation. Lastly, chapter 7 summarizes the study findings, followed by discussion of the limitations of this study and future work. Appendix A shows additional ACC car-following model calibration results under relatively low-speed levels.

CHAPTER 2: LITERATURE REVIEW

There is a lack of well-designed field experiment and comprehensive commercial ACC dataset that encompasses a wide variety of traffic conditions and enables the development of reliable ACC car following models that could accurately reflect the true ACC car following behaviors in microscopic simulation. As a result, the simulation analyses based on these recent models do not provide consistent and accurate estimates of ACC's traffic flow impacts. The literature review will be conducted in the following threes subsections: ACC trajectory data for microscopic modeling, simulation-based ACC car-following model, and traffic flow impacts of ACC.

2.1 ACC Trajectory Data for Microscopic Modeling

To quantify the potential impact and model traffic flow with ACC, several recent empirical studies collected trajectory-level data (Shladover et al, 2012; James et al, 2019; Gunter et al, 2019; Li et al, 2021; Makridis et al, 2021; Shi and Li, 2021b; Li et al, 2022; Zhou et al, 2022; Gloudemans et al, 2023).

Shladover et al. (2012) collected high-speed ACC trajectory data on freeway and proposed a first-order control law in terms of positioning difference and speed difference between the preceding vehicle and the subject vehicle, to represent the car-following dynamics of ACC-equipped vehicles in simulation (Milanés and Shladover, 2014). This simulation-based model, named PATH model, has become one of the most established models for ACC car following (Lu et al, 2017; Liu et al, 2018a; Liu et al, 2018b; Kan et al, 2019).

Gunter et al. (2019) collected large amounts of ACC-controlled trajectory data via seven distinct vehicle models from two different vehicle makes and calibrated the optimal velocity micro-model with a relative velocity term (OVRV) under four main speed profiles, including oscillatory, low speed steps, high speed steps, and speed dips for each vehicle type. They found it very challenging to fit with their model when there exists a lack of symmetry between the acceleration and deceleration of the ACC-equipped vehicles (Gunter et al, 2020).

James et al. (2019) recalibrated four car-following models, including the Autonomous Adaptive Cruise Control (AACC) model, Intelligent Driver Model (IDM), California Partners for Advanced Transit and Highways (PATH) empirical ACC model, and the Technical University of Delft empirical ACC model, using field data from test runs conducted by the Federal Highway Administration on a heavily utilized freeway corridor.

Li et al. (2021) attempted to characterize the empirical car-following behaviors of commercial ACC systems under different traffic conditions based on empirical MA experiments. They claimed that ACC-equipped vehicles could perform quite different behaviors if their headway settings, speed levels, and leader vehicle's oscillation magnitude varied. They also found that the spacing-velocity relationship of ACC vehicles varied under different speed ranges and distinguished from those of human driving vehicles. Li et al (2022) added new field evidence as GA experiments to further understand the ACC equilibrium behaviors via the fundamental diagrams. They found that equilibrium capacities reached above 3500 vehicles per hour at the minimum ACC headway setting, but fast equilibrium speed may pose a safety risk. Their results also suggested that ACC jam spacing could be much larger than in human traffic.

Makridis et al. (2021) developed an open database (OpenACC) for 3000-km of car-following experiments conducted in the real world. They provided insights about the basic properties of the commercial ACC systems, such as controllers' acceleration and deceleration operational domain under normal car-following conditions, response time to perturbations, desired headway settings, etc. (Makridis et al, 2019; Makridis et al, 2020). They also found that ACC systems from different manufacturers behaved very similarly.

Moreover, Shi and Li (2021b) conducted two/three-vehicle platoon experiments with four different headway settings within 10 mph speed fluctuation. It was found that the string stability of the platoon would increase as the headway was set to a larger value.

The details of these major ACC datasets are summarized in Table 2.1, which referred to a previous study with up-to-date datasets and additional information of speed oscillations (Li et al, 2022). Unfortunately, despite covering ACC systems from various vehicle manufacturers, these datasets from Table 2.1 have common limitations: (1) limited speed range: particularly lack of large dataset for low speeds and large speed fluctuations. ACC car following behavior could be nonlinear due to varying power outputs of the internal combustion engine at different speed ranges and respond differently to large traffic disturbance and in stop and go conditions (Shladover et al, 2012; Chon Kan et al, 2021; Chon Kan et al, 2022), and this is especially evident when transitioning from very low speeds or complete stop to higher speeds and vice versa. Naturalistic experiments on freeways cannot guarantee to capture low speed data with good quality, due to the lack of proper safe site or environment (James et al, 2019; Makridis et. al, 2021). Also, some ACC test vehicles in previous studies could not function below 25 mph (40 km/hr) (Milanés and Shladover, 2014; James et al, 2019). In addition, many experiments listed in Table 2.1 focused on string stability of ACC platoons following a minor speed disturbance and those researchers did not see the need to conduct experiments that forced the leading vehicle to decelerate from free-flow speed to very low speed (Gunter et. al, 2020; Li et al, 2021; Shi and Li, 2021b). One exception is that in GA experiments, the following ACC vehicle stopped at intersections to measure the jam spacing (Li et al, 2022); (2) lack of data for car following with heterogeneous desired speeds; and (3) absence of controlled experiments for receiving car following, also known as the relaxation in traffic flow theory (Cohen, 2004; Laval et al, 2008; Zheng et al, 2013; Zhou et al, 2022), when lane changes occur (cut-in).

Table 2.1. Existing commercial ACC datasets (Li et al, 2022).

Existing Datasets	Test Vehicles	Equilibrium Speed Range (mph)	Oscillation (mph)
UC Berkeley PATH (Shladover et al, 2012)	Four-vehicle platoon, Infiniti M56	55 - 67	Small disturbance (< 5 mph)
Federal Highway Administration (James et al, 2019)	Two-vehicle platoon, Cadillac SRX	63 - 73	Small disturbance (< 5 mph)
Vanderbilt University (Gunter et al, 2019)	Two-vehicle platoon, 7 ACC systems	35 - 75	6, 10, 15, 20 (Equilibrium speed at 55 mph)

OpenACC (Makridis et al, 2021)	2/3/5/10-vehicle platoon, 10+ ACC systems	31 - 63 15 - 35	Small disturbance (< 10 mph)
MA experiments (Li et al, 2021)	Three-vehicle platoon, 4 ACC systems	35 - 65 45 - 70	5, 10
University of South Florida (Shi and Li, 2021b)	2/3-vehicle platoon, Lincoln MKZs	35 - 55	2, 4, 6, 8, 10
GA experiments (Li et al, 2022)	Two-vehicle platoon, Tesla Model X	20 - 75	Complete Stop

This research designs and conducts controlled experiments to compile a dataset known as MicroSIMACC, a novel and comprehensive set of trajectories that encompasses longitudinal car following and the effect of lane changes (receiving lane change car following) at full speed range for both internal combustion engine (ICE) vehicles and electric vehicles (EVs). The study will utilize the data to reveal ACC car-following characteristics in terms of their steady-state headways, non-steady state headways under speed disturbance, acceleration and deceleration rates under various speed profiles, gap settings and traffic scenarios, to better understand the performance of ACC controller and their impacts on traffic flow. Those findings as well as dataset itself eventually contribute to developing and calibrating microscopic level car-following models, to be integrated into simulation for performing prospective analyses and developing traffic operations and control strategies for future scenarios. Unlike the experiments summarized in Table 2.1, this research focuses on a more comprehensive and wider range of traffic conditions by testing a very common ACC-equipped vehicle, instead of testing a variety of vehicles (from various manufacturers) under a narrow range of conditions.

2.2 Simulation-based ACC Car-following Model

Conducting a simulation-based study to estimate the impacts of ACC is very important because: (1) the real field test data on the ACC performance are limited; and (2) many studies deal with high market shares for ACC, which is hypothetical and far from the reality. The Intelligent Driver Model (IDM) and the Autonomous Adaptive Cruise Control (AACC) model were the two models developed in the early 2000s to first model the car-following behaviors of automated vehicles. Most of the existing ACC car-following models were recalibrated or improved using these two models as baseline.

The Intelligent Driver Model (IDM) was first developed in 2000 to accurately capture naturalistic human driving behaviors (Treiber et al, 2000). In 2010, the IDM model was expanded to eliminate the 'unnecessarily strong braking reactions' of ACC vehicles during cut-in situations with the introduction of a constant-acceleration heuristic (CAH) (Kesting et al, 2010). The baseline formula of the IDM model were written in equation (2.1) and (2.2):

$$a_{IDM}(s_n, v_n, \Delta v_n) = a_{max}[1 - \left(\frac{v_n}{v_0}\right)^{\alpha} - (\frac{s^*(v_n, \Delta v_n)}{s_n})^2] \tag{2.1}$$

This equation is an interpolation of the tendency to accelerate with $a_{max}^{(n)} * [1 - \left(\frac{v_n}{v_0}\right)^\alpha]$ on a free-flow condition and the tendency to brake with deceleration $-a_{max}^{(n)} * (s^*/s_n)^2$ when vehicle n comes too close to the vehicle in front. The deceleration term depends on the ratio between the desired minimum gap s^* and the actual gap s_n, where the desired gap:

$$s^*(v_n, \Delta v_n) = s_0 + s_1 * \sqrt{\frac{v_n}{v_0}} + T * v_n + \frac{v_n * \Delta v_n}{2 * \sqrt{a_{max} * b}} \tag{2.2}$$

s_0, s_1 represent the jam distance, v_0 is the desired speed (free-flow speed), T is the safe time headway, a_{max} is the maximum acceleration, and b is the desired deceleration.

The major limitation of the IDM model comes from its deceleration part: when the current gap is significantly lower than the desired gap, the deceleration rate becomes unrealistically high. James et al. (2019) confirmed this criticism by recalibrating the latest IDM model using field data from test runs conducted by the Federal Highway Administration on a heavily utilized freeway corridor, where the deceleration part of the trajectory can be barely fitted.

Autonomous Adaptive Cruise Control (AACC) model was first proposed in 2001 (Vander et al, 2001), and this model has considered both the relative speed between the leading and following vehicle, and the difference in physical gap and the desired distance between the leading and following vehicle based on the desired time gap. The reference acceleration of this model can be computed based on the difference between current and intended speed (a_{refv}) or the distance and the speed differences between the current vehicle and the preceding vehicle (a_{refd}). The formula were written in equation (2.3) - (2.5):

$$a_{ref} = \min{(a_{refv}, a_{refd})} \tag{2.3}$$

$$a_{refv} = k(v_{int} - v) \tag{2.4}$$

$$a_{refd} = k_a a_p + k_v(v_p - v) + k_d(r - r_{ref}) \tag{2.5}$$

where v_{int} and v denote the intended and the current speed of the subject vehicle, a_p and v_p denote the acceleration and speed of the preceding vehicle, v denote the speed of the subject vehicle, and r and r_{ref} denote the current and reference gap relative to the preceding vehicle, respectively. k is a constant speed-error factor, while k_a, k_v, and k_d are also constant factors frequently used as in previous studies as 1, $0.58s^{-1}$, and $0.1s^{-2}$.

The AACC model lacks a forward collision warning system (CWS) to initiate driver takeover during critical situations and it considers much vehicle information, including the safety following distance (r_{safe}), the following distance according to the system time setting (r_{system}), a minimum allowed distance (r_{min}), which makes it less efficient to be implemented in the microscopic simulation.

Recently, a few studies have been conducted to model the microscopic car-following behaviors of commercially available ACC vehicles. Note that some of the modeling studies have

been discussed in subsection 2.1, followed by their data collection efforts (Milanés and Shladover, 2014; James et al, 2019; Gunter et al, 2020).

Shang and Stern (2021) calibrated the intelligent driver model (IDM) using car following data collected on commercial ACC vehicles and investigated traffic impacts on freeway capacity under different market penetrations in microscopic simulation. They found that the freeway capacity decreased by up to 35% at higher market penetration rates of commercial ACC-equipped vehicles. Interestingly, Shang et al. (2022) proposed an asymmetric OVRV model and switch model parameters between acceleration and deceleration stage. The calibrated results showed a reduction of spacing error by up to 38% compared with the symmetric OVRV model.

He et al. (2022) augmented five base car-following models with physics-based extensions, including perception delay, linear or nonlinear vehicle dynamics, and acceleration constraints. Various combinations of models and extensions were assessed and compared through vast calibration and validation experiments using measured ACC trajectory data. They found that physics-based extensions provided limited improvements to the accuracy of existing models. They also found that the linear controller with Gipps' spacing policy led to the most accurate model, while the IDM was the most robust model to different input trajectories.

2.3 Traffic Flow Impact of ACC

Several studies investigated the traffic impacts of varying market penetrations of ACC-equipped vehicles via microscopic simulation. Kesting et al. (2007; 2008) used the IDM model and estimated the traffic impacts of ACC under a market penetration rate from 0% to 25%. The results indicated that the ACC vehicles could improve road capacity under small penetration (5%). Moreover, Kesting et al. (2010) claimed that 1% increase of ACC could lead to 0.3% increase of capacity using the improved IDM model with a constant-acceleration heuristic (CAH). However, on the contrary, Shladover et al. (2012) showed the ACC vehicles' impact might be marginal, and Milanés and Shladover (2014) further proved the instability of ACC could bring negative impacts to traffic and reduce the capacity when market penetration is high. More and more recent studies confirmed the string instability of commercial ACC systems from different manufacturers (Gunter et al, 2020; Li et al, 2021; Shi and Li, 2021b), along with the negative traffic impacts from new simulation results (Shang and Stern, 2021).

Research gap exists regarding the traffic impact of ACC with fully electric engines as none of the previous studies has investigated it. This research is intended to clarify the potential difference between ACC-equipped ICE vehicles and ACC-equipped EVs, in terms of traffic flow impacts.

CHAPTER 3: ACC CAR FOLLOWING DATA COLLECTION

3.1 Data Collection Equipment and Vehicle Instrumentation

Conducting experiments through field observations is the most reliable method for this research because there is currently no established simulation tool that could accurately model the behavior of ACC-equipped vehicles under different powertrains. Ideally, installing cameras or detectors on roadways typically yields the most accurate measurement for flow, capacity, density, and mean speeds. However, this method cannot yield any meaningful and viable results in today's traffic stream because it is difficult to determine whether the ACC mode is activated, though there is a large market penetration of vehicles with ACC features. Instead, this study will prospectively assess the impact of ACC-equipped vehicles on capacity by examining OBD (On Board Diagnostics) II data and GPS data collected from carefully designed car following experiments in controlled environments using two or three test vehicles: a leading vehicle as the point of reference, a following vehicle equipped with ACC, and a lane-change vehicle in the lane-change experiments. Furthermore, the empirical data could serve as benchmark data to develop and calibrate car following models that are used as inputs for microscopic simulation, which could scale-up the two/three-vehicle car following experiment to analyses of larger traffic streams.

3.1.1 Internal Combustion Engine (ICE) Vehicle

The field experiments were intended to generate a comprehensive set of trajectory data that encompasses a variety of traffic conditions including full speed range longitudinal car following and receiving lane change car following, using a very common internal combustion engine (ICE) vehicle.

In this study, experiments were conducted using either two or three ACC equipped vehicles (2020 Toyota Corolla LE with a 2,910 lb. curb weight and maximum power output of 139 horsepower at 6,000 rpm from a 1.8-liter naturally aspirated engine) available at Florida Atlantic University (shown in Figure 3.1) to collect trajectory data from the vehicles' onboard computers using the OBD (On Board Diagnostics) II data logger shown in Figure 3.2, which logs acceleration, speed, and distance traveled every 0.2 seconds. These vehicle trajectories were used to extract joint estimates of spacing and headway between the leading and following vehicle.

To ensure accurate reading of the wheel rotations, the tire pressures were checked prior to conducting the experiments. Furthermore, drivers of test vehicles applied a throttle at the same time while the test vehicles were stationary to observe when the changes in engine speed occur in the dataset from each vehicle. If the data showed that the change in engine speed occurred at different times, then it would mean that there's a shift or offset in GPS timestamps in the test vehicles. This could help to synchronize the set of data from both cars and diminish any possibilities of errors due to time off-sets.

Figure 3.1. ACC equipped vehicles in Florida Atlantic University.

(a) OBD II data logger front view

(b) OBD II data logger connected to OBD port

Figure 3.2. OBD II data logger for data collection.

3.1.2 Electric Vehicle (EV)

Specifically, as shown in Figure 3.3, an ICE vehicle (2021 Toyota Camry) with a 3,310 lb. curb weight and maximum power output of 203 horsepower at 6,600 rpm from a 2.5-liter naturally aspirated engine was used as the leading vehicle in the field experiments. For the following vehicle, we selected a mainstream EV (2022 Hyundai IONIQ 5) with a curb weight of 4,414 lbs. and the powertrain delivers 225 horsepower and 258 lb.-ft. of torque, also shown in Figure 3.3. These selections are intended to ensure consistency with previous ICE vehicle experiments (Chon Kan et al, 2021; Chon Kan et al, 2022) by maintaining a similar a weight-to-power ratio. We assume that the EVs selected in this field test could potentially represent a large portion of mainstream ACC-equipped EVs on the road in the near future. Moreover, recent studies demonstrate that the variations between different ACC systems from several manufacturers are not significant (Makridis et al, 2019). Consequently, we anticipate that the findings in this experiment can be generalized in the near future, as mainstream EVs with ACC become more prevalent. The ACC system of EVs used in this study is functional in full-speed range and has four different following gap settings (short, medium, long, and extra-long) for the driver to select from, which can generate a wide range of the headways and spacings.
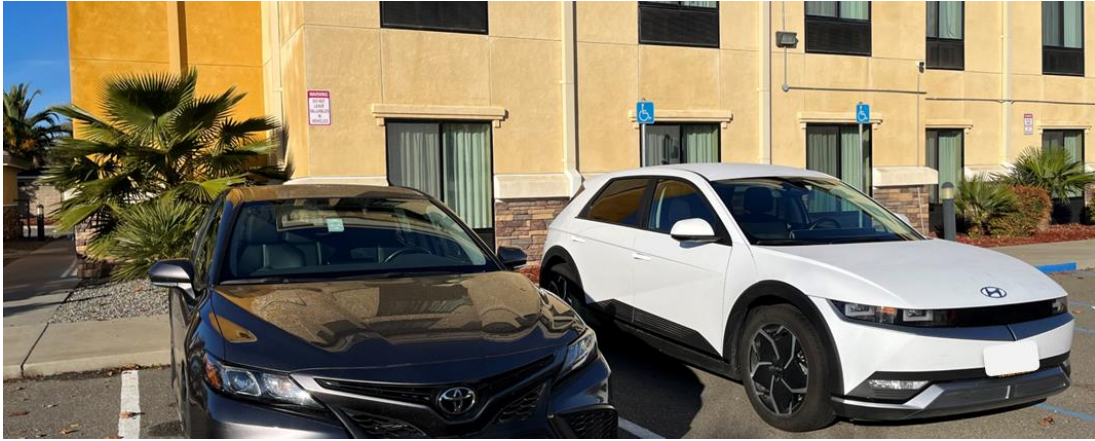
Figure 3.3. Test vehicles (left: 2021 Toyota Camry, right: 2022 Hyundai IONIQ 5).

In addition to testing the Hyundai IONIQ 5, the field test included two other electric vehicles (EVs) from different manufacturers – the 2022 Tesla Model 3 and the 2023 Polestar 2, shown in Figures 3.4 and 3.5, under the same scenarios for comparison. The Tesla Model 3 has a curb weight of 3,686 pounds, and its powertrain generates 221 horsepower and 302 lb-ft of torque. The Polestar 2, on the other hand, has a curb weight of 4,400 pounds and an output of 231 horsepower and 243 lb-ft of torque from its powertrain. Although the power to weight ratio of the Tesla Model 3 is inconsistent and much more favorable compared with the other EVs tested, the Tesla Model 3 was selected to be inclusive of the popular options in today's EV market. EV models from other manufacturers were not attainable or available at the time of field experiments. Also shown in Figures 3.4 and 3.5, an ICE vehicle (2022 Toyota Corolla) with a 2,910 lb. curb weight and maximum power output of 139 horsepower at 6,000 rpm from a 1.8-liter naturally aspirated engine was used as the leading vehicle in the field experiments involving the Tesla Model 3 and Polestar 2 as the following vehicles. As discussed earlier, this is intended to maintain consistency with similar field experiments on the potential capacity impact of ICE with ACC (Chon Kan et al, 2021; Chon Kan et al, 2022). Most importantly, to avoid bias, the vehicles used in the field tests were consumer-grade vehicles obtained from car rental agencies and dealerships, identical to the vehicles available to ordinary consumers and not vehicles specially prepared by the vehicle manufacturers.

Figure 1.4. Test vehicles (left: 2022 Tesla Model 3, right: 2022 Toyota Corolla).

Figure 3.5. Test vehicles (left: 2022 Toyota Corolla, right: 2023 Polestar 2).

Trajectory data from the leading, the lane-change, and the following vehicles were collected using one of the most advanced GPS devices known as Racebox, shown in Figure 3.6. Racebox offers a remarkably high 25 Hz frequency and an excellent 10 cm accuracy, for collecting position data including variables such as latitude, longitude, and altitude every 0.04 seconds and compute cumulative distance travelled, speed and acceleration. The GPS coordinates obtained could also be used to determine spacing and headway between adjacent vehicles.

To ensure the synchronization of the timestamps from both GPS devices and minimize errors, a carefully designed pre-experiment procedure was implemented. This involved performing a synchronized deceleration of both vehicles from a predetermined speed, followed by a frame-by-frame analysis of accompanying video footage. This allowed for the precise alignment of the data sets, thereby reducing errors associated with timestamp offset.

Figure 3.6. RaceBox GPS mounted and connected to phone via Bluetooth.

3.2 Field Experiment Design

3.2.1 Full Speed Range Longitudinal Car-following

This set of ACC car following experiments are intended to simulate steady-state conditions at free-flow speeds and non-steady-state conditions in which traffic approaches the back of queue, travel in the congested state, and return to free-flow speeds after queue discharge, all on isolated public roads.

The detailed experiment procedure is as follows: Initially, both vehicles were aligned in a single lane at a gap of Δ from each other when stationary, and Δ is a fixed distance (1.4 meter that can be easily established using the guidelines or markings on the rearview camera display) between adjacent vehicles. The vehicles then manually accelerated up to the free-flow speed. Four free-flow speeds were tested: 96 km/hr (60 mph), 88 km/hr (55 mph), 72 km/hr (45 mph), and 56 km/hr (35 mph). After both cars reached the free-flow speed, ACC was activated in the following vehicle with short, medium, or long gap setting, which would remain unchanged through the whole procedure. Once the leading vehicle reached the free-flow speed, the following vehicles manually accelerated slightly more to shorten the following distance and then allowed ACC to automatically adjust the spacing and establish the equilibrium state, where the following vehicle returned to the free-flow speed (same as the leading vehicle's speed) and maintained a minimum constant gap with the leading vehicle. This stabilization process is meant to replicate the equilibrium condition at capacity, where many vehicles enter the roadway from various locations and adjust their headways and spacings (following distance or time gap) and eventually reach the equilibrium state with maximum sustained flow or capacity.

At this point, there have not been interruptions that could cause a bottleneck, reduce speed, form queues, or even diminish capacity. To replicate speed fluctuations, we introduced a deceleration from the leading vehicle, and the following vehicle must respond. This could be similar to disruption from reduced speed limits, incidents, or queues near a bottleneck. Both vehicles then returned to the free-flow speed after staying at the lower congested speed for at least 10 seconds. This replicate queue discharge that occurs downstream of a bottleneck. The congested speeds tested include 72 km/hr (45 mph), 56 km/hr (35 mph), 40 km/hr (25 mph), 24 km/hr (15 mph), and complete stop (0 mph); with some not applicable to be paired with lower free-flow speeds. Figure 3.7 shows an example of the speed profile tested in the full speed range longitudinal car following experiment.
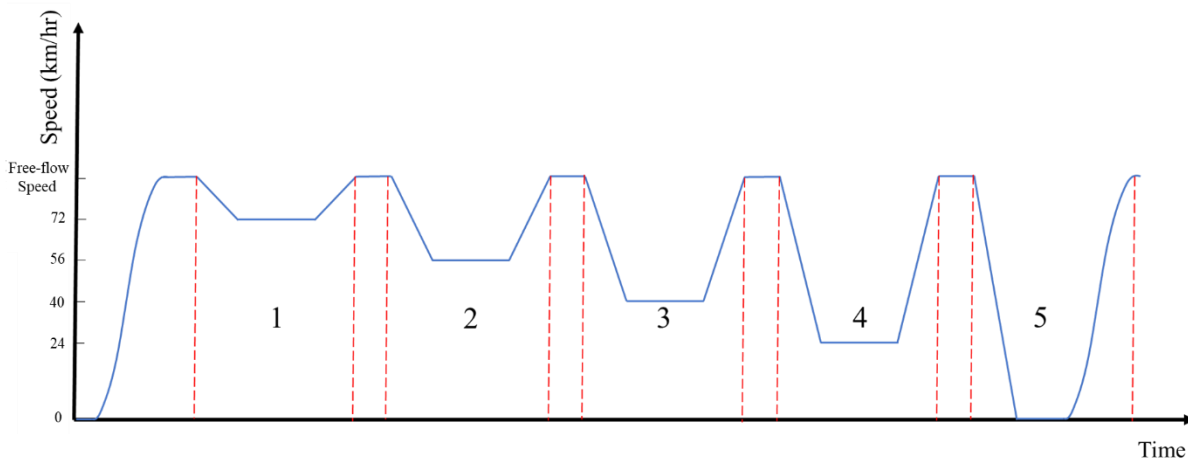
Figure 3.7. Example speed profile of field test.

A total of 17 combinations of free-flow and lower congested speeds were established. Each of these 17 scenarios were tested by setting three different desired speeds for ACC in the following vehicle: with the desired speed set equal to, 8 km/hr (5 mph), or 16 km/hr (10 mph) higher than the free-flow speed. 24 trials were performed for each of the three gap settings on ICE vehicle (16 trials for same desired speed, 4 trials each for 5 mph and 10 mph higher desired speed), and 4 trials were performed for each of the four gap settings on EV (2 trials for same desired speed, 1 trial each for 5 mph and 10 mph higher desired speed). By testing all three/four possible gaps (short, medium, long for both powertrains, and extra-long only for EV) that drivers could set in ACC, 72 trials for ICE vehicle and 16 trails for EV were conducted for each of the 17 car following scenarios.

We expect that such speed fluctuations during the experiment could increase average spacings and headways (time gap) and diminish capacity, especially for ICE vehicle, due to ACC's delayed reaction and gradual acceleration when returning to the free-flow speed (Chon Kan et al, 2021).

3.2.2 Longitudinal Car-following under Higher Desired Speed

With higher ACC desired speed set in the following vehicle, Figure 3.8 illustrated the speed and gap profile of typical ACC car-following behaviors of an ICE vehicle observed in the field. It is obvious that after both vehicles returned to the free-flow speed, there was a period when the following vehicle accelerated up to a speed higher than the free-flow speed (desired speed of leading or front vehicle) to "catch up" with the leading vehicle (period between red and green dotted line). In the meantime, the spacing/gap between two vehicles decreased and returned to almost the minimum equilibrium gap/spacing prior to the speed fluctuation. This field observation will be called "catch-up" process, and such "catch-up" behaviors are expected to decrease the average spacings and headways between two test vehicles and will be modeled separately.

Notice that we cannot rely on the "catch-up" process to recover the initial steady state headway and capacity in the real-world, since it takes a long time and could be easily interrupted. Besides, it could induce additional speed fluctuations upstream, and eventually exchange a smaller gap downstream for a longer gap upstream. The purpose of this test is to present a complete trajectory for developing ACC car-following models in the future.
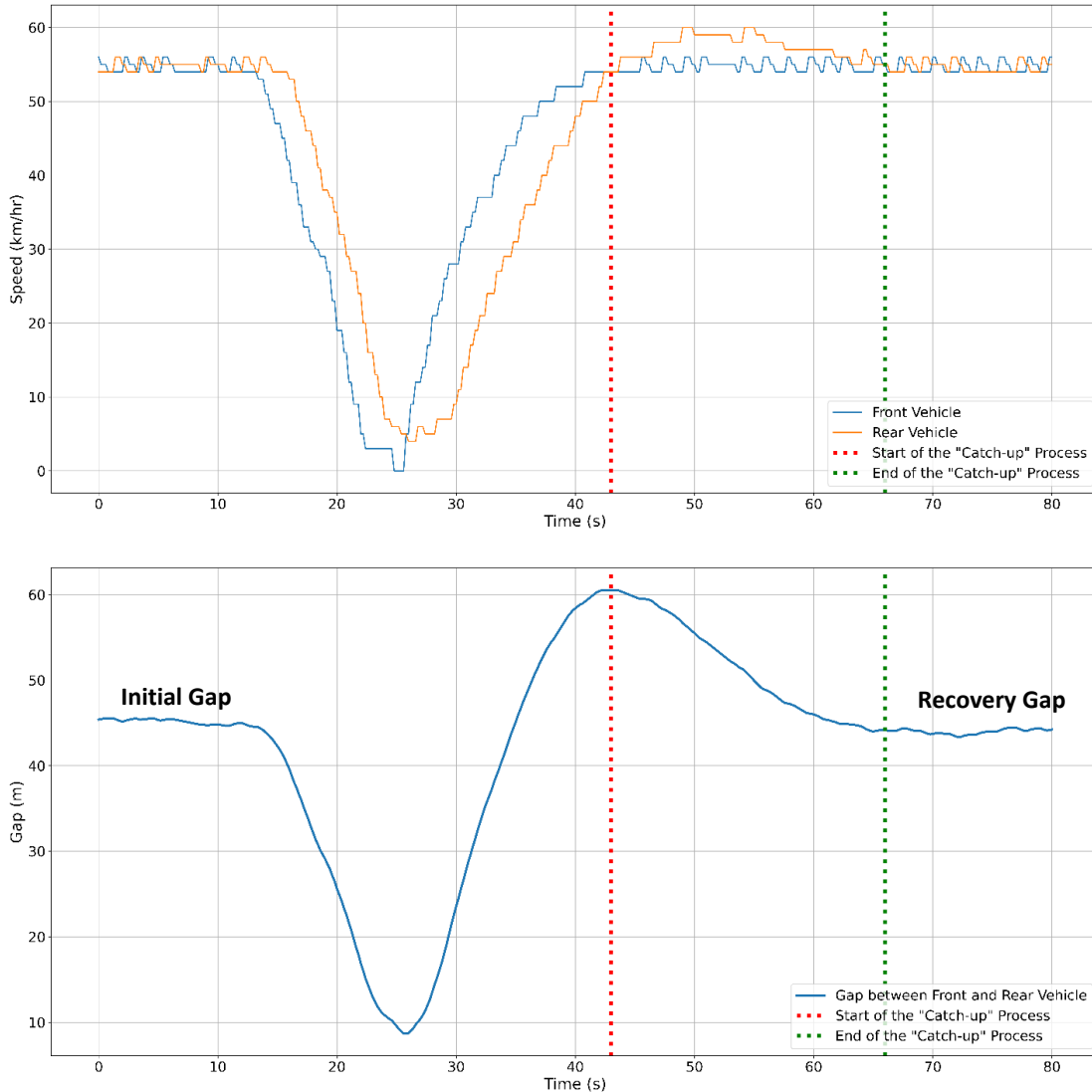
Figure 3.8. Speed and gap vs. time for a typical experiment with higher desired speed.

(Experiment scenario: 56 km/hr free flow speed, 72 km/hr desired speed, long gap).

3.2.3 Receiving Lane Change Car-following

This set of experiments was intended to empirically determine the potential effect of lane changes (performed by human drivers) and the subsequent response from ACC equipped vehicles on capacity. The response from ACC equipped vehicles is known as the relaxation in traffic flow theory (Cohen, 2004; Laval et al, 2008; Zheng et al, 2013; Zhou et al, 2022) or receiving lane change car following in driving behavior models (Liu et al, 2018a; Liu et al, 2018b).

The detailed experiment procedure is as follows: Initially, three vehicles were aligned in a single lane at a gap of Δ (1.4 meter) from each other when stationary, demonstrated in Figure 3.9a. As shown in Figure 3.9b, the front and rear vehicles immediately switched to the left lane, then the drivers of both vehicles manually accelerated at moderate acceleration rate up to the initial free-flow speed. The driver in the leading (front) vehicle then set the cruise control speed to the

free-flow speed after accelerating and remained at that speed throughout the experiment. The driver of the rear vehicle then activated ACC and kept a reasonable following distance.

During this approach, ACC in the rear vehicle may adjust slightly and stabilize again, reaching a steady headway prior to the lane change maneuver. Concurrently, the driver of the middle vehicle that is expected to perform lane changes in the experiment remained in the right lane, and the middle vehicle then rapidly accelerated manually to speeds higher than the free-flow speed for approximately 15 seconds to be ahead of both the front and rear vehicles, also illustrated in Figure 3.9b. Afterwards, the driver of the middle vehicle decelerated to the lane change speed and remained at such until the front and rear vehicles approach from the left lane at the free-flow speed. Shown in Figure 3.9c, this is an example with 96 km/hr (60 mph) free-flow speed and 80 km/hr (50 mph) re speed, and once the middle vehicle is aligned with the gap between the front and rear vehicles, the driver of the middle vehicle was instructed to perform the lane change maneuver manually and accelerate normally to the 96 km/hr (60 mph) free-flow speed during lane change, as the driver would merge or lane change in any normal lane change scenarios. During the lane change maneuver, we expect ACC in the rear vehicle to intervene, decelerate to maintain safe following distance and accelerate back to the free-flow speed once the middle vehicle completes the lane change maneuver, as illustrated by Figure 3.9d and Figure 3.9e.

Two free-flow speeds were tested: 96 km/hr (60 mph) and 56 km/hr (35 mph). For each free-flow speed, three lane change speeds were tested: same as free-flow speed, 8 km/hr (5 mph) lower than free-flow speed, and 16 km/hr (10 mph) lower than free-flow speed. Similarly, as 2-vehicle longitudinal experiments, each scenario was tested by setting three different desired speeds for ACC in the following vehicle: with the desired speed set equal to, 8 km/hr (5 mph), or 16 km/hr (10 mph) higher than the free-flow speed which is also the leading vehicle's desired speed. This controlled experiment is intended to replicate disruptive lane change maneuvers into vehicles more closely spaced in the adjacent lane, and these maneuvers typically occur near freeway entrances and exits as well as arterial intersections where mandatory lane changes from lower speeds to higher speed traffic are the most common. Data were taken after both the middle (lane changer) and rear vehicles returned to the free-flow speed and spacing can be determined to calculate the headway and flow after lane change and the subsequent speed fluctuation in the rear vehicle that performed receiving lane change car following. To compare, data were also obtained from the front and rear vehicles to determine the steady state spacing and distance gap prior to lane change.

For each lane change scenario discussed, 6 trials were performed for each gap setting, and the lane change maneuvers were performed by two different recruited human drivers (3 trials per driver). By testing all three/four available ACC gaps, 18 trials for ICE vehicle and 24 trails for EV were conducted for each lane change scenario.

We expect the headway could increase hence flow could decrease because ACC vehicles have delayed reaction when accelerating again, especially if the lane changer speed is lower than the speeds of the vehicles in the target lane. This could lead to increasing headway and potentially lower capacity, compared to headways and capacities observed in steady state equilibrium conditions prior to lane change.
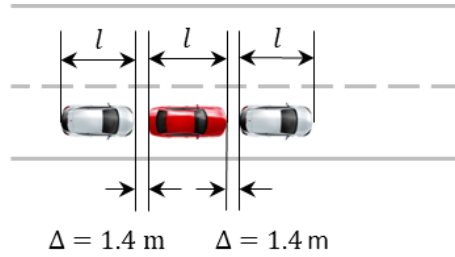
(a) Step 1: Align at complete stop
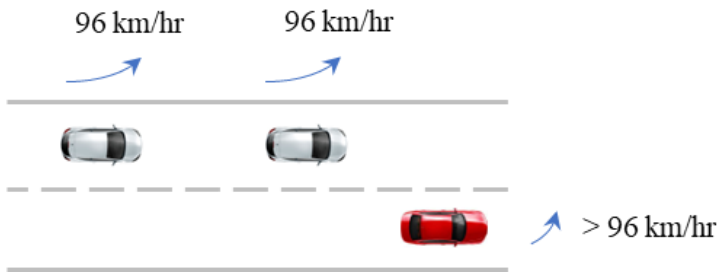
(b) Step 2: all vehicles accelerate to prepare for lane change scenario
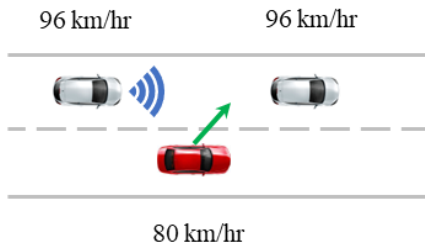
(c) Step 3: middle vehicle (lane changer in red) decelerates to prepare for lane change
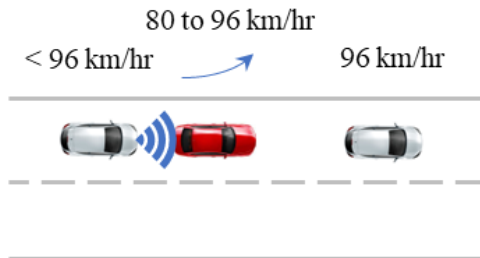
(d) Step 4: middle vehicle performs lane change and the ACC in rear vehicle reacts

(e) Step 5: all three vehicles re-stabilize and return to 96 km/hr steady state
Figure 3.9. Lane change experiment procedures.

17

3.3 Selected Study Site

As mentioned in subsection 3.2, 17 speed scenarios were tested for two-vehicle car-following experiments and 6 speed scenarios were tested for three-vehicle lane-change experiments, with each scenario including three different gap settings (i.e., short, medium, long) for ICE vehicle and four different gap settings (i.e., short, medium, long, extra-long) for EV and three different desired set speeds (i.e., equal to, 8 km/hr (5 mph), or 16 km/hr (10 mph) higher than the free-flow speed) for ACC in the following vehicle. In summary, 23 scenarios were tested:

1. 60 mph (96 kph) to 45 mph (72kph) to 60 mph (96 kph)
2. 60 mph (96 kph) to 35 mph (56 kph) to 60 mph (96 kph)
3. 60 mph (96 kph) to 25 mph (40 kph) to 60 mph (96kph)
4. 60 mph (96 kph) to 15 mph (24 kph) to 60 mph (96 kph)
5. 60 mph (96 kph) to 0 mph (0 kph) to 60 mph (96 kph)
6. 55 mph (88 kph) to 45 mph (72kph) to 55 mph (88 kph)
7. 55 mph (88 kph) to 35 mph (56 kph) to 55 mph (88 kph)
8. 55 mph (88 kph) to 25 mph (40 kph) to 55 mph (88 kph)
9. 55 mph (88 kph) to 15 mph (24 kph) to 55 mph (88 kph)
10. 55 mph (88 kph) to 0 mph (0 kph) to 55 mph (88 kph)
11. 45 mph (72 kph) to 35 mph (56 kph) to 45 mph (72 kph)
12. 45 mph (72 kph) to 25 mph (40 kph) to 45 mph (72 kph)
13. 45 mph (72 kph) to 15 mph (24 kph) to 45 mph (72 kph)
14. 45 mph (72 kph) to 0 mph (0 kph) to 45 mph (72 kph)
15. 35 mph (56 kph) to 25 mph (40 kph) to 35 mph (56 kph)
16. 35 mph (56 kph) to 15 mph (24 kph) to 35 mph (56 kph)
17. 35 mph (56 kph) to 0 mph (0 kph) to 35 mph (56 kph)
18. free-flow speed: 60 mph (96 kph), lane change speed: 50 mph (80 kph)
19. free-flow speed: 60 mph (96 kph), lane change speed: 55 mph (88 kph)
20. free-flow speed: 60 mph (96 kph), lane change speed: 60 mph (96 kph)
21. free-flow speed: 35 mph (56 kph), lane change speed: 25 mph (40 kph)
22. free-flow speed: 35 mph (56 kph), lane change speed: 30 mph (48 kph)
23. free-flow speed: 35 mph (56 kph), lane change speed: 35 mph (56 kph)

Data collections for ICE vehicles were conducted on public roadways during off-peak hours, without interruptions from other road users. US 441 between Atlantic Blvd. and Boynton Beach Blvd (5.0 miles in length) in Delray Beach, Florida, shown in Figure 3.10a, was used to perform scenarios 1-3, 6-8, and 18-20. In addition, the entire section of Connors Highway in Loxahatchee, FL, shown in Figure 3.10b, was used to perform scenarios 4-5, 9-10, 13-14, and 16-17. The lack of intersections, ingress and egress points on this remote highway allowed us to successfully perform larger speed fluctuations to 15 mph and 0 mph. Furthermore, Clinton Moore Rd. between Lyons Rd. and Claridge Oval in Boca Raton, FL, shown in Figure 3.10c, was used to perform scenarios 11 and 12. Finally, Trails End between North University Drive and Pine Island Road Nob Hill Rd. (1.6 miles in length) in Parkland, FL was used to perform scenarios 15, and 21-23 shown in Figure 3.10d. All the four sites have homogenous geometries over their length, and they have no on-ramps and off-ramps.
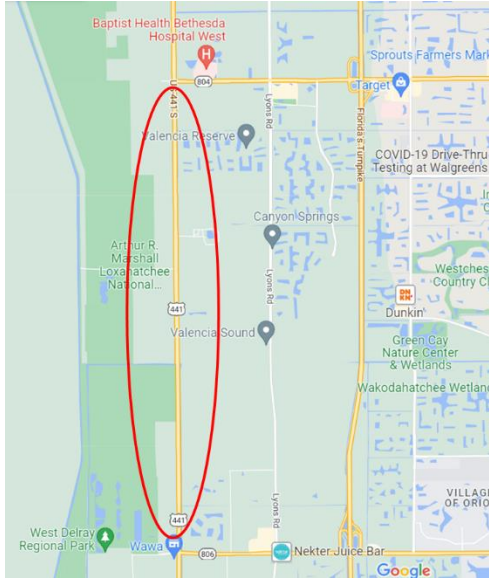
(a) Scenarios 1-3 and 6-8: US 441 in Delray Beach, FL
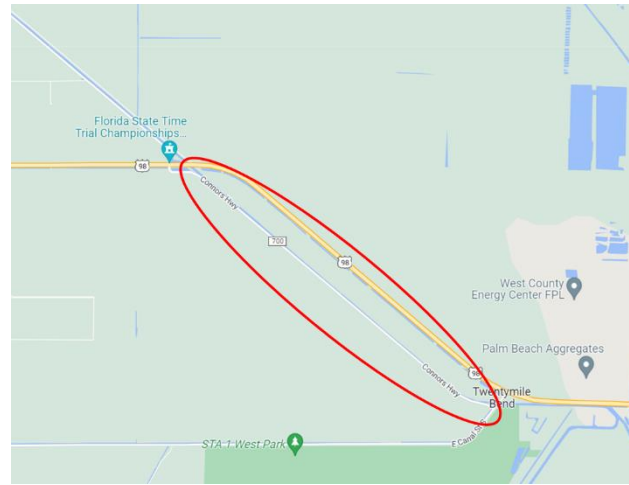
(b) Scenarios 4-5, 9-10, 13-14, and 16-17: Connors Highway in Loxahatchee, FL
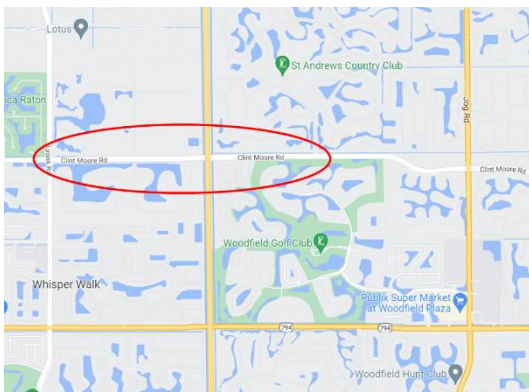
(c) Scenarios 11-12: Clint Moore Rd. in Boca Raton, FL
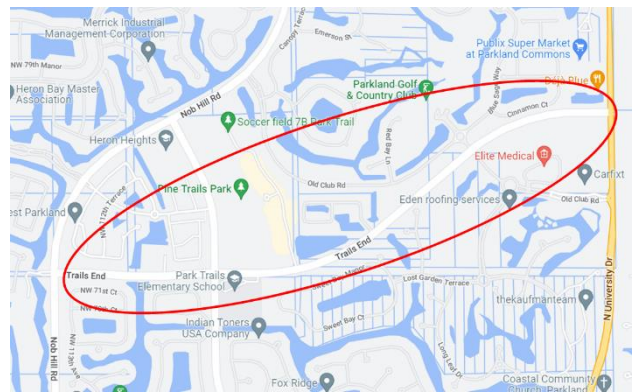
(d) Scenarios 15: Trails End in Parkland, FL

Figure 3.10. Experiment sites for ICE vehicles.

Field experiments for EVs were mainly conducted on isolated portions of rural public roads in Dixon, California, on approximately 10-km stretches of Pendrick, Robben, and Sikes Rds. As shown in Figure 3.11, the remote locations and lack of interference from other road users allowed us to reproduce various traffic conditions efficiently throughout the data collection process. Robben Rd. was primarily used while Pedrick Rd. and Sikes Rd. were alternate locations in case the conditions were less ideal on Robben Rd.

19
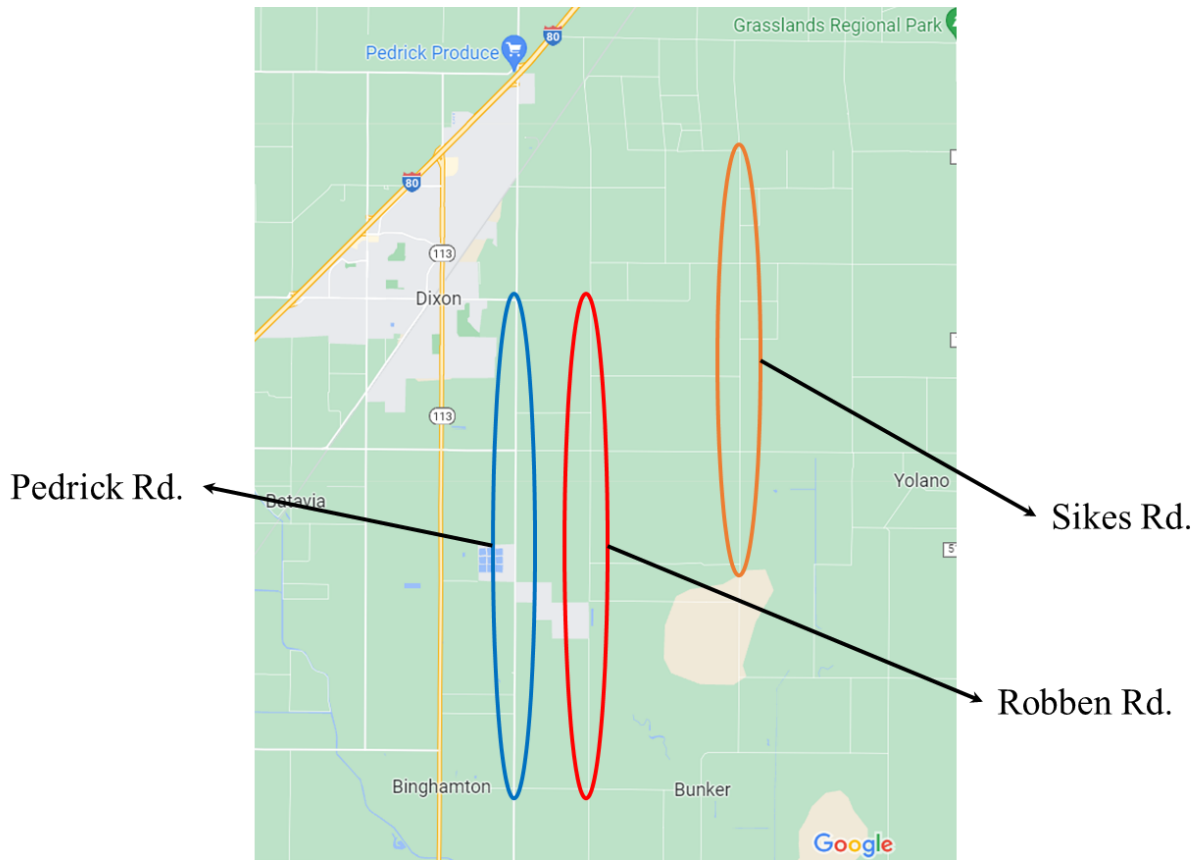
Figure 3.11. Experiment sites for EVs.

3.4 Trajectory Data Analysis

The trajectory analysis to determine spacing is based on the concept of cumulative distance travelled which allows a quantitative and graphic evaluation of the distances driven by the vehicles. The method uses speed collected every 0.2s from OBD data logger and converts that into distance; the differences between the vehicles at a given moment provide the spacing between vehicles and them. We reset the initial gap Δ of 1.4 meters between the leading vehicle's rear bumper and the following vehicle's front bumper at the beginning of every single trial in the lane-change car following experiments and every two trials in the longitudinal car-following experiments, to minimize the cumulative distance errors.

Specifically, we need to find the cumulative distance traveled of each vehicle up to a timestamp t in which the instantaneous photograph of the trajectory was taken to compute the flow and measure the capacity. Having the cumulative distance traveled for each vehicle we can find the difference in traveled distance d_i for each one. Hence, knowing each d_i, as well as vehicle length l and initial gap Δ (i.e., 1.4 meters), we are able to calculate the spacings $s_{12,t}$ and $s_{23,t}$. This is described in detail via equations 3.1 through 3.3 and Figure 3.12.

$$d_{i,t} = \sum_{k=1}^{t} v_{i,k} * \Delta t \qquad (3.1)$$

$$s_{12,t} = d_{1,t} + l + \Delta - d_{2,t} \qquad (3.2)$$

$$s_{23,t} = d_{1,t} + 2l + 2\Delta - d_{3,t} - s_{12,t} \qquad (3.3)$$

where:

$v_{i,t}$: speed reading from the OBD data logger of vehicle i at timestamp t

$d_{i,t}$: cumulative distance traveled of vehicle i at timestamp t

$s_{12,t}$: spacing between vehicle 1 and 2 at timestamp t

$s_{23,t}$: spacing between vehicle 2 and 3 at timestamp t

Δt: time interval between two consecutive OBD data points

l: vehicle length

Δ: initial gap between the leading vehicle's rear bumper and the following vehicle's front bumper
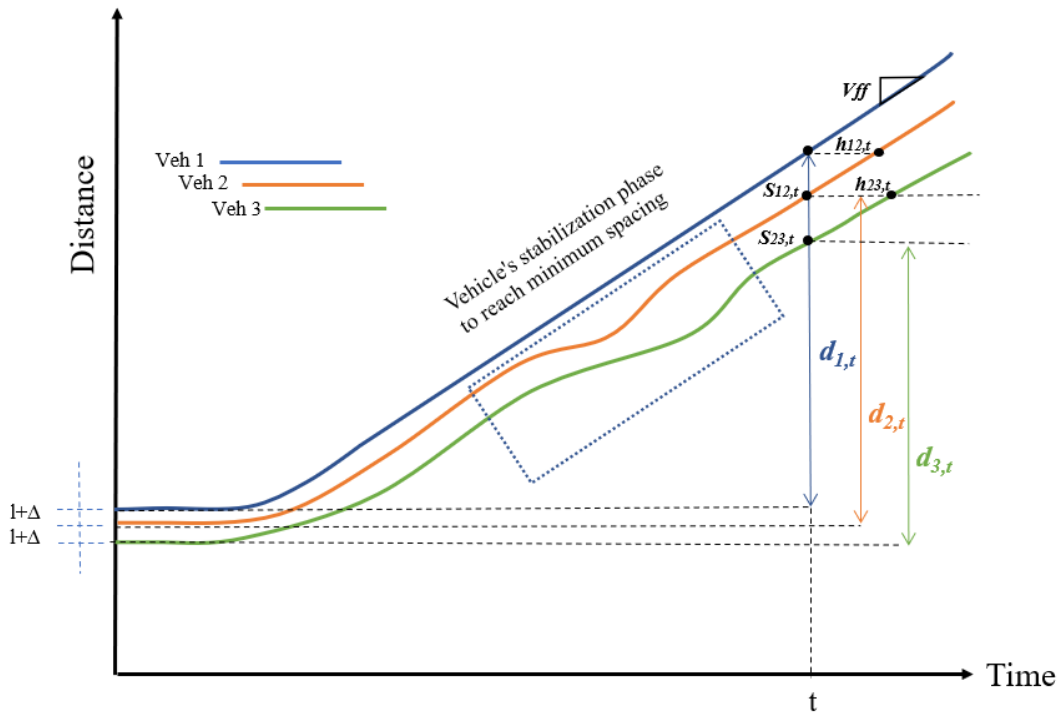
Figure 3.12. Time-space diagram for the determination of spacing s.

3.5 Data Management

MicroSIMACC dataset includes the trajectories of both ACC-equipped ICE vehicles and EVs and has been uploaded on GitHub given the link: https://github.com/microSIM-ACC.

21

For ICE vehicles, three folders are created to separate data collected from different experiment sets: "2-Vehicle ACC Car Following Experiments (CCF, Same Desired Speed)", "2-Vehicle ACC Car Following Experiments (CCF, Higher Desired Speed)", and "3-Vehicle ACC Lane Change Experiments (RCF)". In each folder, the filename can represent the scenarios covered by the data. For instance, the third repeated trial of the 2-vehicle car-following experiment (same desired speed) with long gap setting, free flow speed of 96 km/hr (60 mph) and speed fluctuation down to 40 km/hr (25 mph) will be found in the path "2-Vehicle ACC Car Following Experiments (CCF, Same Desired Speed) \60_25_L_3.csv". The data consists of Time (second), the speed (km/h), distance travelled (m), cumulative distance travelled (m) of each test vehicle, and the travel distance difference (m) between two consecutive vehicles. Sample trajectory data are given in Table 3.1. Column "Speed1 (km/hr)" represents the speed of the leading vehicle, while column "Speed2 (km/hr)" represents the speed of the following ACC-controlled vehicle. Same expression is applied for distance travelled and cumulative distance travelled. Note that an initial gap Δ (i.e., 1.4 m) should be added to the travel distance difference to get the actual distance gap. Engine revolutions per minute (RPM) and mass air flow rate (MAF, unit: g/s) are also included in the ICE dataset but will not be used in this study.

Table 3.1. Sample trajectory data of ACC-equipped ICE vehicles.

Time (s)	Speed1 (km/h)	Speed2 (km/h)	Distance travelled1 (m)	Distance travelled2 (m)	Cumulative distance travelled1 (m)	Cumulative distance travelled2 (m)	Travel distance difference (m)
0	54	54	3	3	609.8889	576.8333	33.05556
0.2	56	54	3.111111	3	613	579.8333	33.16667
0.4	56	54	3.111111	3	616.1111	582.8333	33.27778
0.6	55	54	3.055556	3	619.1667	585.8333	33.33333
0.8	55	54	3.055556	3	622.2222	588.8333	33.38889

For EVs, since the Racebox is utilized as the main data collection equipment to obtain the GPS coordinates of vehicle trajectories, the data are organized in a different way. Data from different manufacturers, including IONIQ5, Polestar 2, and Tesla Model 3, were stored in different folders. Each folder follows the setup presented in Figure 3.13. For instance, a trial with long gap setting, +0 desired speed, free flow speed of 72 km/hr (45 mph) and speed fluctuation down to 24 km/hr (15 mph) will be found in the path "Long\0_desired\45\15". The same information can be obtained from the EV dataset as the ICE vehicle data shown in Table 3.1. The only difference is that the data collection frequency changes from 0.2 second to 0.04 second.
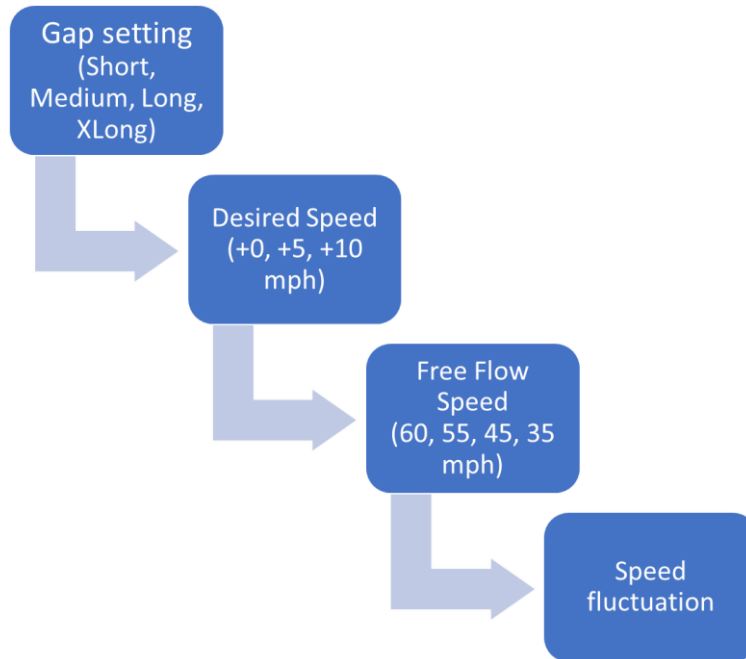
Figure 3.13 Field data organization for EV experiments.

CHAPTER 4: ACC CAR FOLLOWING BEHAVIOR OBSERVATION

4.1 Full Speed Range Longitudinal Car Following

4.1.1 Identical Desired Speeds

Table 4.1 summarized the average minimum headways under steady-state conditions for ACC-equipped ICE vehicle (Toyota Corolla) and ACC-equipped EV (Hyundai IONIQ 5) across a range of free-flow speeds, spanning from 56 km/hr to 96 km/hr. Using the empirical ACC gap preference distribution: 50.4% of drivers choose short gap, 18.5% choose medium, and 31.1% choose long gap (Nowakowski et al, 2010), the theoretical maximum capacity for ICE vehicles can be calculated as 2169 veh/hr, 2036 veh/hr, 1711 veh/hr, and 1574 veh/hr for 96 km/hr (60 mph), 88 km/hr (55 mph), 72 km/hr (45 mph) and 56 km/hr (35 mph) free-flow speeds, respectively. EVs, on the other hand, can achieve considerably shorter headways, reaching as low as 1.23 seconds at constant speeds in steady-state conditions, and potentially yield higher capacities of 2486 veh/hr, 2387 veh/hr, 2229 veh/hr, and 2175 veh/hr, for 96 km/hr (60 mph), 88 km/hr (55 mph), 72 km/hr (45 mph) and 56 km/hr (35 mph) free-flow speeds, respectively. This finding is consistent with initial attempts to quantify the headways adopted by ACC controllers at constant speeds in steady-state conditions (Li et al, 2022). This is a result of EV's instantaneous regenerative braking that allows EVs to safely follow the preceding vehicles more closely at higher speeds. Similar to previous studies on ICE vehicles equipped with ACC (Chon Kan et al, 2021; Chon Kan et al, 2022), it was observed that the minimum headway for EVs increased as the selected ACC gap setting transitioned from short to medium to long, and to extra-long.

Table 4.1. Steady-state minimum headways for various free-flow speeds.

Free Flow Speed: 96 km/hr				
	ACC Gap Selection			
	Short	Medium	Long	Extra Long
ICE Vehicle	1.35	1.95	2.33	/
EV	1.23	1.50	1.77	2.30
Free Flow Speed: 88 km/hr				
	ACC Gap Selection			
	Short	Medium	Long	Extra Long
ICE Vehicle	1.42	2.04	2.60	/
EV	1.27	1.6	1.84	2.35
Free Flow Speed: 72 km/hr				
	ACC Gap Selection			
	Short	Medium	Long	Extra Long
ICE Vehicle	1.68	2.54	3.03	/
EV	1.40	1.69	1.92	2.41
Free Flow Speed: 56 km/hr				
	ACC Gap Selection			
	Short	Medium	Long	Extra Long
ICE Vehicle	1.94	2.77	2.81	/
EV	1.44	1.73	1.96	2.25

Table 4.1 also demonstrated that EVs had much lower variability in the observed minimum headways across different free-flow speeds than ICE vehicles did: the maximum difference across various free-flow speeds was 0.23 seconds for EVs, while this number increased to 0.82 seconds for ICE vehicles. Both numbers were achieved under medium gap setting. This phenomenon indicated that EVs paired with ACC could potentially yield more reliable and consistent capacities in real world traffic.

For ACC-equipped ICE vehicles, the minimum headways under steady-state conditions cannot be sustained once speed fluctuates in non-steady state conditions and the headways can increase by as much as 1.5s. This is consistent with the effect of diminishing discharge flow once queues form at bottlenecks (Cassidy and Bertini, 1999). An example of this phenomenon is shown in Figure 4.1(a), which is a time-space diagram of both the leading and the following vehicle trajectories. The distance between the leader and follower increased after returning to the free-flow speed, which indicated longer spacing and headway therefore diminishing flow. ACC-equipped ICE vehicles exhibit a reaction delay (possibly from the ICE powertrain) and very gradual initial acceleration when returning to free-flow speeds (88 km/hr in this example) during queue discharge. This gradual acceleration corresponds to a rate of approximately 0.5 m/s^2 to 1.0 m/s^2 on a regular basis, which is a very leisurely increase in speed. In the end, the headway increases.

However, unlike ACC-equipped ICE vehicles, these shorter headways adopted by ACC-equipped EVs can be sustained beyond the ideal steady-state conditions. The exceptional powertrain characteristics of fully electric vehicles (EVs) enabled responsive deceleration using regenerative braking when approaching the back of queue when a leading vehicle is decelerating, and most importantly, the instantaneous peak torque allowed for nearly immediate acceleration once the leading vehicle began accelerating during queue discharge. This sustained the shorter headways adopted by EVs with ACC and entails that the potentially higher capacities could be sustained even in non-steady-state conditions, where speeds fluctuate when queues form and dissipate at bottlenecks. As shown by Figure 4.1(b), the ACC-equipped EV follower (Hyundai IONIQ 5) regained its initial minimum headway following a speed fluctuation intended to simulate approaching back of queue and accelerating during queue discharge, which contrasts with the performance of conventional ACC-equipped ICE vehicles, as shown by Figure 4.1(a). EVs produce strong initial acceleration from the instantaneous peak torque, and as illustrated in Figure 4.1(b), the slope of the time-space diagram is steeper for EV's acceleration. In fact, careful examination of field data suggests that EVs can accelerate normally and smoothly at almost twice the rate (1.5 m/s^2 to 2.0 m/s^2).

Moreover, steep decrease in speed and strong deceleration can be found on the trajectories in Figure 4.1(b). This resembles the aggressive regenerative braking of EVs, and the better braking performance allows ACC-equipped EVs to safely follow the leading vehicle at shorter headways. Interestingly, the aggressive regenerative braking applied by the following vehicle Hyundai IONIQ 5 ACC did not amplify the speed change from the 88 km/hr free-flow speed to the 40 km/hr congested speed in this example. This is certainly different from the example shown in Figure 4.1(a), where the ACC-equipped ICE vehicle amplified the speed change relative to the speed fluctuations undertaken by the leading vehicles. Observations from both field tests and trajectories in Figures 4.1 revealed that ACC-equipped EVs immediately applied aggressive regenerative braking that enabled the follower to quickly reach and maintain its desired headway as leader began decelerating, whereas the limited braking capability resulted in the ACC-equipped ICE

vehicle (follower) to decelerate for an extended period to speeds below that of the leading vehicle's final speed in the congested state (after the leader completed decelerating) to finally reach its desired headway, and ultimately amplifies speed change.
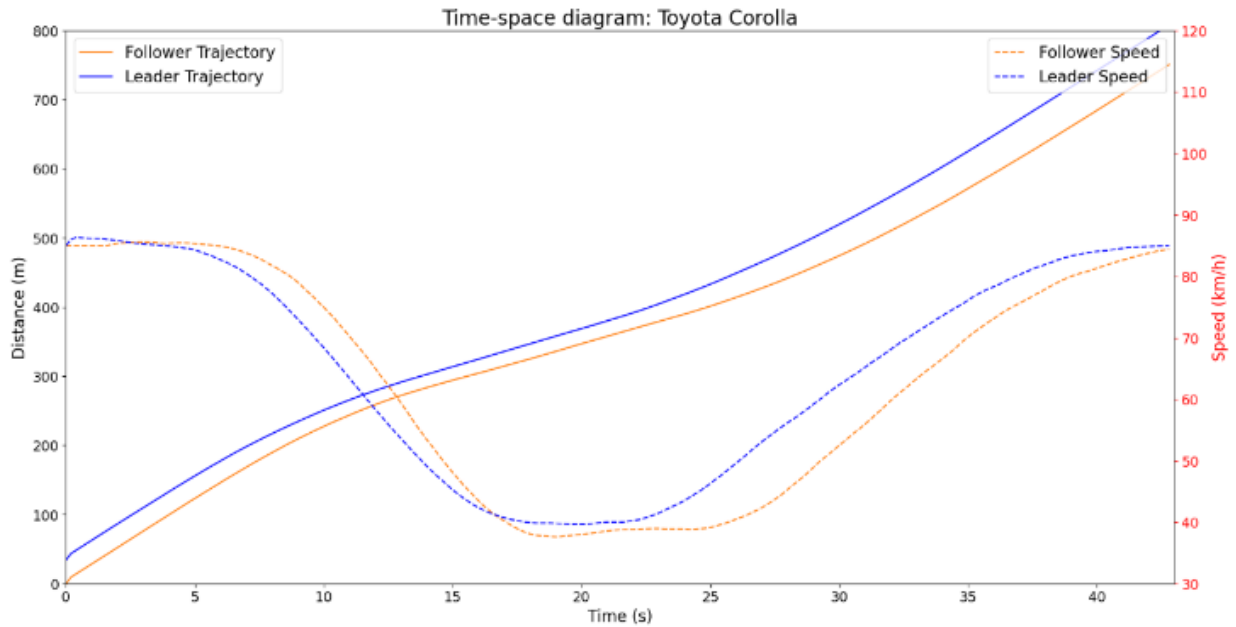
(a) Toyota Corolla (ICE Vehicle)
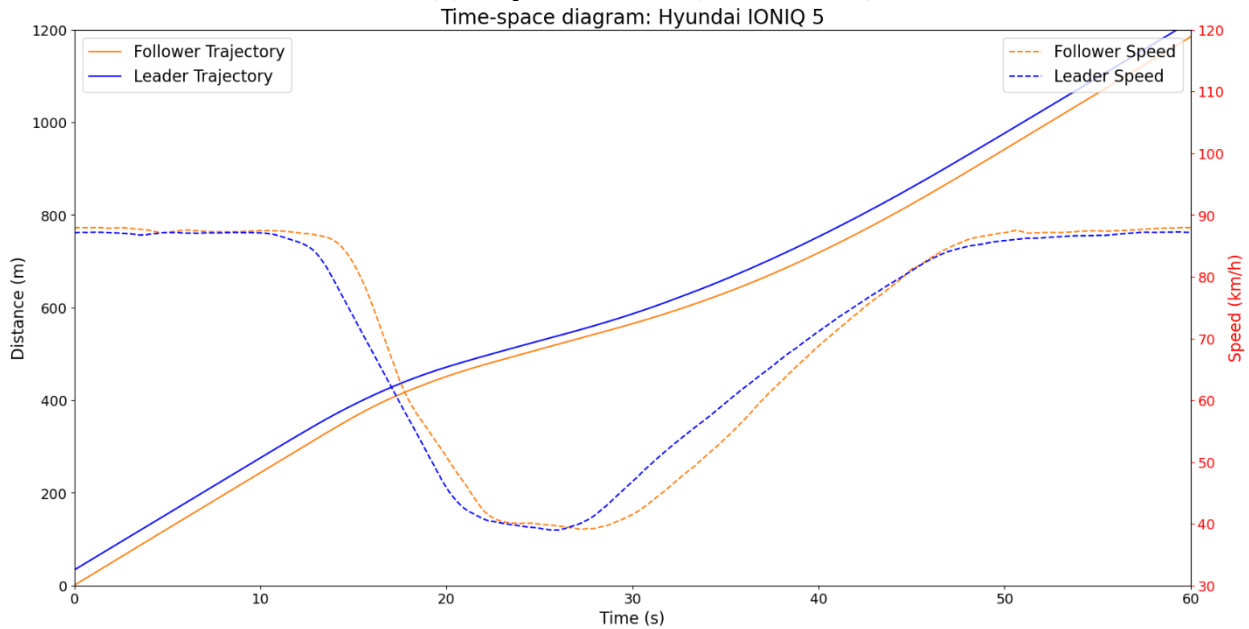
(b) Hyundai IONIQ 5 (EV)

Figure 4.1. Time-space diagram: same desired speed (Experiment scenario: 88 km/hr free-flow speed, 40 km/hr congested speed, short gap).

Overall, we observed that ACC-equipped EVs had nearly identical headway values before and after speed fluctuations (i.e., disturbance), which is much shorter than that of ACC-equipped

ICE vehicles. This highlights the superior capability of the ACC-equipped EVs in maintaining nearly constant and steady headways in dynamic real world traffic conditions.

4.1.2 Additional Observations for ICE Vehicles

For ICE vehicles, it is expected that the increase in headway is amplified as speed changes become more severe (i.e., congested speed becomes lower) under the identical desired speed. In Table 4.2, we showed the headway change, which is the difference between the discharge headways and the corresponding steady-state minimum headways that were always established in the field before the various speed changes, under various free-flow speeds and congested speeds.

Table 4.2. Headway increase for various speed changes under different free-flow speeds, unit: seconds.

Gap setting	Congested Speed (km/hr)						
	88	80	72	56	40	24	0
96 km/hr free-flow speed							
Short	0.21	0.44	0.56	0.77	0.77	0.80	0.84
Medium	0.28	0.50	0.81	1.30	1.14	1.23	1.29
Long	0.35	0.59	0.86	1.47	1.44	1.68	1.51
88 km/hr free-flow speed							
Short	/	/	0.55	0.82	0.98	0.80	0.84
Medium	/	/	0.64	1.05	1.11	1.07	1.13
Long	/	/	0.53	0.95	1.06	1.14	1.18
72 km/hr free-flow speed							
Short	/	/	/	0.44	0.58	0.97	1.02
Medium	/	/	/	0.42	0.81	1.19	1.22
Long	/	/	/	0.47	0.78	1.17	1.25
56 km/hr free-flow speed							
Short	/	/	/	/	0.46	1.01	1.10
Medium	/	/	/	/	0.53	1.03	1.11
Long	/	/	/	/	0.50	0.93	1.05

We observe that, as the speed changes increase in magnitude, the discharge headway generally increases. Interestingly, it is found that the headway increasing patterns can be quite different and it heavily depends on whether the speed changes exceed 32 km/hr (20 mph). The discharge headway does not increase in such an obvious way when the speed changes exceed 32 km/hr (20 mph), compared to the increase when the speed changes is within 32 km/hr (20 mph). This phenomenon can be observed in a clearer way in Figure 4.2, which illustrates the distribution of headway changes under various free-flow speeds and congested speeds. The non-linear headway increasing pattern will be seriously taken into consideration when developing multi-stage ACC car-following models in Chapter 5. Free-flow speeds do not play an important role in headway increase, and similar observations can be found under different free-flow speeds as long as the relative speed change stays the same. Moreover, gap setting does not have a great impact in headway increase either. The headway increase is subtle as the gap setting becomes longer,

compared to that induced by speed changes. In a few cases, longer gap setting does not even guarantee a larger discharge headway.
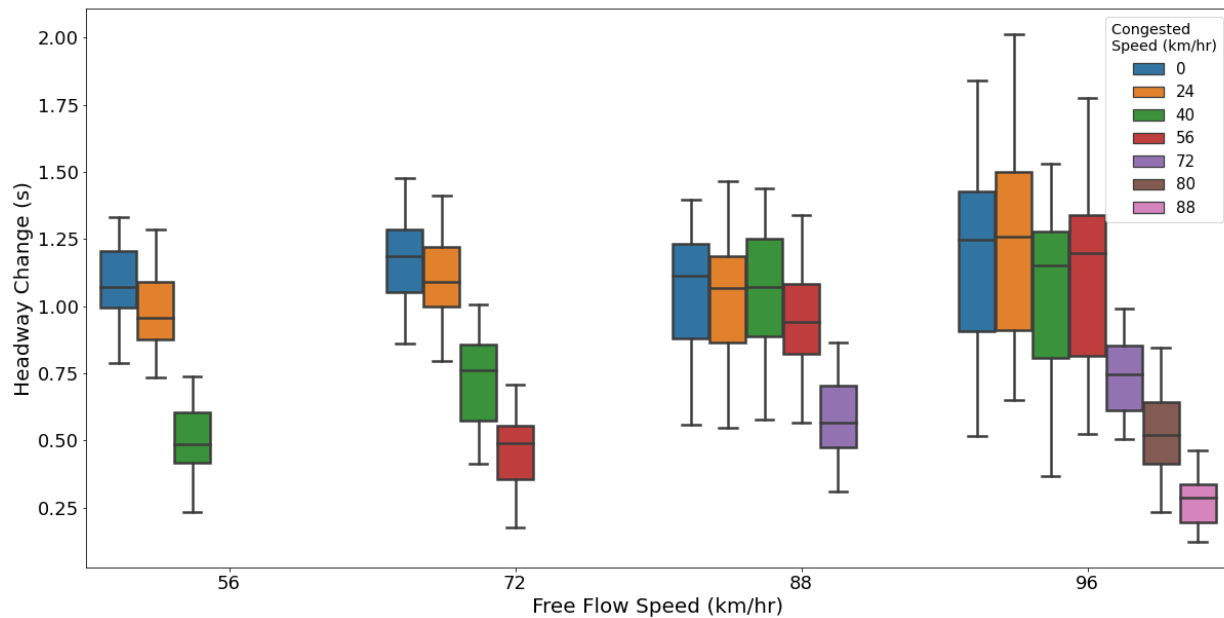
Figure 4.2. Distribution of headway change under various free-flow speeds and congested speeds, unit: seconds.

4.1.3 Heterogeneous Desired Speeds

Indicated by Figure 3.8, the following ACC-equipped ICE vehicle accelerated up to a speed higher than the free-flow speed (desired speed of leading or front vehicle) to "catch up" with the leading vehicle when the desired ACC set speed was higher than the free-flow speed. The increasing headway observed in subsection 4.1.1 would be recovered to a similar level as the initial headway observed at the beginning of the experiment. In fact, after comparing the initial gap with the recovery gap via a standard paired t-test, the results indicated that the average gap even decreased by 1.6 meters in a statistically significant way.

- Average initial gap: 46.07 m
- Average recovery gap: 44.42 m
- Standard deviation of gap difference: 4.90 m
- T-value: - 5.70
- $P > |t|$: 3.03e-10
- Statistically Significant: Yes
- Sample size: 286

Figure 4.3(a) illustrated how ACC-equipped ICE vehicles would accelerate beyond the speed of the leading vehicle to undergo a "catch-up" process before decelerating again to ensure that the minimum headway is maintained. Compared with Figure 4.1 (a), the impact of this "catch-up" process on headway changes can be clearly seen. Such outcome may mainly be explained by the following: (1) a higher desired speed provided the following ACC vehicle an opportunity to

exceed the free-flow speed and shorten the gap with the leading vehicle (i.e., catch-up process); (2) a gap overshooting occurred during the catch-up process, which means that the ACC controller overreacted, a common trait of the string unstable commercial ACC system (Gunter et al, 2020).

For EVs, these field experiments suggest another interesting finding: setting higher desired speed does not affect the car following behavior and no "catch-up" process exists. As ACC-equipped EV accelerates swiftly to follow the lead vehicle and maintain the minimum headway, it would not be possible to accelerate beyond the leading vehicle speed even if the ACC desired speed was set higher, due to the minimum spacing and headway constraint. Figure 4.3(b) shows the speed vs. time plots of an example scenario. As shown, setting ACC desired speeds 8 or 16 km/hr above the desired speed (free-flow speed) of the leading did not alter the car following trajectories, in comparison with the scenario shown in Figure 4.1(b). To testify this finding numerically, we further calculated the headway change during the speed fluctuation by utilizing the initial gap, the recovery gap, and the corresponding free-flow (stable) speed. The results are shown in Table 4.3, which demonstrates that ACC-equipped EVs exhibit minimal headway change, with all cases falling below 0.1 seconds. As a result, minimum headways and maximum flows remain consistent with the steady-state minimum headways depicted in Table 4.1. Notably, even when both vehicles have the same desired speed (a desired speed difference of 0), the headway change remains negligible, thereby preserving the minimum headway. Most of all, ACC-equipped EVs maintain constant headway as speeds fluctuate regardless of how the ACC desired speed was chosen.
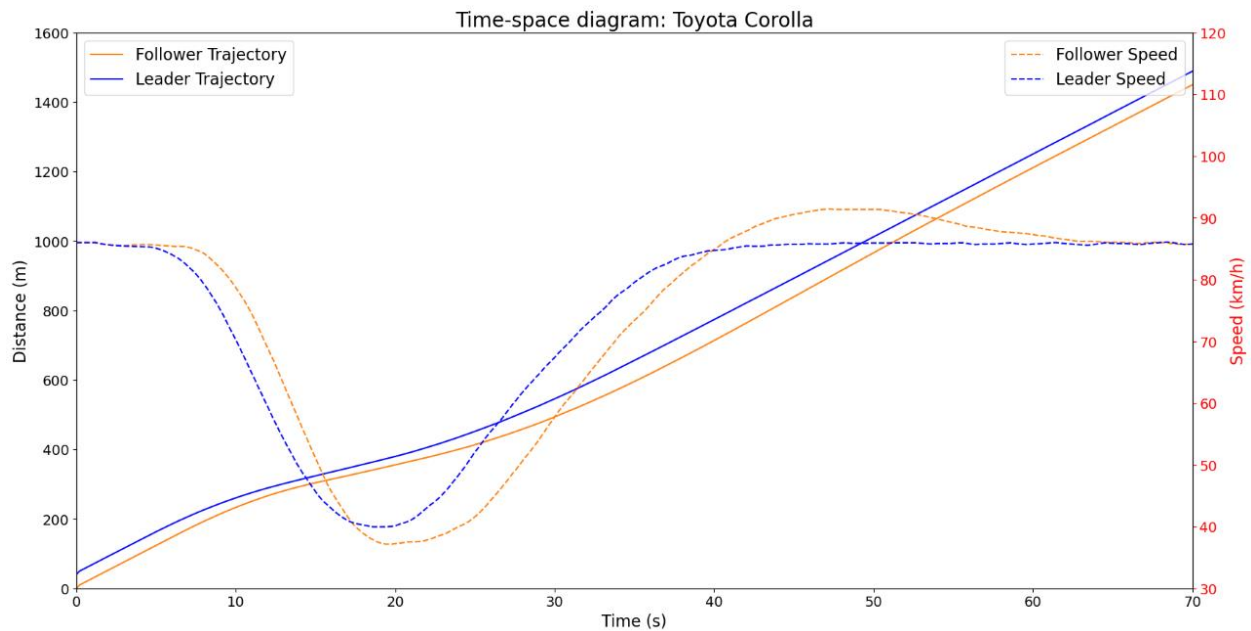
(a) Toyota Corolla (ICE Vehicle)
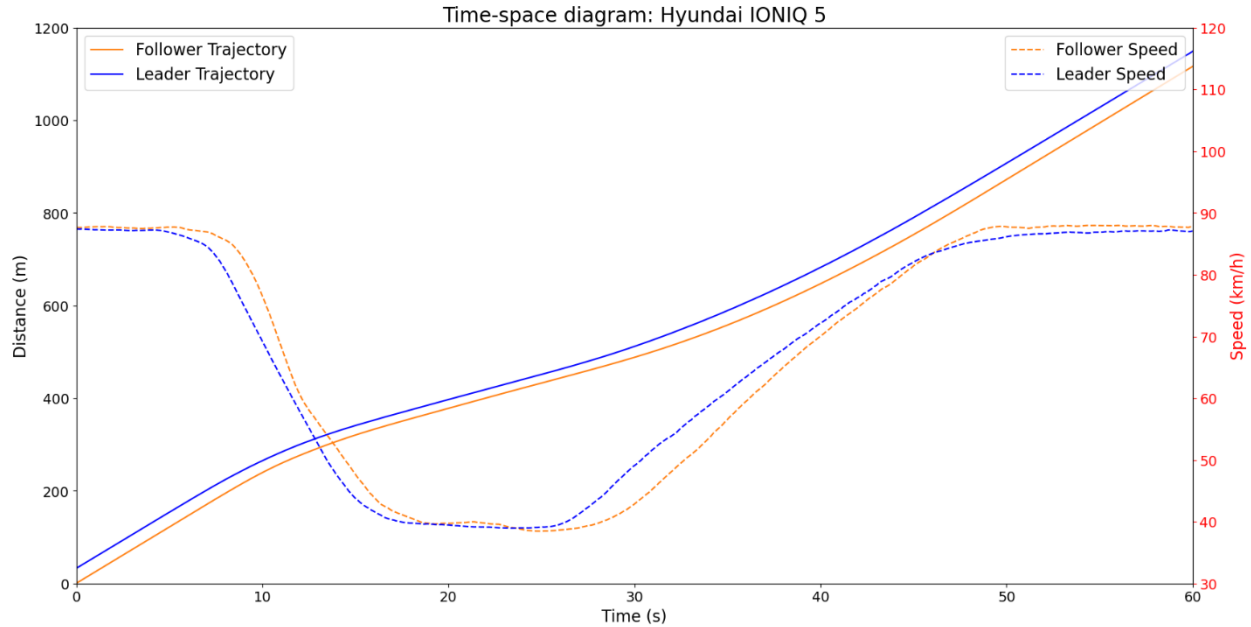
(b) Hyundai IONIQ 5 (EV)

Figure 4.3. Time-space diagram: + 8 km/hr desired speed (Experiment scenario: 88 km/hr free-flow speed, 40 km/hr congested speed, short gap).

Table 4.3. Headway change for various desired speeds.

Gap Setting	Desired Speed (unit: km/hr)	Headway Change (Std, unit: seconds)
Short	0	0.074 (0.090)
	8	0.033 (0.052)
	16	0.013 (0.042)
Medium	0	0.090 (0.075)
	8	0.002 (0.076)
	16	0.021 (0.067)
Long	0	0.058 (0.058)
	8	0.037 (0.041)
	16	0.021 (0.042)
Extra Long	0	0.029 (0.061)
	8	-0.005 (0.025)
	16	0.020 (0.046)

4.1.4 EVs from Different Manufacturers

As mentioned earlier, we conducted comparative tests using ACC equipped EVs from two other manufacturers, the Polestar 2 from a traditional but premium manufacturer Volvo and the Tesla Model 3 from an emerging vehicle manufacturer Tesla, using the same procedures and under similar conditions albeit with fewer repetitions. The observations obtained from testing the Polestar 2 mirrored those from the experiments using the Hyundai IONIQ 5, exhibiting similar minimum headways and sustained almost constant headways even in non-steady-state conditions

when queues are present. As depicted in Figure 4.4, the time-space diagram shows similar trajectories when decelerating while the Polestar 2 approaches the back of queue and when accelerating during queue discharge, though there appears to be a slight amplification of the speed change as opposed to the trajectories in Figure 4.1(b) and Figure 4.3 (b). However, the results for the Tesla Model 3 deviated from our expectations, as evidenced in Figure 4.5. Unlike the car following behavior of other ACC equipped EVs such as the Hyundai IONIQ 5 and Polestar 2, the Tesla Model 3 was unable to regain its initial minimum headway after a speed fluctuation, exhibiting characteristics similar to those of ACC-equipped ICE vehicles. This is reflected in the larger minimum headways and greater variability in minimum headways, leading to a substantial increase. Furthermore, a comparison with the time-space diagrams corresponding to the same experimental scenario for the ACC equipped ICE vehicle tested in (Chon Kan et al, 2021; Chon Kan et al, 2022) show that the Tesla Model 3's car following behavior is much similar to that of an ACC equipped ICE vehicle. It appears that the ACC equipped by Telsa does not utilize the advantages of EV powertrain, especially the instant peak torque that provides immediate acceleration during queue discharge, instead, the ACC equipped by Tesla gradually accelerates at a leisurely pace as the leading vehicle accelerates during queue dissipation. Similarly, the same "catch-up" process associated with ACC-equipped ICE vehicles that is shown in Figure 4.3(a) can be found in Figure 4.6, when the desired speed of the follower (Tesla Model 3) is set higher than that of the leader.
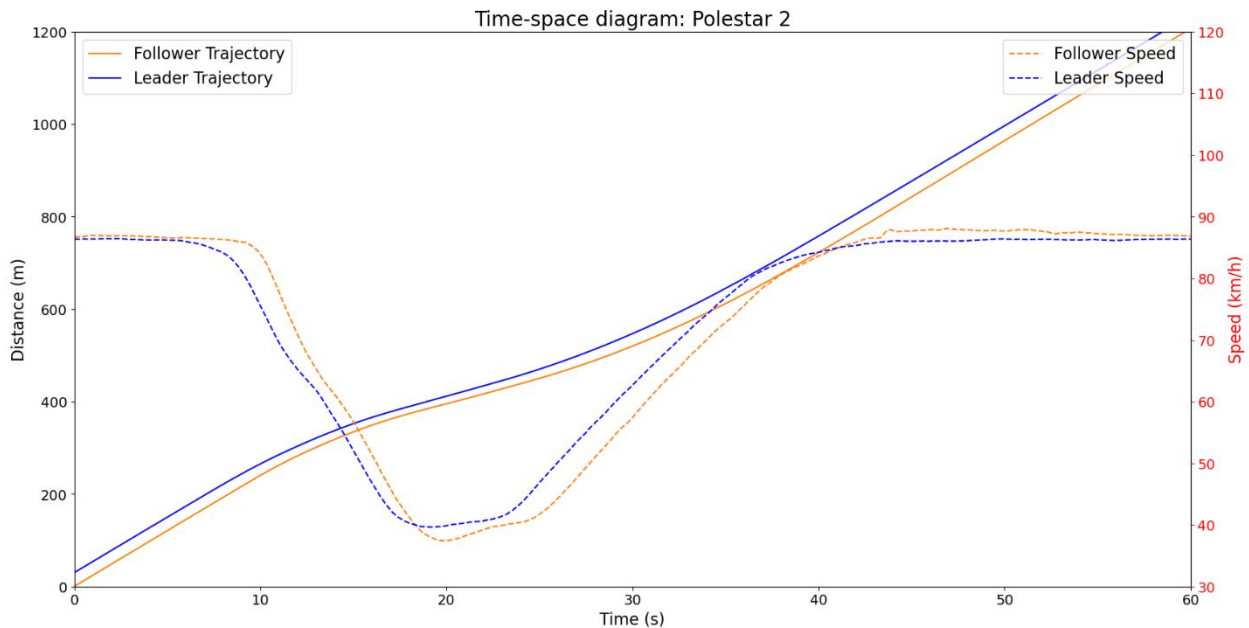
Figure 4.4. Polestar time-space diagram: 88 to 40 to 88 km/hr, short gap, same desired speeds.
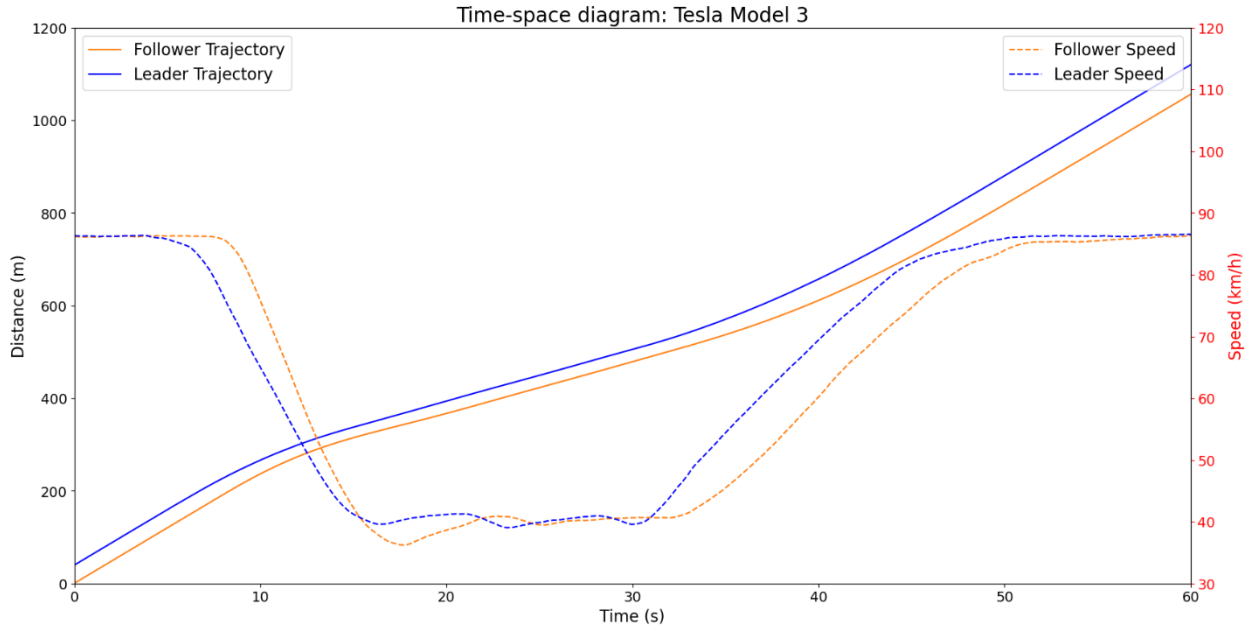
Figure 4.5. Tesla time-space diagram: 88 to 40 to 88 km/hr, short gap, same desired speeds.
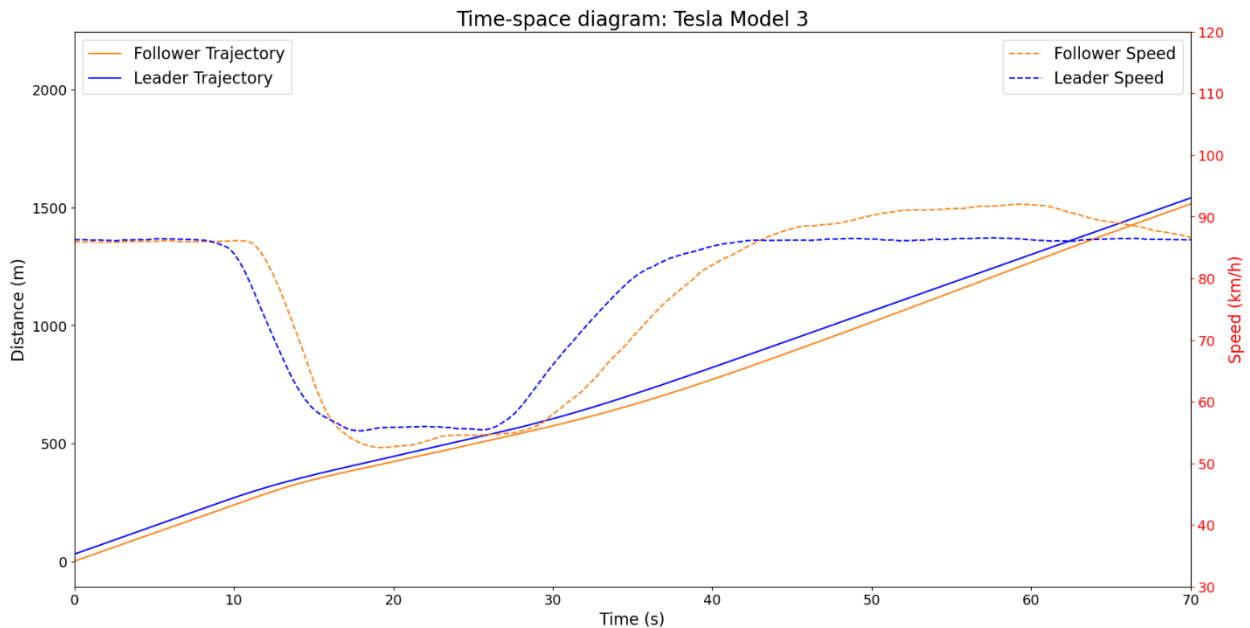
Figure 4.6. Tesla time-space diagram: 88 to 40 to 88 km/hr, short gap, +8 km/hr desired speed.

To shed light on the divergent behavior of Tesla, as compared to the other ACC-equipped EVs such as the Hyundai IONIQ 5 and Polestar 2, we delved into the distribution of accelerations and decelerations. As demonstrated in Figure 4.7, the analysis revealed that while in operation with ACC, Tesla Model 3 exhibits smoother acceleration and deceleration rates, with a higher distribution of lower acceleration rates and deceleration rates as compared to the Hyundai IONIQ 5 in the same set of experiments. This observation provides a crucial insight into the behavior of

Tesla's ACC system, suggesting that its algorithm is configured to exhibit a more sluggish behavior akin to that of ACC-equipped ICE vehicles, despite its powertrain capabilities to be more responsive.

As an added note, the same string unstable behavior can be observed when examining Tesla Model 3's trajectory in ACC mode, shown in both Figure 4.5 and Figure 4.6. The speed change was amplified relative to the speed change underwent by the leading vehicle, same as the trajectories that correspond to ACC-equipped ICE vehicles, shown in Figures 4.1(a) and 4.3(a). Of course, this has broader implications for shockwaves and queue propagation that requires further analyses.

Nevertheless, this set of experiments provides very important initial insights on the potential benefits of electric powertrain to vehicle automation going forward. The data generated from these carefully planned experiments could be used to develop and validate microscopic level models for car following, which could be used as the underlying assumption in a scaled-up simulation of macroscopic traffic. Ultimately, the true capacity benefit that EVs with automation could offer would be validated and affirmed given the appropriate models and simulation tools developed based on empirical observations.
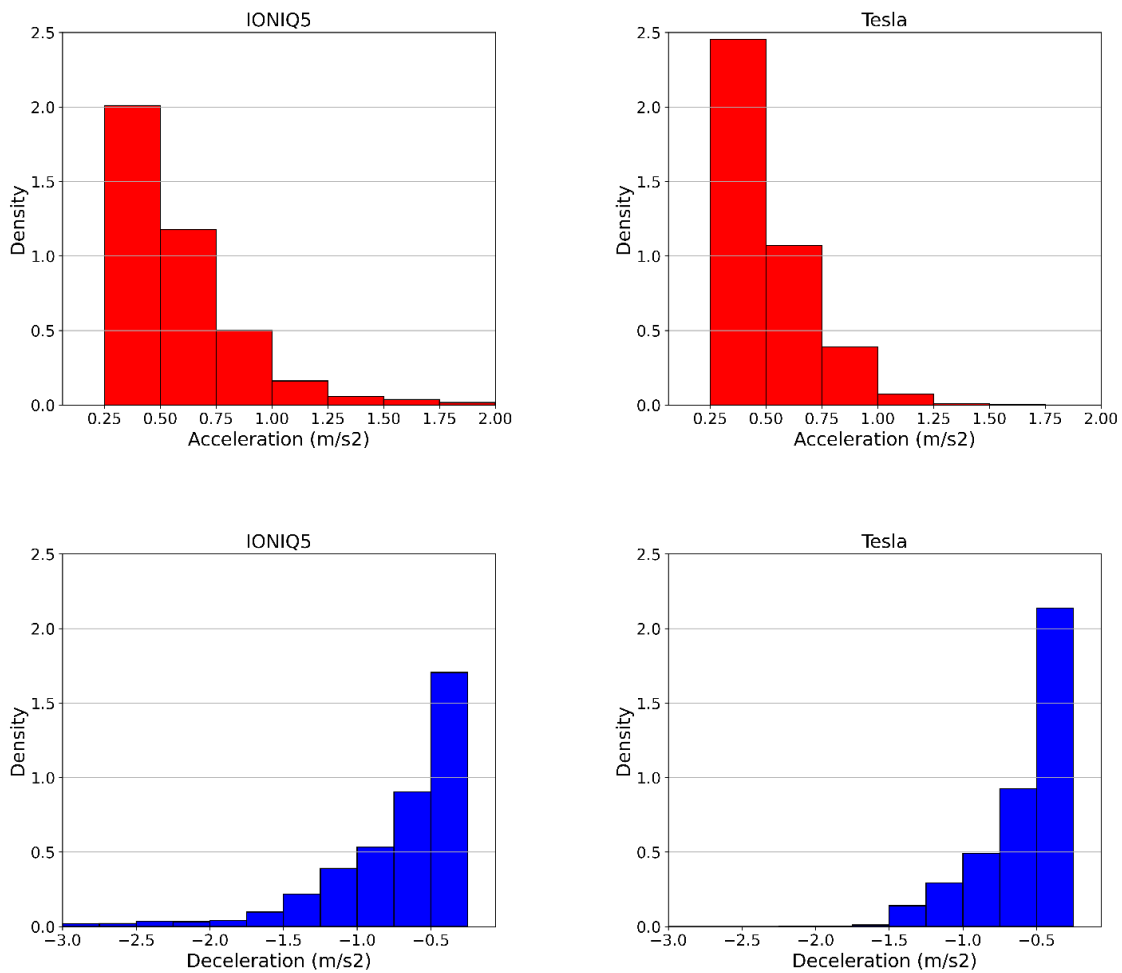
Figure 4.7. IONIQ 5 and Tesla acceleration and deceleration rates distributions.

4.2 Receiving Lane Change Car Following

4.2.1 Gap Comparison between ICE Vehicles and EVs

To conduct the gap comparison analysis under different setups, we first define the gap difference as $d_{gap,alc} - d_{gap,blc}$ for distance gap and $t_{gap,alc} - t_{gap,blc}$ for time gap. Table 4.4 compares the gaps before and after lane change between ICE vehicles and EVs. A few conclusions can be made based on the results shown in the table: first, EVs are more likely to adopt shorter gaps after lane change. In fact, almost all after lane-change gaps became shorter, indicating that the minimum gap adopted by ACC-equipped EVs are fairly short. On the contrary, for ICE vehicles, only a few scenarios showed decreases in the stabilized gap after lane change and the minimum gap adopted is much larger, and this could lead to lower capacity; second, it is worth noting that both ICE and EV began with similar gaps prior to the lane change maneuver, and this further reinforces that EVs with ACC have the potential to adopt much shorter gaps or headways after lane change to improve capacity while ICE vehicles increase gaps after lane change and further reduces capacity. All of the above are consistent with our expectation that EV with ACC could utilize its responsive braking and acceleration to adopt and maintain shorter headways and gaps, and ultimately leads to improved road capacity.

Table 4.4. Gap comparison between ICE vehicle and EV under different cut-in scenarios.

Target Lane Free-flow Speed (mph)	LC Speed (mph) /Engine	Gap Setting	Gap (distance, time) Before LC (m, s)	Gap (distance, time) After LC (m, s)	Gap Difference (distance, time) Δ (m, s)
35	25/ICE	Short	25.46 (1.64)	31.2 (2.01)	5.74 (0.37)
		Medium	33.44 (2.15)	41.41 (2.66)	7.97 (0.51)
		Long	39.11 (2.51)	47.41 (3.05)	8.3 (0.53)
	25/EV	**No Data Available due to Dangerous Driving**			
	30/ICE	Short	28.19 (1.81)	27.15 (1.75)	-1.05 (-0.07)
		Medium	38.72 (2.49)	33.88 (2.18)	-4.84 (-0.31)
		Long	41.67 (2.68)	45.16 (2.9)	3.49 (0.22)
	30/EV	**Short**	**22.62 (1.45)**	**14.88 (0.96)**	**-7.74 (-0.5)**
		Medium	**26.6 (1.71)**	**17.33 (1.11)**	**-9.27 (-0.6)**
		Long	**31.22 (2.01)**	**19.09 (1.23)**	**-12.13 (-0.78)**
		Extra Long	**38.34 (2.46)**	**26.72 (1.72)**	**-11.62 (-0.75)**
	35/ICE	Short	26.3 (1.69)	24.93 (1.6)	-1.37 (-0.09)
		Medium	36.67 (2.36)	35.11 (2.26)	-1.56 (-0.1)
		Long	46.07 (2.96)	36.23 (2.33)	-9.84 (-0.63)
	35/EV	**Short**	**26.91 (1.73)**	**18.9 (1.22)**	**-8.01 (-0.51)**
		Medium	**30.38 (1.95)**	**18.49 (1.19)**	**-11.89 (-0.76)**
		Long	**31.59 (2.03)**	**23.56 (1.51)**	**-8.03 (-0.52)**
		Extra Long	**35.14 (2.26)**	**31.91 (2.05)**	**-3.23 (-0.21)**
60	50/ICE	Short	41.81 (1.57)	34.66 (1.3)	-7.16 (-0.27)
		Medium	49.67 (1.86)	54.94 (2.06)	5.27 (0.2)
		Long	62.65 (2.35)	68.87 (2.58)	6.22 (0.23)
	50/EV	**Short**	**43.18 (1.62)**	**37.72 (1.41)**	**-5.45 (-0.2)**
		Medium	**52.99 (1.99)**	**39.86 (1.49)**	**-13.12 (-0.49)**
		Long	**62.44 (2.34)**	**50.22 (1.88)**	**-12.22 (-0.46)**
		Extra Long	**67.01 (2.51)**	**58.2 (2.18)**	**-8.81 (-0.33)**
	55/ICE	Short	39.94 (1.5)	35.29 (1.32)	-4.65 (-0.17)
		Medium	56.06 (2.1)	57.81 (2.17)	1.76 (0.07)
		Long	68.7 (2.58)	72.6 (2.72)	3.9 (0.15)
	55/EV	**Short**	**41.32 (1.55)**	**32.08 (1.2)**	**-9.24 (-0.35)**
		Medium	**52.54 (1.97)**	**40.83 (1.53)**	**-11.72 (-0.44)**
		Long	**60.99 (2.29)**	**47.45 (1.78)**	**-13.54 (-0.51)**
		Extra Long	**66.35 (2.49)**	**58.09 (2.18)**	**-8.26 (-0.31)**
	60/ICE	Short	38.59 (1.45)	33.44 (1.25)	-5.16 (-0.19)
		Medium	52.03 (1.95)	52.16 (1.96)	0.13 (0)
		Long	66.15 (2.48)	67.33 (2.52)	1.19 (0.04)
	60/EV	**Short**	**26.5 (0.99)**	**23.69 (0.89)**	**-2.8 (-0.11)**
		Medium	**42.42 (1.59)**	**38.66 (1.45)**	**-3.75 (-0.14)**
		Long	**49.15 (1.84)**	**46.02 (1.73)**	**-3.13 (-0.12)**
		Extra Long	**50.26 (1.88)**	**55.81 (2.09)**	**5.54 (0.21)**

4.2.2 Additional Observations for ICE Vehicles

After we investigated the few scenarios where ICE vehicles had a shorter stabilized gap after lane-change, a clear pattern can be found: for smaller speed difference between the target lane and lane changer (i.e., 0 or 8 km/hr) under short gap setting, the stabilized gap after lane change can become smaller than the stabilized gap before lane change, leading to a gap decrease; in contrast, for larger speed differences between the target lane and the lane changer (i.e., 16 km/hr) under medium and long gap setting, a severe gap increase could be observed after the lane change.

This pattern can be explained reasonably via the time series of speed and gap of front, middle, and rear vehicles. Figure 4.8 and 4.9 illustrate the speed and acceleration when the gap increases or decreases after lane change, respectively. Figure 4.8 shows the car following behavior if the lane-changer speed is much smaller than the target lane free-flow speed with ACC set at long gap (i.e., 56 km/hr target lane free-flow speed, 40 km/hr lane change speed). The red dotted line in the figure indicates approximately when the lane change occurred. We can easily see that the rear vehicle was traveling much faster than the middle vehicle (lane changer) during lane change. Besides, the long gap setting guarantees that the desired gap of the rear vehicle is relatively large and the tolerance for the shorter gap is relatively low. Therefore, the response of the rear vehicle to the lane change behaviors became very aggressive to ensure safety by adopting larger desired gap and following distances, which led to a large speed change (i.e., decrease of 19 km/hr) and eventually a longer gap after the lane change (i.e., ~9.5 meters increase).

Similarly, Figure 4.9 gives a representative example of how the rear vehicle would react if the lane-changer speed is similar to the target lane free-flow speed with ACC set at short gap (i.e., 96 km/hr target lane free-flow speed, 96 km/hr lane changer speed). When the lane change occurred, the speed of the rear vehicle was almost identical to that of the middle vehicle (lane changer). Short gap setting also ensures that the desired gap of the rear vehicle can be relatively small and thus the tolerance for the shorter gap is relatively high. As a result, the rear vehicle reacted gently with minor to moderate speed change (i.e., 5 km/hr) and eventually stabilized at a shorter gap after the lane change (i.e., ~11 meters decrease).

In summary, for ICE vehicles, lane change maneuvers could increase headways and potentially reduce capacity like earlier regular car following experiments, especially when the target-lane speed is larger than the lane-change speed and the ACC selected gap setting is medium or long. EVs with ACC have the potential to adopt much shorter gaps or headways after lane change to improve capacity.
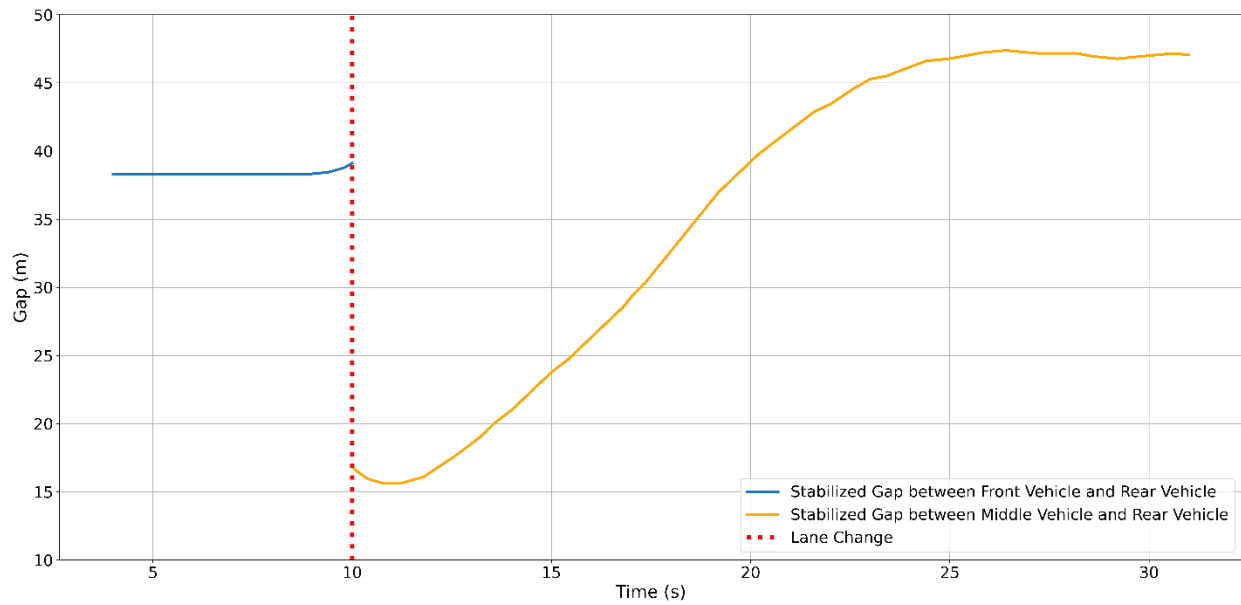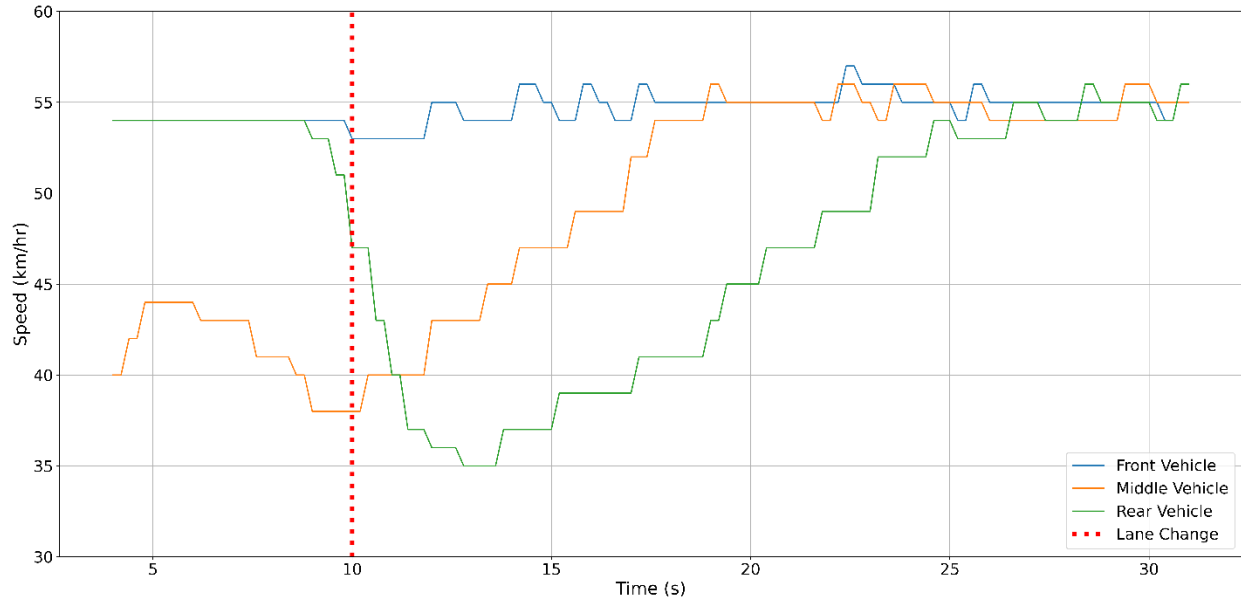
Figure 4.8. Speed and gap vs. time for 56 km/hr target lane free-flow speed, 40 km/hr lane change speed, and long gap.
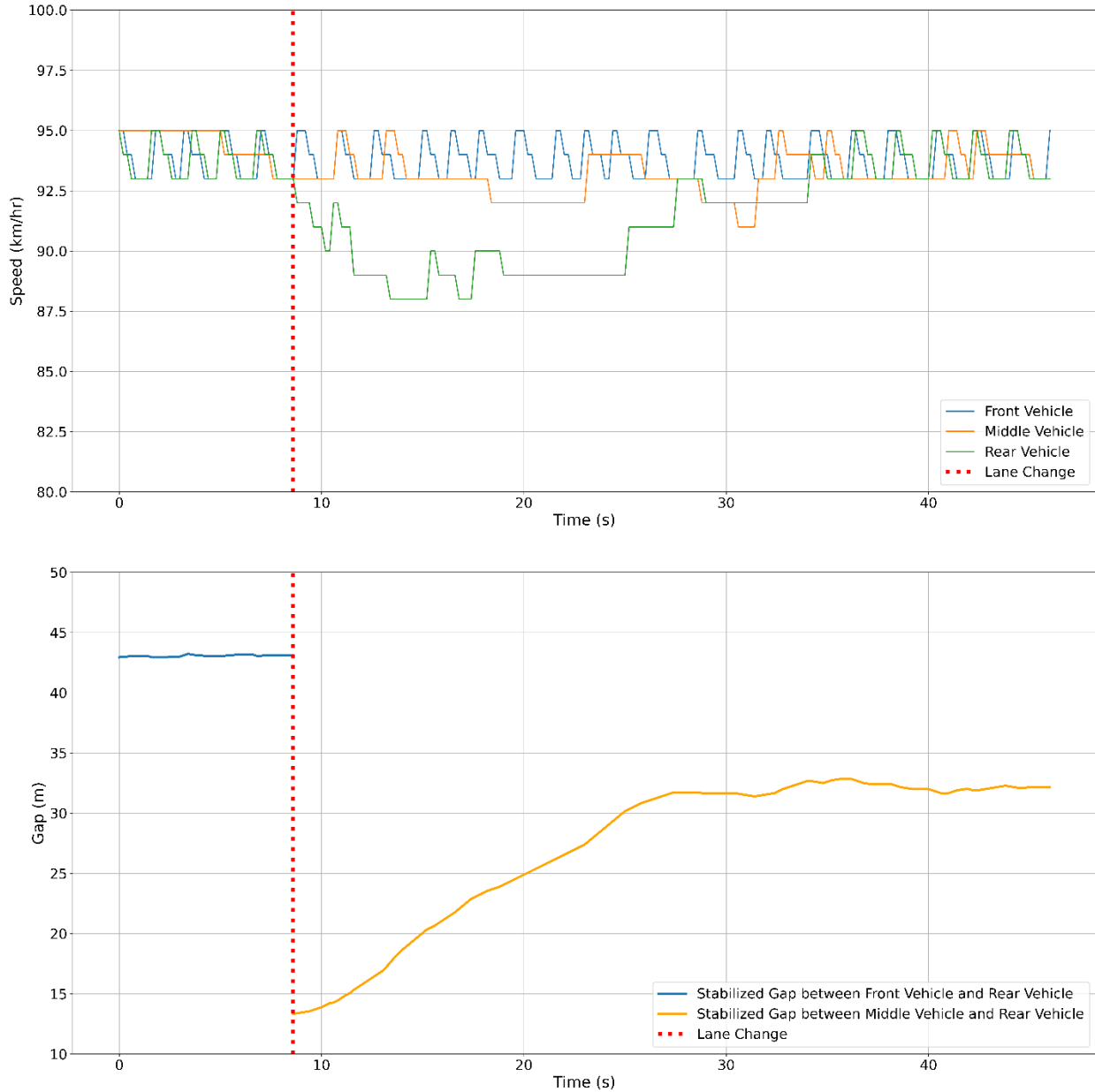
Figure 4.9. Speed and gap vs. time for 96 km/hr target lane free-flow speed, 96 km/hr lane change speed, and short gap.

Supposing a scenario where only ACC equipped vehicles are considered, and using the behavioral distribution proposed by Nowakowski, we can capture the ACC car-following behaviors under different powertrains and estimate the potential changes in discharge flow: for ICE vehicles, the discharge flow could possibly be reduced by as much as 40% for various free-flow speeds (96 km/hr, 88 km/hr, 72 km/hr, 56 km/hr) when the congested speeds approach complete stops (i.e., 0 km/hr); for EVs, the discharge flow could probably maintain at a similar level as human drivers. Of course, this initial finding needs to be verified using microscopic simulations of larger traffic streams, and the underlying car following behavior in simulations could be modeled using the trajectory data collected in this experiment, both of which will be discussed in detail in chapter 5.

CHAPTER 5: ACC CAR FOLLOWING MODEL DEVELOPMENT, CALIBRATION AND IMPLEMENTATION

After we observed the new ACC car-following characteristics for both powertrains in Chapter 4, the major challenge is how to consider the "variable gap pattern" when speed fluctuations occur, especially for the ICE vehicles. Therefore, for the model development, improvement suggestions over the conventional "constant gap" models, which force the follower to adopt a constant desired gap with the leader by accelerating much more aggressively if the vehicles were farther apart, would be brought up. The California Partners for Advanced Transportation Technology (PATH) model (also known as OVRV model), is a well-known "constant gap" model, which has been proven, calibrated and validated, and discussed in detail in several studies (Milanés and Shladover, 2014; Hao et al, 2018a; Hao et al, 2018b; Kan et al, 2019; James et al, 2019; Gunter et al, 2020; Shang et al, 2022). In this study, we called the PATH model as symmetric constant gap (SCG) model in the rest of the chapter and used it as a basis to show how a "constant gap" model would be improved in general.

5.1 Symmetric Constant Gap Model (SCG Model)

To model the full speed range ACC car-following behavior, the following model was adopted as the basis of model development (Milanés and Shladover, 2014; Liu et al, 2018b):

$$a_{sv} = k_1(d - t_{hw}v_{sv} - L) + k_2(v_l - v_{sv}) \tag{5.1}$$

where a_{sv}: acceleration recommended by the ACC controller to the subject vehicle [m/s²]; k_1: gain in positioning difference between the preceding vehicle and the subject vehicle; k_2: gain in speed difference between the preceding vehicle and the subject vehicle; d: distance gap between the subject vehicle's front bumper and the preceding vehicle's front bumper [m]; t_{hw}: desired time gap of the ACC controller (s); L: length of the preceding vehicle [m]; v_l: current speed of the preceding vehicle [m/s]; v_{sv}: current speed of the subject vehicle [m/s]. The first term $k_1(d - t_{hw}v_{sv} - L)$ is the gap regulation term intended to correct the error between current and desired gaps, while the second term $k_2(v_l - v_{sv})$ refers to the speed regulation intended to adjust the difference between the current and desired speeds.

There are two major limitations of this symmetric constant gap model: (1) known by its name, the model makes a simulated vehicle to adopt a constant desired gap with the leading vehicle by forcing the vehicle to accelerate aggressively if there are gap errors. It is especially evident when the field data suggested that gaps increased when the leading vehicle accelerates back to the free flow speed especially for a ACC-equipped ICE vehicle, and this leads to capacity drop due to the longer average headway when compared to the initial headway under steady equilibrium condition. The constant gap model cannot capture this "increasing gap" phenomenon and forces the following vehicles to follow more closely instead. This would be problematic for congested freeways and arterials with stop-and-go conditions near traffic signals since the severity of ACC's impact on capacity is underestimated; (2) the linear model parameters have only been calibrated for higher speeds (i.e., above 56 mph) but not the low speeds associated with congestion at freeway bottlenecks and arterials with signalized intersections. This could be problematic as we observed that acceleration and deceleration of ACC vehicle control algorithms (especially those equipped internal combustion engine) often behave differently across large ranges of speed, and a piecewise linear function may be considered to account for such variations while avoiding excessive computation time of complex non-linear models. Other minor issues include that the model does

not consider the reaction time or the delay of the ACC system, which could lead to an unrealistic simulation of the vehicle trajectories. Besides, the model does not consider acceleration and deceleration strength limits of different powertrains, and both of which are characteristics of commercial ACC systems meant to ensure comfort and safety. All of the above should be accounted for in the improved model.

In subsection 5.2 and 5.3, we will discuss the above limitations of the current symmetric constant gap model as well as possible solutions in more detail. Afterwards, a new ACC car-following model was developed to overcome these limitations, and different model parameters were calibrated using various scenarios tested in the field experiments. Since the ICE powertrains showed much more variable and speed dependent car following behaviors including an obvious 'increasing gap' phenomenon compared to the EV powertrains, the model for ICE vehicle is expected to be more challenging than that for EV. Therefore, we will propose the new model for ICE vehicle first, and then add supplementary contents to the EV one if necessary.

5.2 New Asymmetric Variable Gap Model (ASVG Model) for ICE vehicle

5.2.1. Asymmetric model structure to capture distinguished car following behaviors during deceleration (approach back of queue) vs. acceleration (queue discharge).

The most important car following characteristic of the commercial ACC-equipped ICE vehicles observed in the field is that the gap between the subject ACC-equipped vehicle and the leading vehicle will increase after a speed fluctuation, especially when the vehicles were traveling at the minimum gap. This has been demonstrated by prior field experiments (Lapardhaja et al, 2021) and can lead to a capacity drop. Also, this is evident in arterial conditions with stop-and-go at signals. This is caused by the delay reaction of ACC when accelerating, and the limited torque and power in ICE at lower speeds could further exacerbate this increase in gap. However, the original SCG model fails to capture this phenomenon because the SCG model includes a gap regulation term $K_1(d - t_{hw}v_{sv} - L)$ during this acceleration, which will force the subject vehicle accelerate rapidly to follow the leading vehicle and maintain a fixed distance gap with the leading vehicle after both vehicles return to the desired speed. One of the simplest ways to overcome this limitation is to remove the gap regulation term and only keep the speed regulation term $K_2(v_l - v_{sv})$ during acceleration. Figure 5.1 shows the distance gap variation pattern during a typical speed fluctuation of both original SCG model, and the modified model without gap regulation during acceleration, respectively. We can easily see that the gap increase pattern could be captured with this small modification. In summary, to capture the new observation of increasing gap, the model evolved from equation 1 to equation 5.2 shown below:

$$a_{sv}(t) = \begin{cases} k_{1\_1}(d - t_{hw}v_{sv} - L) + k_{2\_1}(v_l - v_{sv}) & \text{if } a_{sv}(t-1) \leq 0 \\ k_{2\_2}(v_l - v_{sv}) & \text{if } a_{sv}(t-1) > 0 \end{cases} \quad (5.2)$$

(a) SCG Model	**(b) ASVG Model**
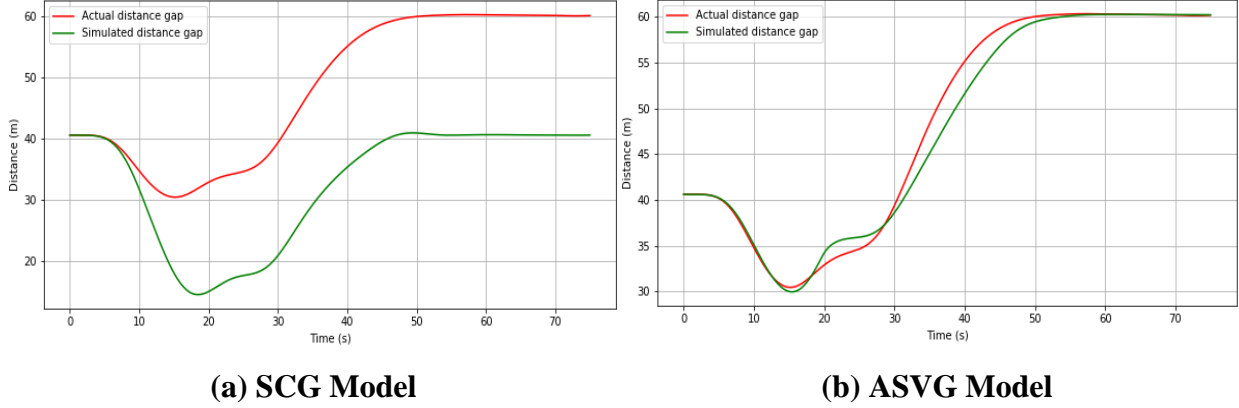
Figure 5.1. Illustration of the distance gap with different car-following models.

5.2.2. Nonlinear model structure to capture various acceleration and deceleration car following behaviors across large speed ranges (speed oscillation magnitudes).

Unlike the acceleration car following, we suggest maintaining the gap regulation term but vary the type of gap regulation (either time gap or distance gap) based on the extent of speed fluctuation. Based on the comparison with field data shown by Figure 4.2, the gap regulation term will remain the same as the term in symmetric constant gap model $K_1(d - t_{hw}v_{sv} - L)$ when the speed fluctuation range is smaller than 20 mph (e.g., 60 to 55/50/45 mph). Basically, this term ensures that the vehicle's time gap will maintain as its desired time gap after stabilization, and thus we call it "time gap regulation". When the range of fluctuation is larger than 20 mph (e.g., 60 to 35/25/15/0 mph), the gap regulation term should switch to a "distance gap regulation" $K_1'(d - t_{hw}v_{initial} - L)$, which means that the following vehicle will try to maintain a constant distance gap rather than a time gap with the preceding vehicle. Figure 5.2 compares the gap variation pattern under large and small speed fluctuations. We can easily see the difference from these plots: during the deceleration, it is the time gap that fluctuates around its desired value for the small speed fluctuation case, while it becomes the distance gap that fluctuates around a fixed value for the large speed fluctuation case. One reasonable explanation is that the following vehicle should get more powerful restrictions to ensure the safety when the speed fluctuation becomes larger, and a "distance gap regulation" can definitely provide a stronger deceleration stimulus than a "time gap regulation". Besides the special speed oscillation boundary at 20 mph, piecewise linear parameter sets at different speed levels were also added to the new model to account for the nonlinear car following behaviors across large speed ranges. In summary, to capture the alternate gap regulation under different speed fluctuations, the model evolved from equation 5.2 to equation 5.3 shown below:

$$a_{sv}(t) = \begin{cases} k_{1\_1}(d - t_{hw}v_{free} - L) + k_{2\_1}(v_l - v_{sv}) & \text{if } a_{sv}(t-1) \leq 0 \text{ and } \Delta V \geq 20 \text{ mph} \\ k_{1\_2}(d - t_{hw}v_{sv} - L) + k_{2\_2}(v_l - v_{sv}) & \text{if } a_{sv}(t-1) \leq 0 \text{ and } \Delta V < 20 \text{ mph} \\ k_{2\_3}(v_l - v_{sv}) & \text{if } a_{sv}(t-1) > 0 \end{cases} \quad (5.3)$$

where ΔV represents speed fluctuation magnitude [mile/hr] and v_{free} represents the free-flow speed [m/s].

(a) Distance gap, 60-25 mph

(b) Distance gap, 60-45 mph

(c) Time gap, 60-25 mph

(d) Time gap, 60-45 mph
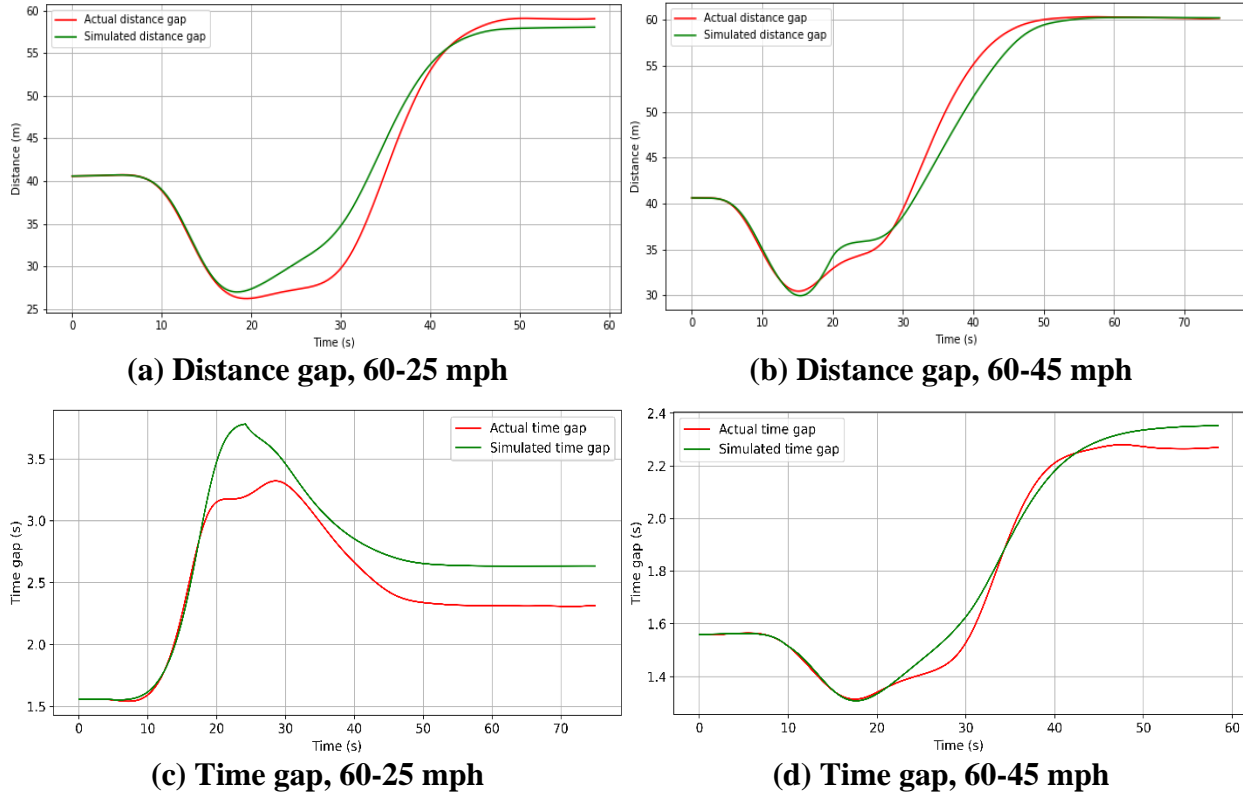
Figure 5.2. Illustration of the time gap and distance gap with different speed fluctuation magnitude.

5.2.3. Other minor adjustments

Further inspection of the field data suggests that the model also requires a smooth transition between acceleration and deceleration to capture the real-world car following behavior. Hence, a smoothing algorithm was developed as Figure 5.3 shows:

where $a'_{sv}(t)$ represents the desired acceleration at time step t if the new mode is applied.
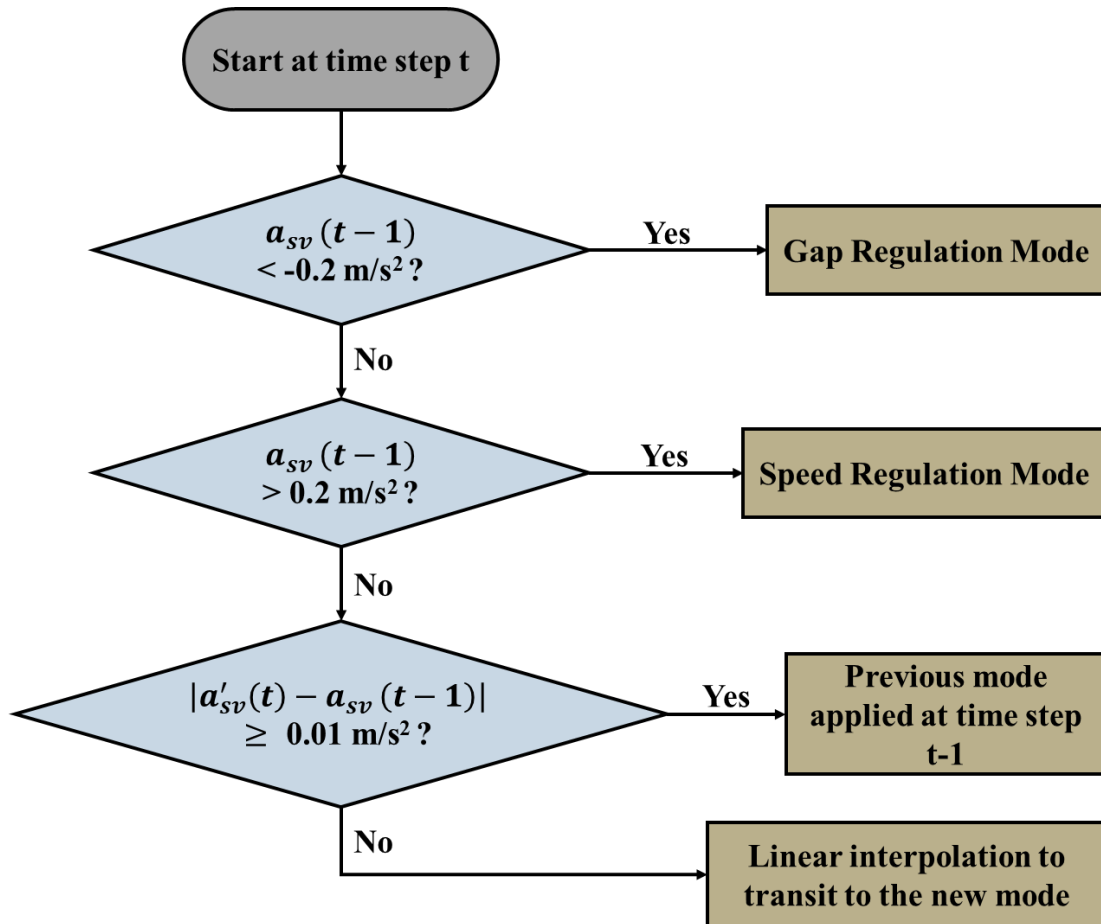
Figure 5.3. Flow chart of the smoothing algorithm to transit between acceleration and deceleration.

It is worth mentioning that the transition threshold of the acceleration should be selected carefully. On the one hand, the threshold cannot be too large. Otherwise, the model's performance will be greatly affected. On the other hand, the threshold cannot be too small, otherwise the desired acceleration difference could be too large to make the transition happen within the entire threshold. In this study, the threshold is selected as -0.2 - 0.2 m/s². Figure 5.4 shows the simulated speed profile of a typical speed fluctuation scenario before and after applying the smoothing algorithm.
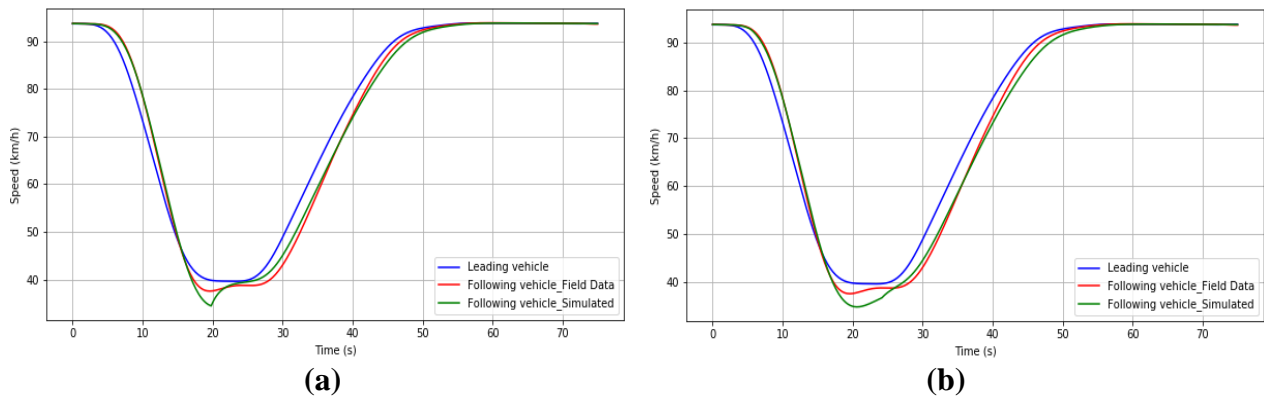
Figure 5.4. Illustration of the speed profiles with a fluctuation of 60-25 mph (a) before, and (b) after applying the smoothing algorithm.

43

Delay/reaction time τ is another important characteristic of the commercial ACC systems as demonstrated in prior field tests (Makridis et al, 2019; Chon Kan et al, 2021), which has not been considered in the original SCG model. The reaction delay is an important cause of increase in time and distance gaps after speed fluctuation. Any information obtained from the preceding vehicle should have a time delay before they can be used to estimate the desired acceleration of the subject vehicle. In detail, the distance between two vehicles' front bumper $d(t - \tau)$ applied in the gap regulation term and the preceding vehicle's speed $v_l(t - \tau)$ applied in the speed regulation term should both add a delay when calibrating the models. We expect that the longer the desired gap is set, the longer the reaction time should be. Figure 5.5 compares the delay of three gap settings under the same scenario (i.e., 60-25 mph speed fluctuation). These plots prove the importance of adding the delay as an additional parameter to the model calibration because without it, the simulated trajectories show significant discrepancy from the field data.

Finally, we should consider several constraints of the commercial ACC system under a ICE powertrain to represent the real-world traffic, including: 1) reasonable thresholds for calibration parameters K_1, K_2, τ; 2) physical constraint: maximum acceleration and deceleration limits; 3) speed constraints: speed can never go over the free-flow speed (only for the same desired speed scenarios); 4) acceleration constraints: acceleration can never be positive if the leading vehicle is decelerating at congested conditions. These constraints will be added to the optimization problem to solve the optimal parameter set with the minimal error.
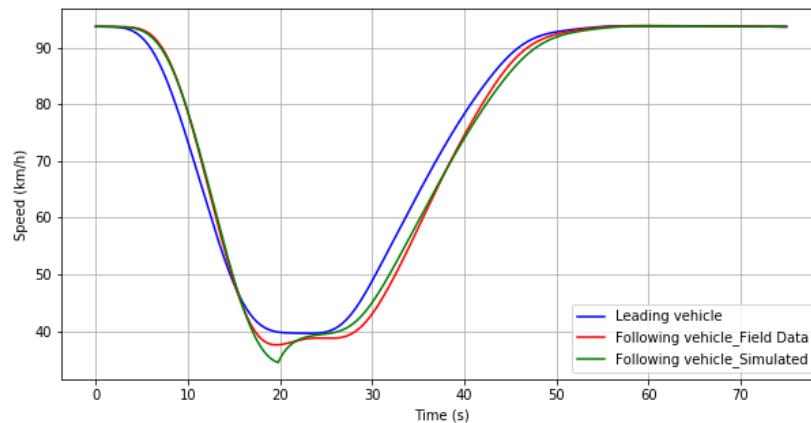
(a) short gap
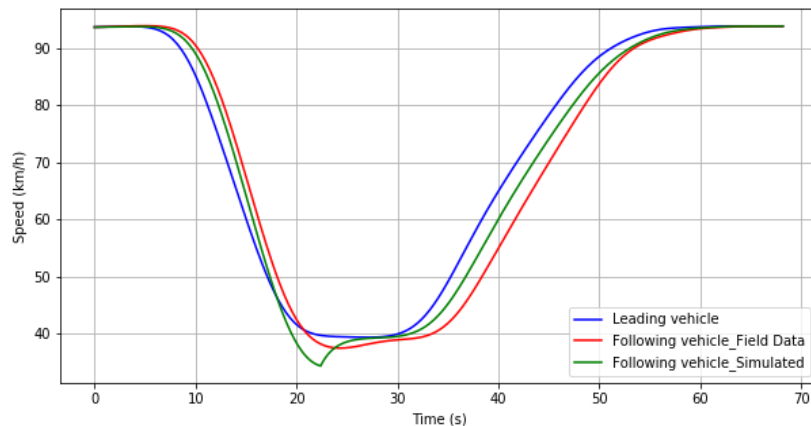
(b) medium gap
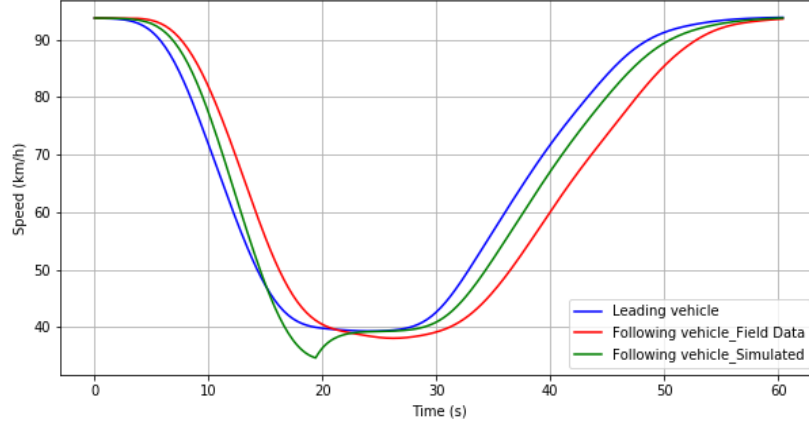
(c) long gap

Figure 5.5. Illustration of the speed profiles with a fluctuation of 60-25 mph under different gap settings.

5.3 New Asymmetric Variable Gap Model (ASVG Model) for EVs

For EV version of the new ACC car-following model, similar adjustments would be applied as ICE version did, with one exception: when adopting the piecewise linear parameter sets to capture the nonlinear car following behaviors across large speed ranges, the speed oscillation boundary at 20 mph to alternate between 'distance gap regulation' and 'time gap regulation' would be removed, as the EV car following behaviors during deceleration were much more consistent than ICE vehicle and the phenomena observed in Figure 5.2 did not exist in the EV dataset.

Besides, it is important to emphasize that the EV car following behaviors observed in the filed did not show an obvious "increasing gap" phenomenon as ICE vehicle did and appeared to have a "constant gap" pattern in the trajectory plot (i.e., Figure 4.1(a) and Figure 4.1(b)) when the follower returned to the free-flow speed. Although slight gap changes were found through the detailed numbers in the data, a further investigation would be conducted to compare the model results with field data in terms of speed errors and decide whether an asymmetric model is still necessary or the original SCG model is sufficient.

To summarize, the new ACC car-following model that will be developed and calibrated in this study is presented as equation 5.4 for ICE vehicles and equation 5.5 for EVs. This model will be called asymmetric variable gap model (ASVG) in the rest of the paper.

$$
a_{sv}(t) = \begin{cases} K_{1\_1}\big(d(t-\tau) - t_{hw}v_{free} - L\big) + K_{2\_1}(v_l(t-\tau) - v_{sv}) \\ \quad if\ a_{sv}(t-1) \le 0\ and\ \Delta V \ge 20\ mph \\ K_{1\_2}(d(t-\tau) - t_{hw}v_{sv} - L) + K_{2\_2}(v_l(t-\tau) - v_{sv}) \\ \quad if\ a_{sv}(t-1) \le 0\ and\ \Delta V < 20\ mph \\ K_{2\_3}\big(v_l(t-\tau) - v_{sv}(t)\big) \\ \quad if\ a_{sv}(t-1) > 0 \end{cases} \tag{5.4}
$$

$$
a_{sv}(t) = \begin{cases} K_{1\_2}(d(t-\tau) - t_{hw}v_{sv} - L) + K_{2\_2}(v_l(t-\tau) - v_{sv}) \\ \quad if\ a_{sv}(t-1) \le 0 \\ K_{2\_3}\big(v_l(t-\tau) - v_{sv}(t)\big) \\ \quad if\ a_{sv}(t-1) > 0 \end{cases} \tag{5.5}
$$

45

5.4 Model Calibration

Once we determine the model structure, the next step is to solve a proper optimization problem to obtain the parameter set with the best performance. Typically, the objective should be to minimize the speed error between the simulation and the observation data. Therefore, the optimization problem in our study is presented as follows:

Objective:

$$\text{Minimize } \text{RMSE}\,(v_{simulated}, v_{observed})$$

Constraints:

for ICE vehicles:

$$a_{sv}(t) = \begin{cases} K_{1\_1}\big(d(t-\tau) - t_{hw}v_{free} - L\big) + K_{2\_1}(v_l(t-\tau) - v_{sv}) \\ \quad if \ a_{sv}(t-1) \leq 0 \ and \ \Delta V \geq 20 \ mph \\ K_{1\_2}(d(t-\tau) - t_{hw}v_{sv} - L) + K_{2\_2}(v_l(t-\tau) - v_{sv}) \\ \quad if \ a_{sv}(t-1) \leq 0 \ and \ \Delta V < 20 \ mph \\ K_{2\_3}\big(v_l(t-\tau) - v_{sv}(t)\big) \\ \quad if \ a_{sv}(t-1) > 0 \end{cases} ;$$

$$v_{sv}(t) = v_{sv}(t - \Delta t) + a_{sv}(t)\Delta t;$$

$$d(t) = d(t - \Delta t) + (v_l(t) - v_{sv}(t))\Delta t;$$

$$0 \leq K_{1\_1}, K_{1\_2} \leq 1, \text{unit: s}^{-2};$$

$$0 \leq K_{2\_1}, K_{2\_2}, K_{2\_3} \leq 1, \text{unit: s}^{-1};$$

$$0 \leq \tau \leq 4.0, \text{unit: seconds};$$

$$-1.75 \leq a_{sv} <=1.05, \text{unit: m/s}^2;$$

$$v_{sv} \leq v_{free};$$

for EVs:

$$a_{sv}(t) = \begin{cases} K_{1\_2}(d(t-\tau) - t_{hw}v_{sv} - L) + K_{2\_2}(v_l(t-\tau) - v_{sv}) \\ \quad if \ a_{sv}(t-1) \leq 0 \\ K_{2\_3}\big(v_l(t-\tau) - v_{sv}(t)\big) \\ \quad if \ a_{sv}(t-1) > 0 \end{cases} ;$$

$$v_{sv}(t) = v_{sv}(t - \Delta t) + a_{sv}(t)\Delta t;$$

$$d(t) = d(t - \Delta t) + (v_l(t) - v_{sv}(t))\Delta t;$$

$$0 \leq K_{1\_2} \leq 1, \text{unit: s}^{-2};$$

$$0 \leq K_{2\_2}, K_{2\_3} \leq 1, \text{unit: s}^{-1};$$

$$0 \leq \tau \leq 4.0, \text{unit: seconds};$$

$$-3.0 \leq a_{sv} <=2.0, \text{unit: m/s}^2;$$

$$v_{sv} \leq v_{free};$$

where $v_{simulated}$: simulated speed profiles [m/s]; $v_{observed}$: observed speed profiles [m/s]; $d_{simulated}$: simulated distance gap profiles [m]; $d_{observed}$: observed distance gap profiles [m]; v_{free}: free-flow speed [m/s]; ΔV: speed fluctuation magnitude [mile/hr].

The threshold for each constraint was determined based on field observations and some simple simulation trials of the collected data. The acceleration and deceleration limits of EVs under normal conditions are much higher than those of ICE vehicles. As a results, we can see that the boundaries of deceleration and acceleration for ICE vehicles is -1.75 m/s^2 and 1.05 m/s^2, while the boundaries for EVs are -3.0 m/s^2 and 2.0 m/s^2.

Two classic constant gap models, shown as equation 5.6 and equation 5.7, have also been recalibrated so that a speed error comparison can be made across the two models and the new ASVG model for both ICE vehicle and EV. The model with smaller root mean squared errors (RMSEs) will be eventually chosen and implemented in microscopic simulation.

(1) Symmetric constant gap model (SCG):

$$a_{sv}(t) = K_1(d(t-\tau) - t_{hw}v_{sv} - L) + K_2(v_l(t-\tau) - v_{sv}) \tag{5.6}$$

(2) Asymmetric constant gap model (ASCG):

$$a_{sv}(t) = \begin{cases} K_{1\_1}(d(t-\tau) - t_{hw}v_{sv} - L) + K_{2\_1}(v_l(t-\tau) - v_{sv}) \\ \qquad\qquad if\ a_{sv}(t-1) \le 0 \\ K_{1\_2}(d(t-\tau) - t_{hw}v_{sv} - L) + K_{2\_2}(v_l(t-\tau) - v_{sv}) \\ \qquad\qquad if\ a_{sv}(t-1) > 0 \end{cases} \tag{5.7}$$

Given the fact that we would mainly test the model performance in the microscopic simulation on freeway, the numerical analysis for ICE vehicle and EV under 60 mph free-flow speed were listed in Table 5.1 and Table 5.2, respectively. The rest of the results under relatively low free-flow speeds were included in Appendix A, shown in Table A.1 and Table A.2. The best model with the smallest speed error is marked in bold. We can clearly see from Table 5.1 that the new ASVG model for ICE vehicle outperforms the two constant gap models under most of the scenarios. The RMSE of the ASVG model ranges from 0.2 to 0.5, indicating an overall good fitness to the field data. The SCG model is much worse than the other two, proving the distinguished car-following behaviors between acceleration and deceleration for ICE vehicles. Besides, the ASCG model performs slightly worse than the new model under the large speed oscillation (i.e., > 10 mph). This model also has very small positioning difference gain K_{1_2} (i.e., ~1e-3) during acceleration, showing the necessity of removing the gap regulation term to capture the increasing gap after the speed fluctuation. Last but not least, both SCG and ASCG models can perform a bit better than the ASVG model when the free-flow speed is 60 mph and the speed fluctuation is less than 10 mph, proving the traditional models' capability of capturing more consistent car-following behaviors under free-flow condition with little disturbance on freeway.

Interestingly, Table 5.2 shows an opposite trend in terms of RMSE performance across the three models. The SCG model is better than the other two asymmetric models, indicating the consistent car-following behaviors between acceleration and deceleration for EVs. The new ASVG model still performs well with RMSE ranging from 0.3 and 0.5, while the ASCG model performs the worst in most cases, since the model can neither capture the consistent behaviors or the increasing gap after speed fluctuation. Those results are consistent with the field observations that EVs can provide more consistent response to the leading vehicle and "increasing gap" phenomenon after speed fluctuation exists but is not as obvious as ICE vehicles. As a result,

removing the gap regulation term during acceleration for EVs won't bring as much benefit as for ICE vehicles.

Ultimately, we will adopt the ASVG model to capture the increasing gap or variable headway for ICE vehicles, and the SCG model to capture more consistent car following behaviors for EVs. Both models have piecewise linear parameters under different speed levels and gap settings, along with proper smoothing algorithms to transfer among those various scenarios.

Table 5.1. RMSE comparison among SCG model, ASCG model, and ASVG model: ICE vehicle, 60 mph (96 km/hr) free-flow speed.

Free-flow speed	Congested Speed	Gap Setting	SCG Model	ASCG Model	ASVG Model
60	0	L	0.806	0.46	**0.337**
	0	M	0.792	0.479	**0.402**
	0	S	0.818	0.661	**0.488**
	15	L	0.807	0.413	**0.357**
	15	M	0.766	0.481	**0.411**
	15	S	0.824	0.697	**0.482**
	25	L	0.792	0.375	**0.348**
	25	M	0.757	**0.441**	0.452
	25	S	0.722	0.596	**0.485**
	35	L	0.877	0.433	**0.344**
	35	M	0.873	0.521	**0.384**
	35	S	0.602	0.416	**0.349**
	45	L	0.691	0.333	**0.29**
	45	M	0.627	0.337	**0.299**
	45	S	0.371	**0.3**	0.33
	50	L	0.391	**0.223**	0.245
	50	M	0.465	**0.278**	0.325
	50	S	0.321	**0.207**	0.209
	55	L	0.275	**0.22**	0.311
	55	M	0.231	**0.187**	0.228
	55	S	0.168	**0.139**	0.23

Table 5.2. RMSE comparison among SCG model, ASCG model, and ASVG model: EV, 60 mph (96 km/hr) free-flow speed.

Free-flow speed	Congested Speed	Gap Setting	SCG Model	ASCG Model	ASVG Model
60	0	X	**0.268**	0.468	0.314
	0	L	**0.318**	0.462	0.345
	0	M	**0.318**	0.424	0.387
	0	S	**0.269**	0.389	0.39
	15	X	**0.269**	0.573	0.344
	15	L	**0.313**	0.516	0.335
	15	M	**0.313**	0.563	0.373
	15	S	**0.27**	0.451	0.368
	25	X	**0.272**	0.81	0.331
	25	L	**0.318**	0.659	0.329
	25	M	**0.317**	0.576	0.357
	25	S	**0.271**	0.532	0.411
	35	X	**0.335**	0.525	0.359
	35	L	0.393	0.764	**0.359**
	35	M	**0.401**	0.696	0.411
	35	S	**0.341**	0.595	0.48
	45	X	**0.32**	0.752	0.327
	45	L	0.39	0.644	**0.343**
	45	M	0.403	0.547	**0.401**
	45	S	**0.342**	0.662	0.472

The calibrated parameters of 60 mph free-flow speed for ICE vehicle's ASVG model and EV's SCG model were included in Table 5.3 and Table 5.4, respectively. Similarly, Table A.3 and Table A.4 in Appendix A showed model parameters under other free-flow speeds. For the new ASVG model, Model Version 1 represents "distance gap regulation", while Model Version 2 represents "time gap regulation", during the deceleration. The results were rounded to three decimal places. Based on the results in Table 5.3, some patterns for the new ICE car-following model could be found and reasonably explained:

1. When calibrating the ASVG models, we tested both model versions for all the scenarios, and the results confirm the phenomenon observed in Figure 5.2 that when the speed fluctuation is larger than 20 mph, a "distance gap regulation" should be applied during deceleration, and when the speed fluctuation is smaller than 20 mph, a "time gap regulation" should be applied. 20 mph were chosen as the boundary since different gap variation patterns were observed between 15 mph and 25 mph speed oscillation magnitude.

2. In general, shorter gap setting and larger speed fluctuation lead to larger control gains that correspond to the speed difference and the position difference with the preceding vehicle and vice versa. This pattern is reasonable and expected because the ACC controller reacts more aggressively to ensure safety.

3. For the high-speed cases with larger speed ranges, the model relies more heavily on speed regulation term K_{2_1} and K_{2_2} when the long gap is selected, while it relies more heavily on gap regulation term K_{1_1} and K_{1_2} when the gap setting is short. The potential explanation could

be that it would be more critical to maintain a safe gap between vehicles when the initial gap has already been small enough, while it becomes more important to consider the comfort when initial gap is large, which makes the speed regulation more suitable to control the vehicle.

4. For the low-speed cases where the maximum speed is low and speed fluctuations are relatively smaller, the model does not depend on the gap regulation unless the vehicles made complete stops. The results are consistent with the second pattern we summarized above. We need to point out that having only speed regulation will make the model simpler, but the model will also be more sensitive to the data collected. This means that any small changes to the data will lead to a relatively large shift in the model coefficients, compared to the model with both speed and gap regulation. That is another important reason why we do not apply only speed regulation in the model.

5. The delay fluctuates between 0 and 2.0 seconds. It does not impact on the errors within a reasonable threshold, nor does it directly relate to the initial free-flow speed, speed fluctuation magnitude, and gap settings based on the results shown in Table 5.1. Further investigations are required to get a better understanding of how the delay/reaction time works in the commercial ACC systems.

On the other hand, due to the more consistent behaviors at acceleration/deceleration of EVs over ICE vehicles, a more simplified model parameter set was considered. As shown in Table 5.4, the delay term could be pre-determined before the calibration as most scenarios showed a similar system reaction on average within a small range around 0.4 seconds. One interesting finding is that positioning difference gain K_1 is close to zero (i.e., <1e-3) under certain circumstances when the congested speed is reaching 15 mph or a complete stop, and the gap setting is long or extra-long. This phenomenon indicated that the gap variation could not be ignored while the collision risks were relatively low under those large speed fluctuations and long gap settings, as a result, the gap regulation term in those cases played a minor role in determining the EV car-following behaviors. Besides, similar as ICE car following model, both positioning difference gain K_1 and speed difference gain K_2 of EV model had an increasing trend over shorter gap setting and larger speed fluctuation.

The newly calibrated parameters were applied to both the ASVG model for ICE vehicles and SCG model for EVs and simulated the vehicle's trajectories. Figure 5.6 and Figure 5.7 showed the comparison of observed and simulated speed profiles and distance gap using the new ASVG model under some typical scenarios, respectively. In general, the new model can simulate the trajectories very well under a wide variety of speed fluctuations and gap settings for both freeways and arterials. The model's capability has been greatly expanded to realistically model freeway and arterials. Besides, from Figure 5.7, we can easily see that the gap growth is positively related to the speed fluctuation magnitude: the larger the speed fluctuation magnitude is, the larger gap increasing we can observe. Moreover, it is worth noting that there are a few cases where the new model does not fit the trajectories very well, including the first fourth cycles shown in Figure 5.6 (a) and Figure 5.7 (a). The reason is because some experiments were not conducted in a perfectly controlled environment due to some human mistakes or test site constraints. The speed profiles indicate that they do not have a complete stabilization process where both vehicles should return to free-flow speed after the minimal gap is achieved.

Lastly, additional efforts would be undertaken to provide a comprehensive model with a single set of parameters that captures all of the traffic conditions that ACC vehicles could

encounter, instead of separate parameter sets for each of the representative scenarios tested in the field. Those efforts would be discussed in subsection 5.7 before the simulations could begin.

Table 5.3. Calibrated parameters of ICE vehicle under 60 mph (96 km/hr) free-flow speed.

Free-flow Speed (mph)	Congested Speed (mph)	Gap Setting			Model Version
		Short	**Medium**	**Long**	
60	55	$\tau = 0.0$ $K_{1\_2} = 0.030$ $K_{2\_2} = 0.202$ $K_{2\_3} = 0.167$	$\tau = 0.2$ $K_{1\_2} = 0.019$ $K_{2\_2} = 0.113$ $K_{2\_3} = 0.145$	$\tau = 0.4$ $K_{1\_2} = 0.015$ $K_{2\_2} = 0.050$ $K_{2\_3} = 0.129$	Version 2
	50	$\tau = 0.0$ $K_{1\_2} = 0.031$ $K_{2\_2} = 0.318$ $K_{2\_3} = 0.211$	$\tau = 1.0$ $K_{1\_2} = 0.010$ $K_{2\_2} = 0.182$ $K_{2\_3} = 0.169$	$\tau = 2.0$ $K_{1\_2} = 0.007$ $K_{2\_2} = 0.084$ $K_{2\_3} = 0.197$	Version 2
	45	$\tau = 0.0$ $K_{1\_2} = 0.001$ $K_{2\_2} = 0.399$ $K_{2\_3} = 0.260$	$\tau = 0.8$ $K_{1\_2} = 0.016$ $K_{2\_2} = 0.350$ $K_{2\_3} = 0.221$	$\tau = 0.2$ $K_{1\_2} = 0.000$ $K_{2\_2} = 0.388$ $K_{2\_3} = 0.156$	Version 2
	35	$\tau = 0.0$ $K_{1\_1} = 0.048$ $K_{2\_1} = 0.525$ $K_{2\_3} = 0.359$	$\tau = 0.0$ $K_{1\_1} = 0.016$ $K_{2\_1} = 0.469$ $K_{2\_3} = 0.217$	$\tau = 0.0$ $K_{1\_1} = 0.008$ $K_{2\_1} = 0.392$ $K_{2\_3} = 0.183$	Version 1
	25	$\tau = 0.0$ $K_{1\_1} = 0.059$ $K_{2\_1} = 0.443$ $K_{2\_3} = 0.419$	$\tau = 0.0$ $K_{1\_1} = 0.030$ $K_{2\_1} = 0.438$ $K_{2\_3} = 0.296$	$\tau = 0.0$ $K_{1\_1} = 0.011$ $K_{2\_1} = 0.418$ $K_{2\_3} = 0.228$	Version 1
	15	$\tau = 0.0$ $K_{1\_1} = 0.000$ $K_{2\_1} = 0.843$ $K_{2\_3} = 0.498$	$\tau = 0.0$ $K_{1\_1} = 0.005$ $K_{2\_1} = 0.717$ $K_{2\_3} = 0.335$	$\tau = 0.0$ $K_{1\_1} = 0.004$ $K_{2\_1} = 0.564$ $K_{2\_3} = 0.258$	Version 1
	0	$\tau = 0.0$ $K_{1\_1} = 0.009$ $K_{2\_1} = 0.873$ $K_{2\_3} = 0.426$	$\tau = 0.0$ $K_{1\_1} = 0.016$ $K_{2\_1} = 0.765$ $K_{2\_3} = 0.321$	$\tau = 0.0$ $K_{1\_1} = 0.011$ $K_{2\_1} = 0.566$ $K_{2\_3} = 0.265$	Version 1

Table 5.4. Calibrated parameters of EV under 60 mph (96 km/hr) free-flow speed.

Free-flow Speed (mph)	Congested Speed (mph)	Gap Setting			
		Short	Medium	Long	Extra-Long
60	45	$K_1 = 0.046$ $K_2 = 0.442$	$K_1 = 0.046$ $K_2 = 0.476$	$K_1 = 0.033$ $K_2 = 0.466$	$K_1 = 0.021$ $K_2 = 0.425$
	35	$K_1 = 0.06$ $K_2 = 0.434$	$K_1 = 0.042$ $K_2 = 0.561$	$K_1 = 0.028$ $K_2 = 0.535$	$K_1 = 0.011$ $K_2 = 0.497$
	25	$K_1 = 0.046$ $K_2 = 0.668$	$K_1 = 0.028$ $K_2 = 0.735$	$K_1 = 0.009$ $K_2 = 0.676$	$K_1 = 0$ $K_2 = 0.551$
	15	$K_1 = 0.026$ $K_2 = 0.831$	$K_1 = 0.023$ $K_2 = 0.746$	$K_1 = 0.004$ $K_2 = 0.701$	$K_1 = 0$ $K_2 = 0.569$
	0	$K_1 = 0.02$ $K_2 = 0.926$	$K_1 = 0.005$ $K_2 = 0.935$	$K_1 = 0$ $K_2 = 0.797$	$K_1 = 0$ $K_2 = 0.583$
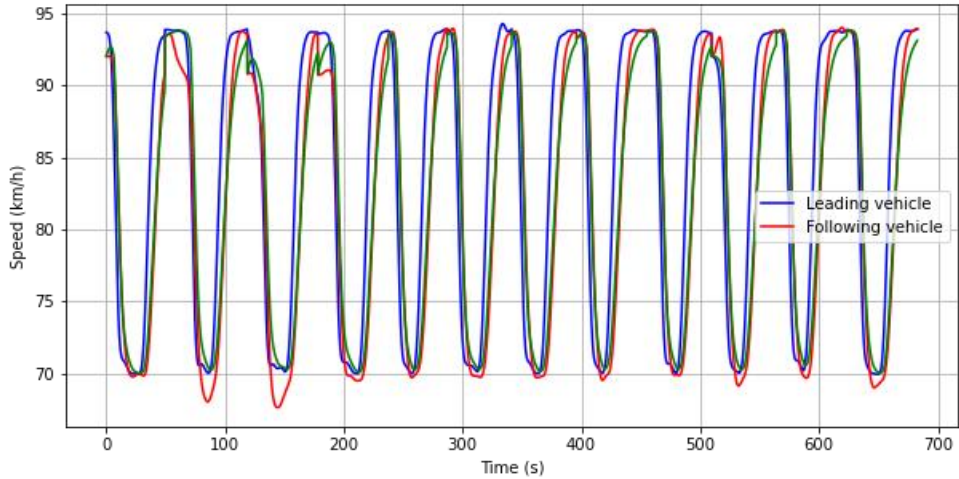
(a) 60-45 mph, long gap
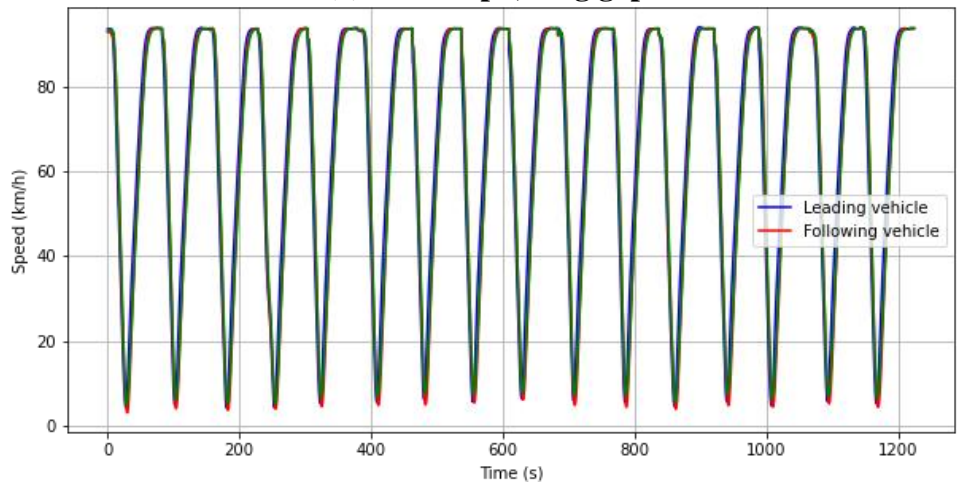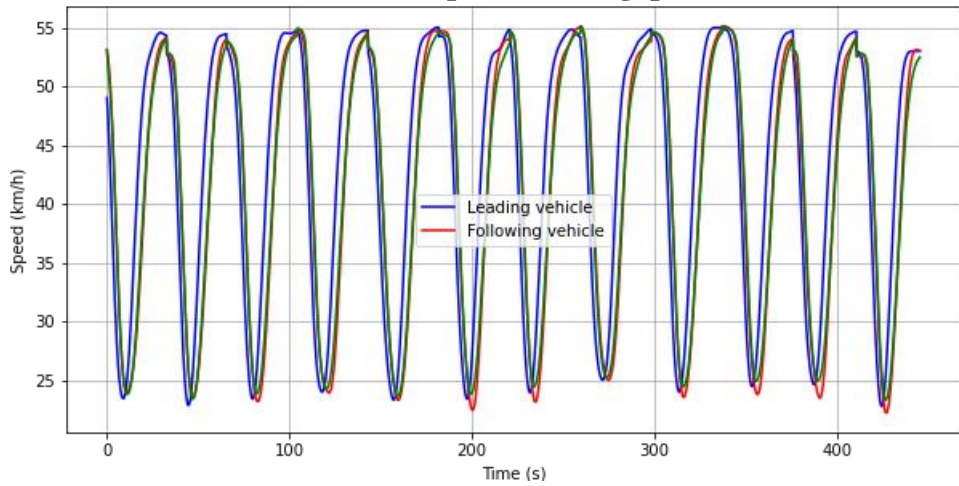
(b) 60-0 mph, medium gap

(c) 35-15 mph, medium gap
Figure 5.6. Illustration of the simulated speed for some typical bottleneck scenarios.
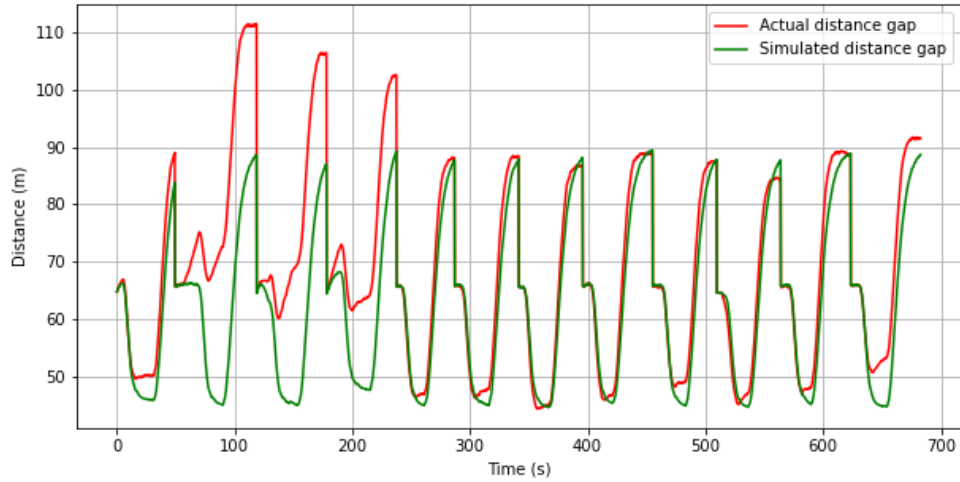
(a) 60-45 mph, long gap
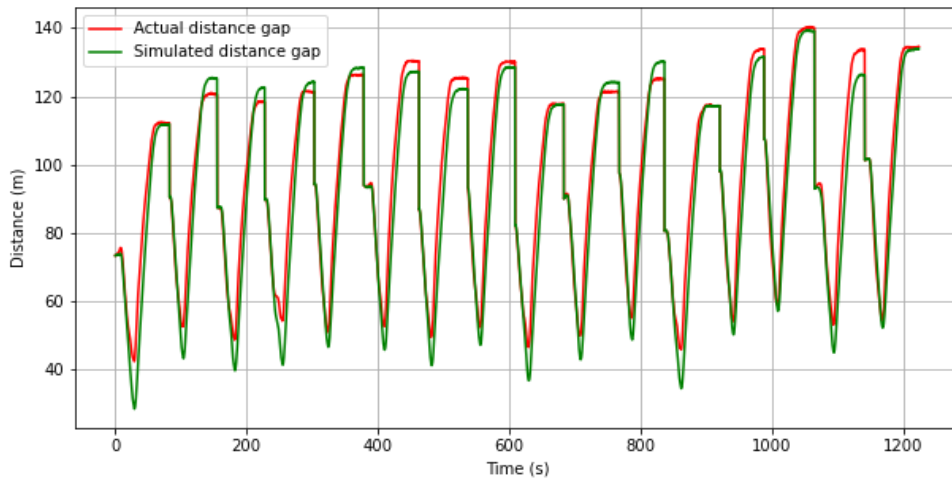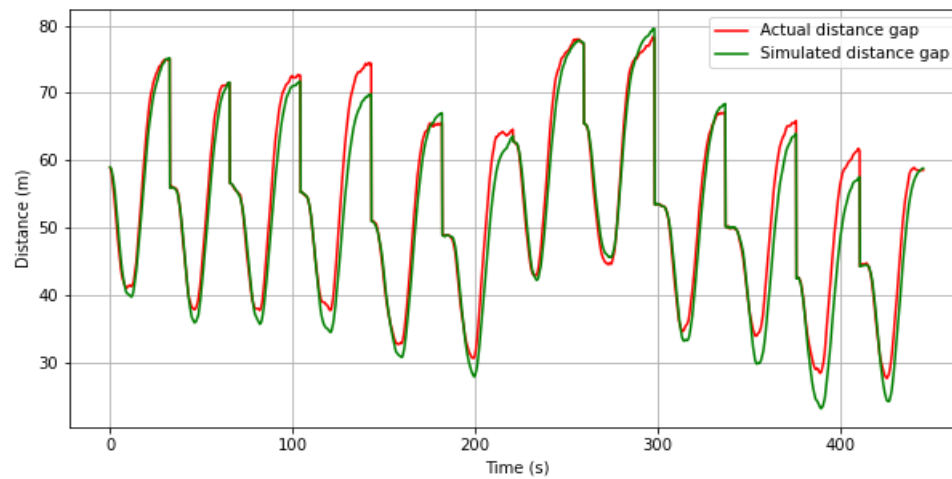
(b) 60-0 mph, medium gap

(c) 35-15 mph, medium gap

Figure 5.7. Illustration of the simulated gap for some typical bottleneck scenarios.

5.5 Car-following Behaviors under Heterogeneous Desired Speed

As indicated by Figure 3.8, in the regular 2-vehicle longitudinal car-following experiments, there exists a period when the following ACC-equipped ICE vehicle accelerates up to a speed higher than the stable free-flow speed (desired speed of leading or front vehicle) to "catch up" with the leading vehicle after both vehicles return to the free-flow speed. This phenomenon is called "catch-up" process, and it leads to the gap between two vehicles decreasing to a similar level as the stabilized gap prior to the speed fluctuation. The "catch-up" process for ACC-equipped ICE vehicle will be modeled separately since the new ASVG model developed in subsection 5.4 cannot capture the recover gap during this process. Note that ACC-equipped EVs do not have such a "catch-up" behavior due to the instantaneous torque and strong acceleration power, and therefore, the special model developed in this subsection only suits ICE vehicles.

Two reasonable assumptions have been made to simplify the model development: 1) gap settings will affect the car-following behaviors throughout the entire experiment, since they determine the most important characteristics in the car following, the desired gap; 2) the lowest speed reached during the speed fluctuation stage (i.e., congested speed) will not affect the catch-up car-following behaviors, since their influence should be fully reflected by the increasing gap when both vehicles first come back to the free-flow speed.

The SCG model, shown by equation 5.6, is preferred to capture the catch-up car-following behaviors as this model has proved its capability to capture the overshooting characteristics of ACC-controlled vehicles. All the calibrated parameter sets under different gap setting and stable speeds are listed in Table 5.5. Based on the results, some patterns could be found and reasonably explained:

1. For short gap, both k_1 and k_2 fall into a limited range. The ratios between the minimum and maximum k_1 and k_2 are 0.76 and 0.64, respectively, indicating that there exists similar catch-up behaviors across different stable (free-flow) speeds.

2. For medium gap, there is a large difference in k_1 at 35 and 45 mph stable speeds. The ratio between the two k_1 values is 0.35, indicating that significant difference exists between free-flow (stable) speeds of 35 and 45 mph with medium gap. However, both k_1 and k_2 show strong similarity at 45 and 55 mph stable speeds. The ratios between the two k_1s and k_2s are 0.81 and 0.96, respectively.

3. For the long gap, similar conclusions can be drawn as the medium gap. There is a large difference in k_1 at 35 and 45 mph stable speeds, and the ratio between the two k_1 values is 0.25, while both k_1 and k_2 show strong similarity at 45 and 55 mph stable speeds, with a ratio of 0.81 and 0.80 respectively.

4. The delay τ fluctuates between 0 and 3.8 seconds under different scenarios. It does not impact on the speed errors, nor does it directly relate to the stable speed and gap settings based on the results shown in Table 5.5. This is consistent with the delay term of the ASVG model developed in subsection 5.4. Therefore, the delay term does not necessarily reflect the true reaction time of the ACC-controlled vehicle. This will require further refinement in future work.

Using the newly calibrated parameters and the improved model, trajectories of the catch-up process were simulated, as shown in Figure 5.8 and Figure 5.9 (only the catch-up process to enlarge the details, not the entire experiment). Comparison of the observed and simulated speed

profiles demonstrate that the new model can simulate the catch-up car-following behaviors very well under a wide variety stable speeds and gap settings. Figure 5.9 shows that the simulated gap can be perfectly fitted to the observed gap during the whole catch-up process, which further confirms the strong capability of the SCG model to regulate the gap to its desired level.

Lastly, additional efforts could be undertaken to integrate this enhance model with the "cat-up" process into a comprehensive and adaptive ACC modeling framework that switches modes and model structures depending on the presence of heterogeneity in ACC desired set speeds.

Table 5.5 Summary of calibrated parameters in the catch-up car-following model.

Gap Setting	Stable Speed (mph)	Gain in positioning difference K_1 (s^{-2})	Gain in speed difference K_2 (s^{-1})	Delay τ (s)
Short	35	0.019	0.080	2.0
	45	0.025	0.125	0.4
	55	0.023	0.121	1.0
Medium	35	0.006	0.037	3.8
	45	0.021	0.048	0.2
	55	0.017	0.050	0.0
Long	35	0.004	0.036	3.8
	45	0.016	0.095	0.6
	55	0.013	0.076	0.0
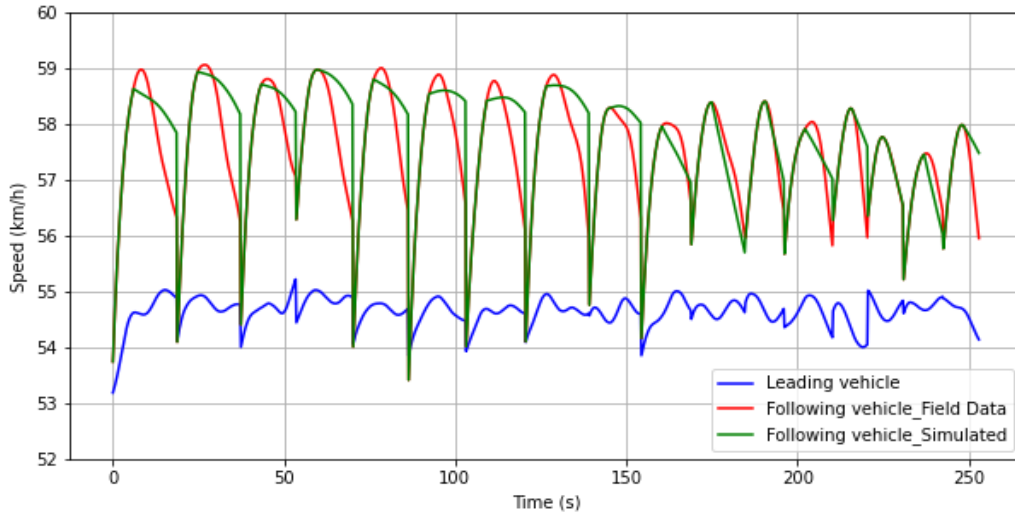
(a) 35 mph (56 kph), long gap
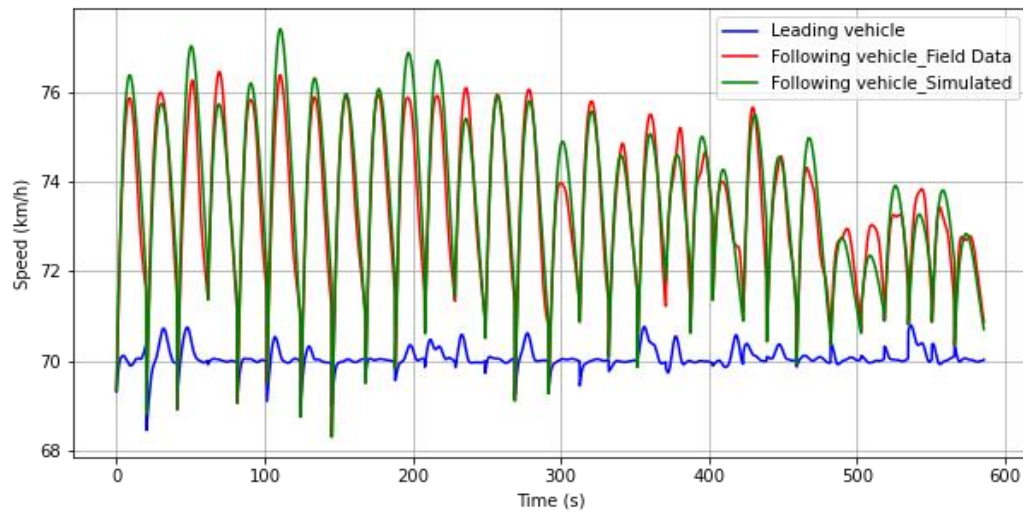
(b) 45 mph (72 kph), medium gap
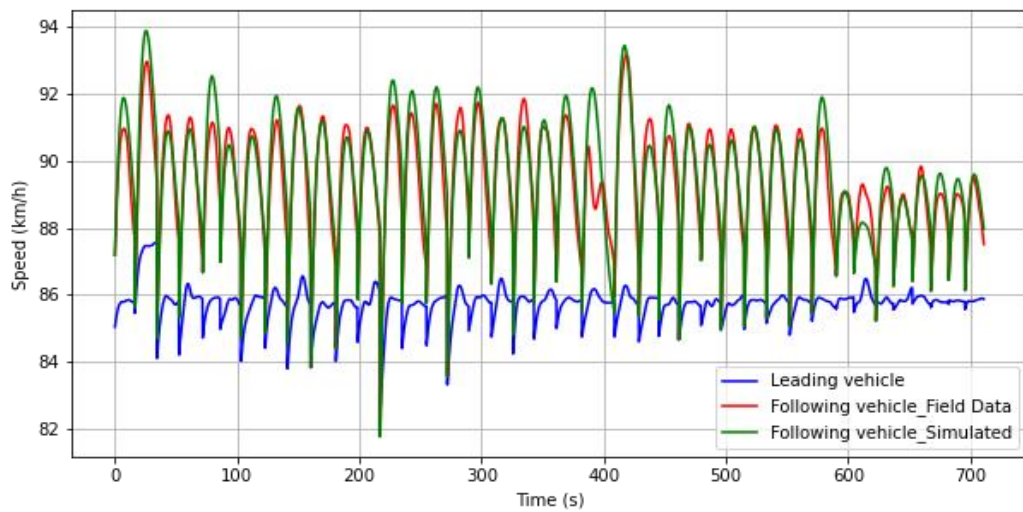
(c) 55 mph (88 kph), short gap
Figure 5.8. Illustration of the simulated speed for some typical catch-up scenarios.
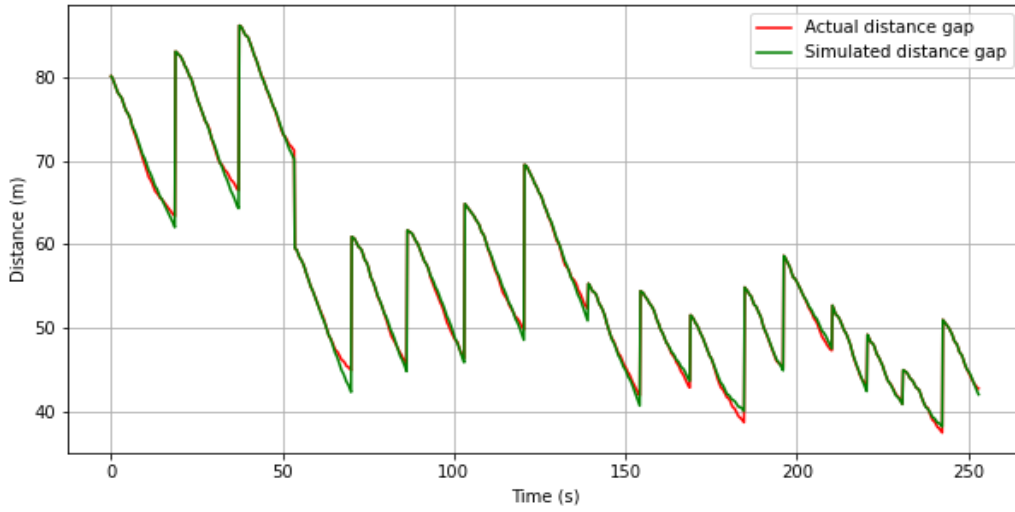
(a) 35 mph (56 kph), long gap
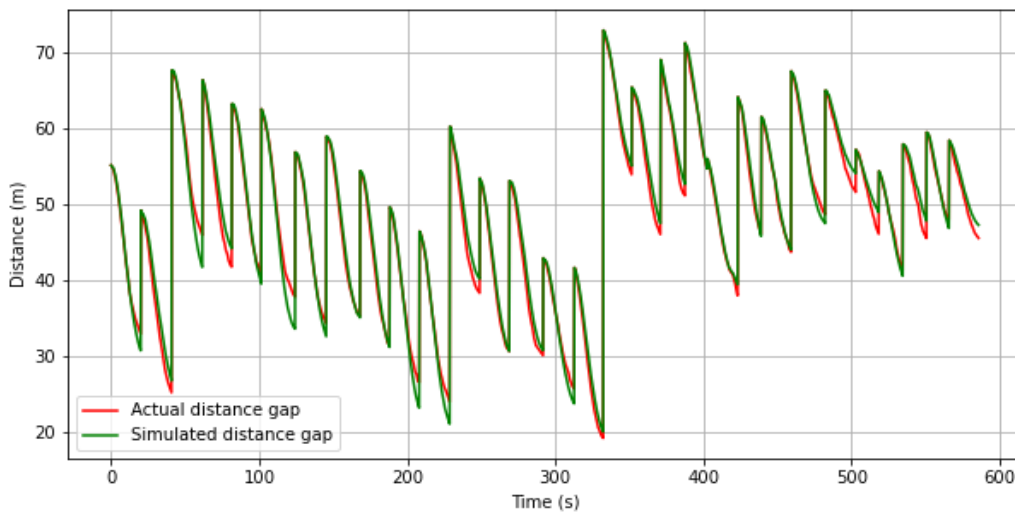
(b) 45 mph (72 kph), medium gap
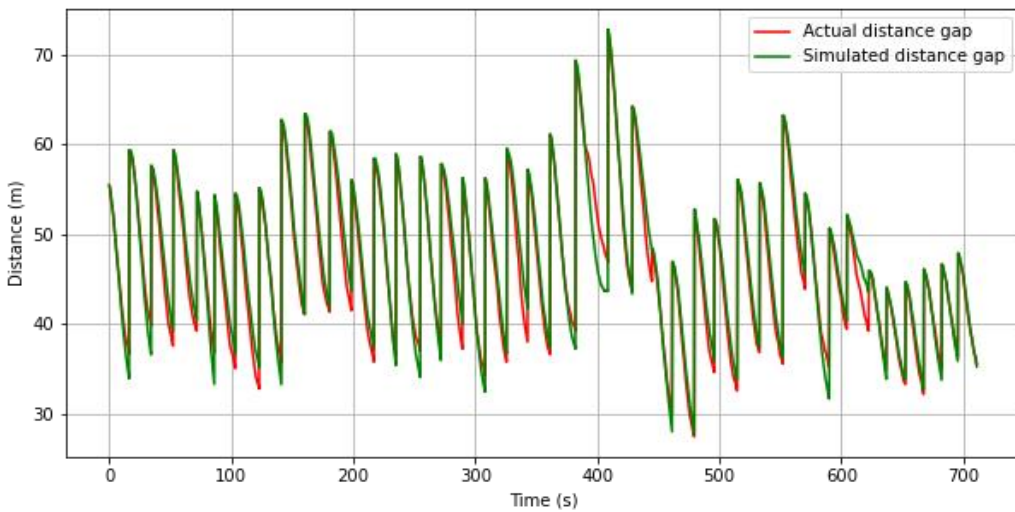
(c) 55 mph (88 kph), short gap

Figure 5.9. Illustration of the simulated gap for some typical catch-up scenarios.

5.6 Receiving Lane-change Car-following Model

This subsection intends to further quantify the impact of ACC's receiving lane-change car following behaviors on the distance and time gaps that resemble typical multi-lane freeways with both free-flow and congested conditions, by comparing the performance between internal combustion powered vehicles and fully electric vehicles. More importantly, a microscopic receiving-lane-change car following model (RCF model) will be developed using trajectory data collected from the carefully designed 3-vehicle lane-change experiments described in subsection 3.2.3, which will address internal combustion powered vehicles and provide an initial peek at fully electric vehicles.

5.6.1 Updated Desired Time Gap

A new desired time gap set needs to be adapted to the model, reflecting the latest design of ACC controller embedded in commercial ACC vehicles. The minimum steady-state headways shown in Table 4.1 are converted to the minimum safety time gaps shown in Table 5.6, which indicates that the desired gap varies not only by ACC selected gap setting, but free-flow speed as well. Besides, ICE vehicle and EV paired with ACC also show some difference in desired time gap, due to EV's responsive regenerative braking that allows for safe operation at shorter gaps or headways. In this study, since the lane-change experiments were conducted at the free-flow speed of 60 mph and 35 mph, only the desired time gap at the corresponding speed level are shown in the table.

Table 5.6. Minimum safety time gap (s) under different gap settings and free-flow speed.

Gap Setting	Desired Time Gap (s)			
	ICE vehicle		EV	
	60 mph	35 mph	60 mph	35 mph
Short	1.18	1.64	1.06	1.14
Medium	1.78	2.47	1.33	1.43
Long	2.16	2.51	1.60	1.66
Extra Long	/		2.13	1.95

5.6.2 Reduced Time Gap

Similar as the new model developed in the previous subsections, we develop the new receiving lane-change car following model on a basis of the conventional SCG model shown by equation 5.6. The first major update to the SCG model is to develop a time-variant desired time gap $\dot{t}_{hw}$ instead of maintaining desired time gap t_{hw}. Otherwise, the recalibrated model parameters cannot accurately replicate the field observed receiving-car following behavior, including the speed profiles and the gap between the following vehicle and the preceding vehicle. The unsatisfactory fit could be attributed to the following vehicle's overestimated deceleration in response to the cut-in maneuver, which leads to the simulated speed lower than the field observed speeds during the deceleration phase. To address this, a reduced time gap $\dot{t}_{hw}$ needs to be applied once the cut-in vehicle's lane change maneuver is detected by the ACC controller of the following vehicle. $\dot{t}_{hw}$'s formula is shown as equation 5.7:

$$\dot{t}_{hw} = t_{min} + (t_{hw} - t_{min}) * \frac{n}{I_s}, \ n \le I_s \tag{5.7}$$

where I_s represents the total number of transition time steps, n represents the current time since the detection of the cut-in maneuver, t_{min} is the minimum temporal time gap the ACC controller will adapt and it should be proportional to be the original desired time gap t_{hw}. A reasonable search range of this variable is between 0.3- 0.7 t_{hw} based on the preliminary examination of the field data. Figure 5.10 gives a representative example of the simulated speed profile and distance gap with constant desired time gap on the left and time-variant desired time gap on the right, while the free-flow speed is 60 mph, lane-change speed is 50 mph, and the gap setting is medium. It proves that applying a reduced time gap is necessary to capture the realistic and less aggressive ACC deceleration in response to the lane change maneuver, keep a relatively higher speed at the beginning of the lane-change, and maintain a shorter distance gap before acceleration.

(a) Speed, Constant Time Gap t_{hw} (b) Speed, Reduced Time Gap $\dot{t}_{hw}$

(c) Distance Gap, Constant Time Gap t_{hw} (d) Distance Gap, Reduced Time Gap $\dot{t}_{hw}$
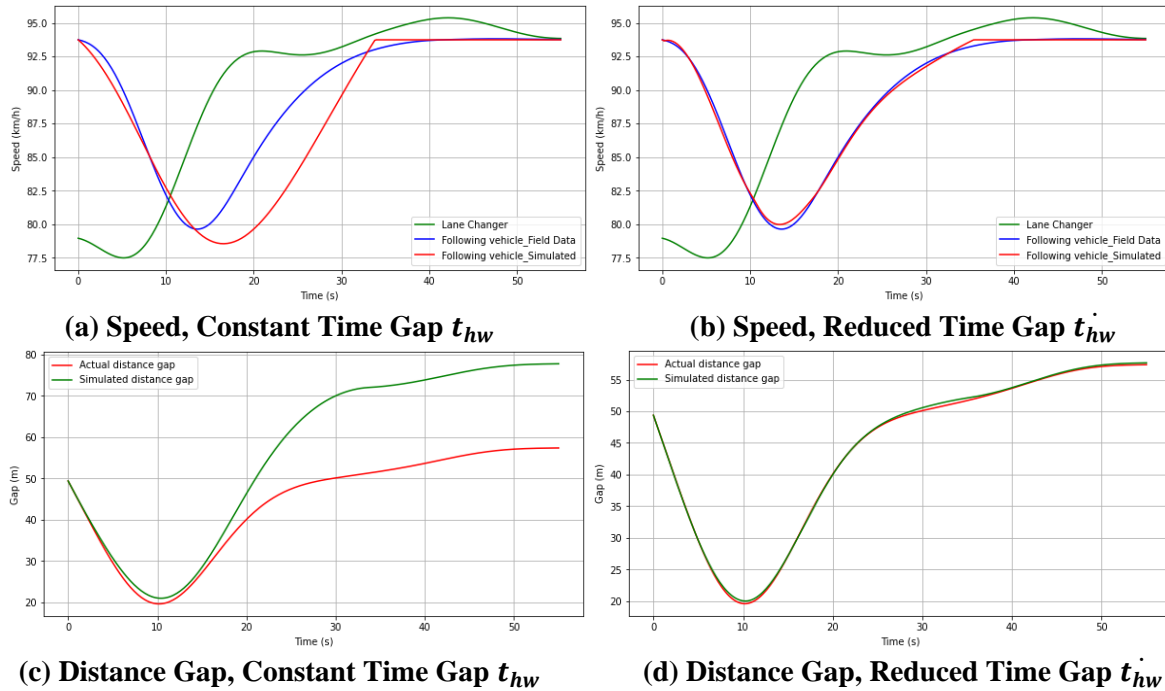
Figure 5.10. Simulated speeds and distance gaps with different car-following models (Free-flow speed: 60 mph, lane-change speed: 50 mph, gap setting: medium).

5.6.3 Asymmetric Car-following Behaviors

Another important change to the SCG model is to apply an asymmetric car-following model structure to capture the difference in car following behaviors between acceleration and deceleration stages. The simplest solution is to apply different gap gain k_2 and speed gain k_3 shown in equation 5.6. Adding the time-variant reduced time gap into consideration, the final receiving-lane-change car-following model (RCF model) will be written as equation 5.8:

$$a_{sv}(t) = \begin{cases} K_{1\_1}{}'(d(t-\tau) - \dot{t}_{hw}v_{sv} - L) + K_{2\_1}{}'(v_{lc}(t-\tau) - v_{sv}) \\ \qquad if\ a_{sv}(t-1) \leq 0 \\ K_{1\_2}{}'(d(t-\tau) - \dot{t}_{hw}v_{sv} - L) + K_{2\_2}{}'(v_{lc}(t-\tau) - v_{sv}) \\ \qquad if\ a_{sv}(t-1) > 0 \end{cases} \qquad (5.8)$$

where v_{lc}: the lane-change speed [m/s].

60

Figure 5.11 compares the symmetric and asymmetric model structure in terms of their simulated speed and distance gap, while the free-flow speed is 35 mph, lane-change speed is 25 mph, and the gap setting is long. The figure indicates that the symmetric structure fails to provide enough acceleration strength to let the following vehicle speed up and eventually leads to a longer distance gap than expected after the lane-change process.

(a) Speed, Symmetric Structure

(b) Speed, Asymmetric Structure

(c) Distance Gap, Symmetric Structure

(d) Distance Gap, Asymmetric Structure

Figure 5.11. Simulated speeds and distance gaps with different car-following models (Free-flow speed: 35 mph, lane-change speed: 25 mph, gap setting: long).

5.6.4 Smoothing algorithm to transition between acceleration and deceleration

Further inspection of the field data suggests that the model also requires a smooth transition between acceleration and deceleration to capture the real-world car following behavior. Hence, a simple linear smoothing algorithm was developed and the RCF model will be rewritten as equation 5.9:

$$a_{sv}(t) = \begin{cases} a'_{dcc}(t) & a_{sv}(t-1) \leq -0.05 \\ a'_{acc}(t) & a_{sv}(t-1) \geq 0.05 \\ a'_{acc}(t) * \dfrac{a_{sv}(t-1)+0.05}{0.1} & \\ -a'_{dcc}(t) * \dfrac{a_{sv}(t-1)-0.05}{0.1} & -0.05 < a_{sv}(t-1) < 0.05 \end{cases} \tag{5.9}$$

where $a'_{dcc}(t)$ and $a'_{acc}(t)$ represents the desired acceleration at time step t if calculated by equation 5.8 [m/s^2].

It is worth mentioning that the transition threshold of the acceleration should be selected carefully. On the one hand, the threshold cannot be too large. Otherwise, the model performance will be greatly affected. On the other hand, the threshold cannot be too small, otherwise the desired

acceleration difference could be too large to make the transition happen within the entire threshold. In this study, the threshold is selected as -0.05 - 0.05 m/s². Figure 5.12 shows the simulated speed profile of a typical cut-in scenario before and after applying the smoothing algorithm.
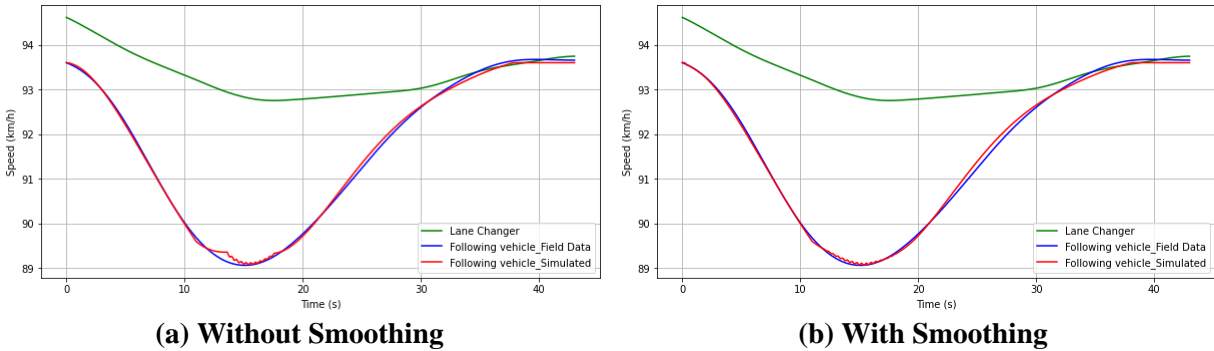
(a) Without Smoothing   (b) With Smoothing

Figure 5.12. Simulated speeds with and without the smoothing algorithm (Free-flow speed: 60 mph, lane-change speed: 60 mph, gap setting: short).

5.6.5 Model Comparison

After solving a similar linear optimization problem as the one in subsection 5.4, optimal model parameters of ACC-equipped ICE vehicles a few cut-in scenarios are shown as follows:

60 mph Free-flow speed, 50 mph lane-change speed, medium gap setting: $K_{1\_1}' = 0.021$, $K_{2\_1}' = 0.155$, $K_{1\_2}' = 0.03$, $K_{2\_2}' = 0.215$, $I_s = 17$, $t_{min} = 0.31\ t_{hw}$;

60 mph Free-flow speed, 60 mph lane-change speed, short gap setting: $K_{1\_1}' = 0.0245$, $K_{2\_1}' = 0.225$, $K_{1\_2}' = 0.042$, $K_{2\_2}' = 0.225$, $I_s = 11$, $t_{min} = 0.48\ t_{hw}$.

Small changes to each parameter can have a great impact on the receiving lane-change car-following behaviors. Larger speed difference and shorter gap setting when lane change occurs can generally lead to longer transition period and smaller minimal reduced time gap.

As for EVs, more detailed investigation is required but similar model framework will be applied as they still have apparent asymmetric car following behaviors. Figure 5.13 and Figure 5.14 are examples of how the new RCF model can fit the EV cut-in scenarios. The setup is the same as that for ICE vehicles. Optimal model parameters of ACC-equipped EVs under the same cut-in scenarios are shown below:

60 mph Free-flow speed, 50 mph lane-change speed, medium gap setting: $K_{1\_1}' = 0.06$, $K_{2\_1}' = 0.45$, $K_{1\_2}' = 0.045$, $K_{2\_2}' = 0.18$, $I_s = 3$, $t_{min} = 0.82 * t_{hw}$ (Figure 5.13);

60 mph Free-flow speed, 60 mph lane-change speed, short gap setting: $K_{1\_1}' = 0.10$, $K_{2\_1}' = 0.145$, $K_{1\_2}' = 0.025$, $K_{2\_2}' = 0.145$, $I_s = 3.6$, $t_{min} = 0.7 * t_{hw}$ (Figure 5.14).

The preliminary results are consistent with our expectation that greater gain in speed difference and position difference, larger reduced minimum gap and shorter transition time will occur compared to those for ICE under the same condition. Instantaneous torque and regenerative braking characteristics allow EV with ACC to deliver stronger acceleration and deceleration so that they can respond more quickly and instantaneously to cut-in vehicles and be less dependent on reduced time gap.

(a) Speed   (b) Distance Gap
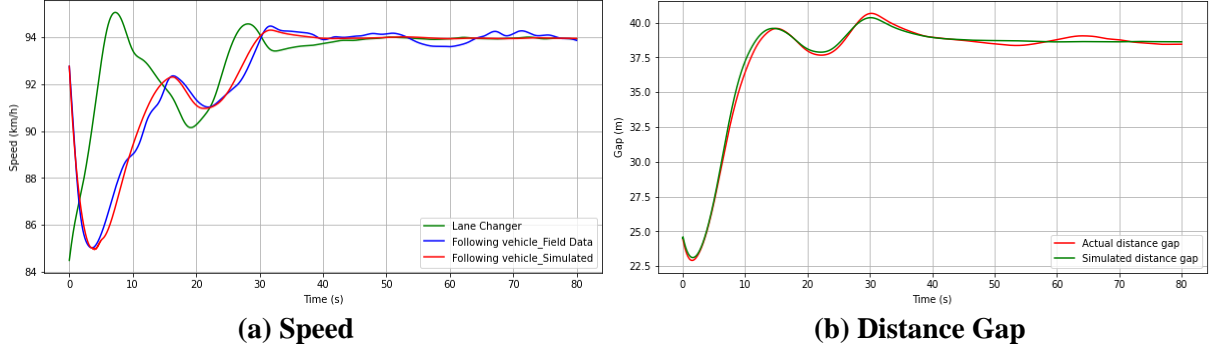
Figure 5.13. Simulated speeds and distance gap with adjusted RCF model for EV.
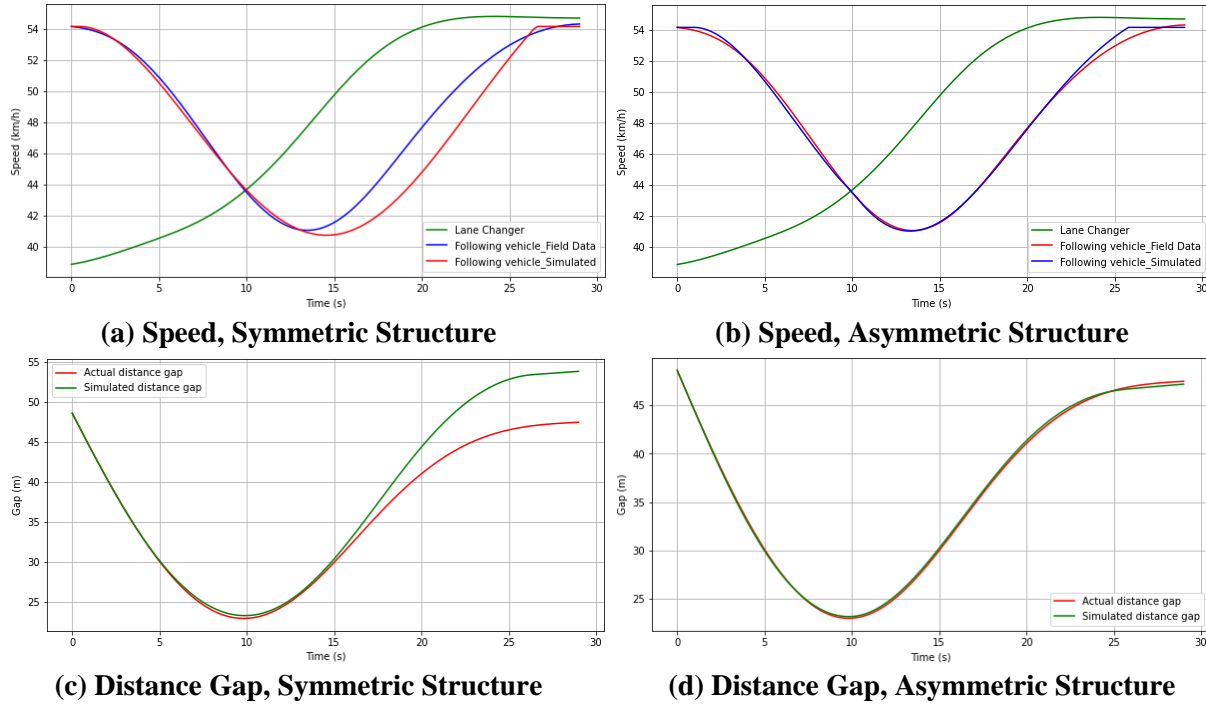**(Free-flow speed: 60 mph, lane-change speed: 50 mph, gap setting: medium).**

(a) Speed   (b) Distance Gap
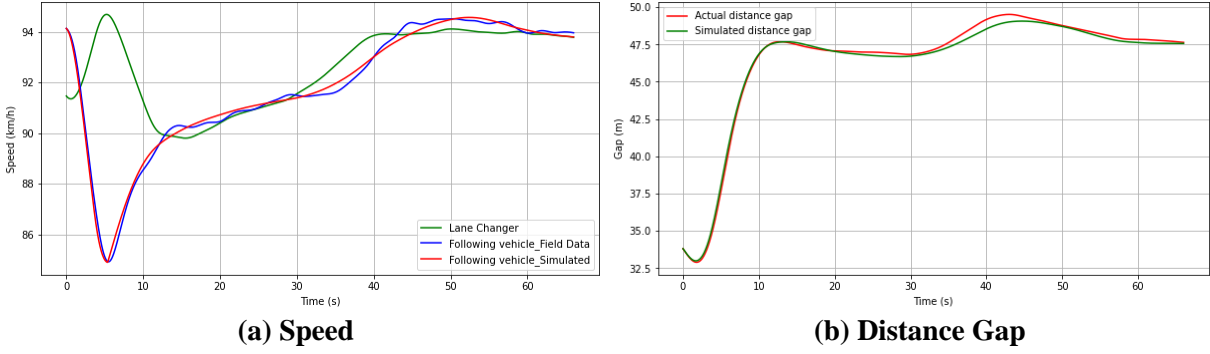
Figure 5.14. Simulated speeds and distance gaps with adjusted RCF model for EV
(Free-flow speed: 60 mph, lane-change speed: 60 mph, gap setting: short).

5.7 ACC Car Following Model Framework

To integrate the common CF model under free-flow condition (subsection 5.1), CCF model (subsection 5.2-5.4) with catch-up behaviors of ICE vehicle under heterogeneous desired speeds (subsection 5.5), RCF model (subsection 5.6) into a comprehensive ACC car-following model framework, we need to decide the boundary to switch between two new models (CCF vs. RCF). Once the cut-in maneuvers take place, one most obvious characteristic is a sudden change in the object/vehicle that the ACC is following. Therefore, we rely on the change of longitudinal distance gap between the following vehicle and the preceding vehicle to choose the model. If the decrease of the longitudinal distance gap within one time step is larger than one vehicle length plus the minimal safety distance gap, then we should apply the RCF model. Otherwise, the CCF model will be used. The boundary distance gap change will be calculated as equation 5.10:

$$\Delta d_{min} = d_{safe} + L = d_{lc} - d_l + d_{jam} + L$$
$$= v_{lc} * \tau_r + \frac{v_{lc}^2}{2 * b_{lc}} - \frac{v_f^2}{2 * \hat{b}_l} + d_{jam} + L \tag{5.10}$$

where d_l: the travelled distance of the leader if it applies a most severe braking to complete stop [m], d_{lc}: the travelled distance of the lane changer in response to leader's braking [m], d_{jam}: the jam gap [m], τ_r: the reaction time of the human driver [s], b_{lc}: the most severe braking that the lane changer wishes to undertake [m/s²], $\hat{b}_l$: the lane changer's estimate of leading vehicle's most severe braking capabilities [m/s²]. Assuming the two vehicle's braking capabilities are the same, then equation 5.10 can be simplified to equation 5.11:

$$\Delta d_{min} = v_{lc} * \tau_r - \frac{v_f^2 - v_{lc}^2}{2 * b} + d_{jam} + L \tag{5.11}$$

Therefore, the pseudo code of switching between two new ACC car-following models is presented in Figure 5.15. The threshold for each constraint is determined based on field observations and some simple simulation trials of the collected data.

If $d(t_0 - 1) - d(t_0) \leq \Delta d_{min}$**:**

    For $t \geq t_0$ **and** $v_{sv}(t) = v_l(t) = v_f$ **not holds:**

$$a_{sv}(t) = \begin{cases} K_{1\_1}\big(d(t-\tau) - t_{hw}v_f - L\big) + K_{2\_1}(v_l(t-\tau) - v_{sv}) \\ \quad if\ a_{sv}(t-1) \leq 0\ and\ \Delta V \geq 20\ mph \\ K_{1\_2}(d(t-\tau) - t_{hw}v_{sv} - L) + K_{2\_2}(v_l(t-\tau) - v_{sv}) \\ \quad if\ a_{sv}(t-1) \leq 0\ and\ \Delta V < 20\ mph \\ K_3\big(v_l(t-\tau) - v_{sv}(t)\big) \\ \quad if\ a_{sv}(t-1) > 0 \end{cases};$$

$$v_{sv}(t) = v_{sv}(t - \Delta t) + a_{sv}(t)\Delta t;$$

$$d(t) = d(t - \Delta t) + (v_l(t) - v_{sv}(t))\Delta t;$$

    Else:

        For $t \geq t_0$ **and** $v_{sv}(t) = v_l(t) = v_f$ **not holds:**

$$a_{sv}(t) = \begin{cases} K_{1\_1}'(d(t-\tau) - t_{hw}'v_{sv} - L) + K_{2\_1}'(v_{lc}(t-\tau) - v_{sv}) \\ \quad if\ a_{sv}(t-1) \leq 0 \\ K_{1\_2}'(d(t-\tau) - t_{hw}'v_{sv} - L) + K_{2\_2}'(v_{lc}(t-\tau) - v_{sv}) \\ \quad if\ a_{sv}(t-1) > 0 \end{cases};$$

$$v_{sv}(t) = v_{sv}(t - \Delta t) + a_{sv}(t)\Delta t;$$

$$d(t) = d(t - \Delta t) + (v_{lc}(t) - v_{sv}(t))\Delta t;$$

$$t_{hw}' = t_{min} + (t_{hw} - t_{min}) * \frac{t - t_0}{I_s},\ t \leq t_0 + I_s;$$

$$t_{hw}' = t_{hw},\ t > t_0 + I_s;$$

    Where:

$$0 \leq K_{1\_1}, K_{2\_1}, K_{1\_1}', K_{2\_1}' \leq 1, \text{unit: } s^{-2};$$

$$0 \leq K_{2\_1}, K_{2\_2}, K_{1\_2}', K_{2\_1}', K_3 \leq 1, \text{unit: } s^{-1};$$

$$0.3t_{hw} \leq t_{min} \leq 0.7t_{hw}$$

$$5 \leq I_s \leq 20, \text{unit: seconds};$$

$$0 \leq \tau \leq 4.0, \text{unit: seconds};$$

$$-1.75 \leq a_{sv} <= 1.05, \text{unit: } m/s^2;$$

$$v_{sv} \leq v_f;$$

$$a_{sv} \leq 0\ if\ a_l < 0;$$

Figure 5.15. Pseudo code of congested car following model (CCF) and receiving-lane-change car following model (RCF) integration.

The comprehensive ACC car-following model framework will be briefly represented as the flow chart shown in Figure 5.16. Under free-flow condition where the gap between the following vehicle and the preceding vehicle is relatively large, the gap will maintain at a similar level if small speed change occurs, and thus, the original PATH model or SCG model can sufficiently capture the ACC car following behaviors. However, with denser traffic with shorter gaps, it is necessary to apply the new CCF model and RCF model, which depends on the detection of a cut-in object. As in this case, the gap varies greatly due to many factors, including ACC selected gap setting, free-flow speed, speed fluctuation magnitude, lane-change speed, etc. A more comprehensive model can help capture those variations and asymmetric car following behaviors between acceleration and deceleration. Note that ACC desired set speed can lead to great car following behavior changes after speed fluctuations, which was discussed and modeled in subsection 5.5. Those changes will not affect the general ACC car following model framework shown in Figure 5.16 and can be treated as a special case when implementing into the microscopic simulation.
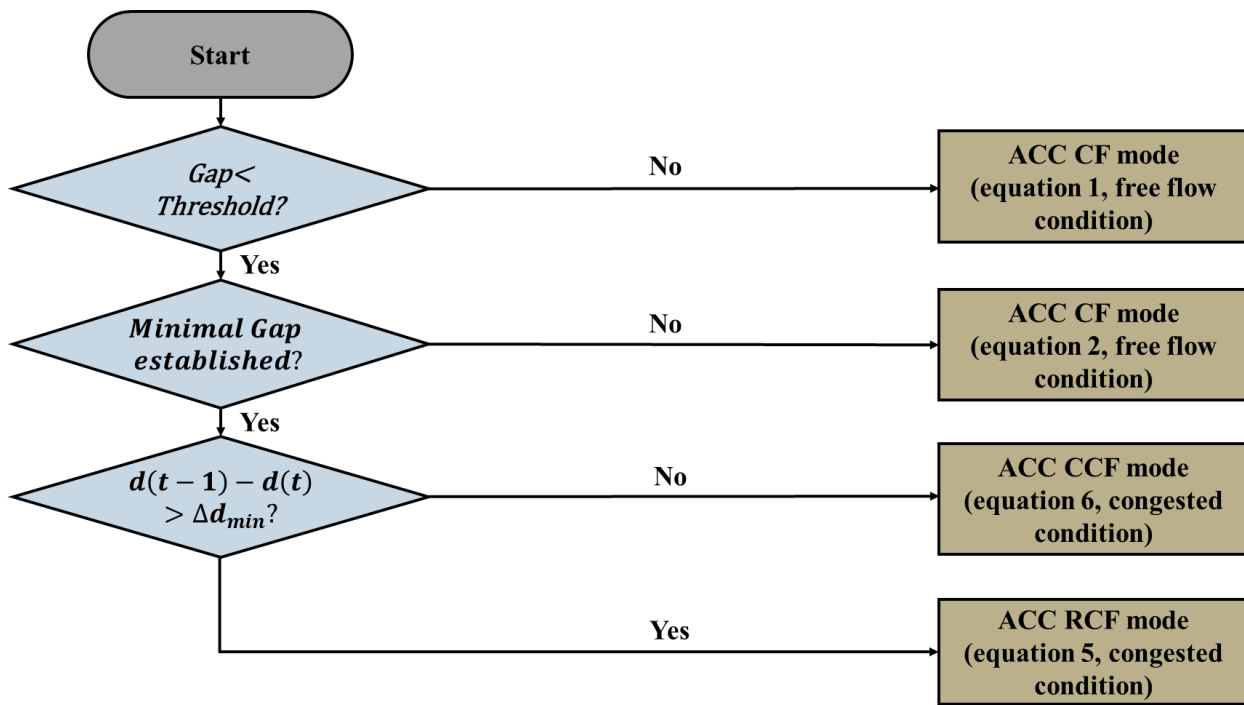
Figure 5.16. Adaptive cruise control (ACC) car following model framework.

5.8 Model Implementation in Microscopic Simulation

Applying the comprehensive model framework along with calibrated parameter sets for both ICE vehicles and EVs, the ACC car-following models were implemented into AIMSUN (TSS, 2020) via microSDK to enable simulation analysis. We followed the model structure proposed in the previous subsections and made some new efforts to capture all the traffic conditions that ACC vehicles could encounter. This required us to select the appropriate speed dependent parameter set and smoothly interpolate the parameters between the scenarios covered in our field experiments, instead of separate parameter sets for each of the representative scenario tested. In other words, a proper transition algorithm should be proposed to make the model continuous in the domain of vehicle velocity. In this study, a linear interpolation technique was applied to help the ACC car-

following model make a transition from one scenario to another, if the current speed profile of ACC vehicles fell into certain buffers. We have to define a few lists and variables, which will be used in the flow chart of the model implementation procedure shown below:

- Counting variable i: represents the ith speed profile the algorithm works through, where the speed profile is sorted from the largest to the smallest;
- $v_{bound}(i)$: represents the lower speed boundary of the ith speed profile;
- $v_{buffer_{lower}}(i)$: represents the lower buffer boundary within the ith speed profile ranges, if the speed is smaller than this value, we should apply the linear interpolation with the parameters under the $(i+1)^{th}$ speed profile;
- $v_{buffer_{upper}}(i)$: represents the upper buffer boundary within the ith speed profile ranges, if the speed is larger than this value, we should apply the linear interpolation with the parameters under the $(i-1)^{th}$ speed profile;
- $k(i)$: represents the calibrated model parameter set within the ith speed profile ranges.

For the ACC car-following model linear interpolation, two boundary cases were considered:

(1) When the $v_{sv}(t) < v_{buffer_{lower}}(i)$, the linear interpolation takes place with the lower-level scenario:

$$
\begin{aligned}
k = k(i) * \left(1 - \frac{v_{buffer_{lower}}(i) - v_{sv}(t)}{v_{buffer_{lower}}(i) - v_{buffer_{upper}}(i-1)}\right) + k(i-1) \\
* \left(\frac{v_{buffer_{lower}}(i) - v_{sv}(t)}{v_{buffer_{lower}}(i) - v_{buffer_{upper}}(i-1)}\right)
\end{aligned}
\tag{5.12}
$$

(2) When the $v_{sv}(t) > v_{buffer_{upper}}(i)$, the linear interpolation takes place with the upper-level scenario:

$$
\begin{aligned}
k = k(i) * \left(1 - \frac{v_{sv}(t) - v_{buffer_{upper}}(i)}{v_{buffer_{lower}}(i+1) - v_{buffer_{upper}}(i)}\right) + k(i+1) \\
* \left(\frac{v_{sv}(t) - v_{buffer_{upper}}(i)}{v_{buffer_{lower}}(i+1) - v_{buffer_{upper}}(i)}\right)
\end{aligned}
\tag{5.13}
$$

Figure 5.17 shows the flow chart of the implementation of ACC car-following models.
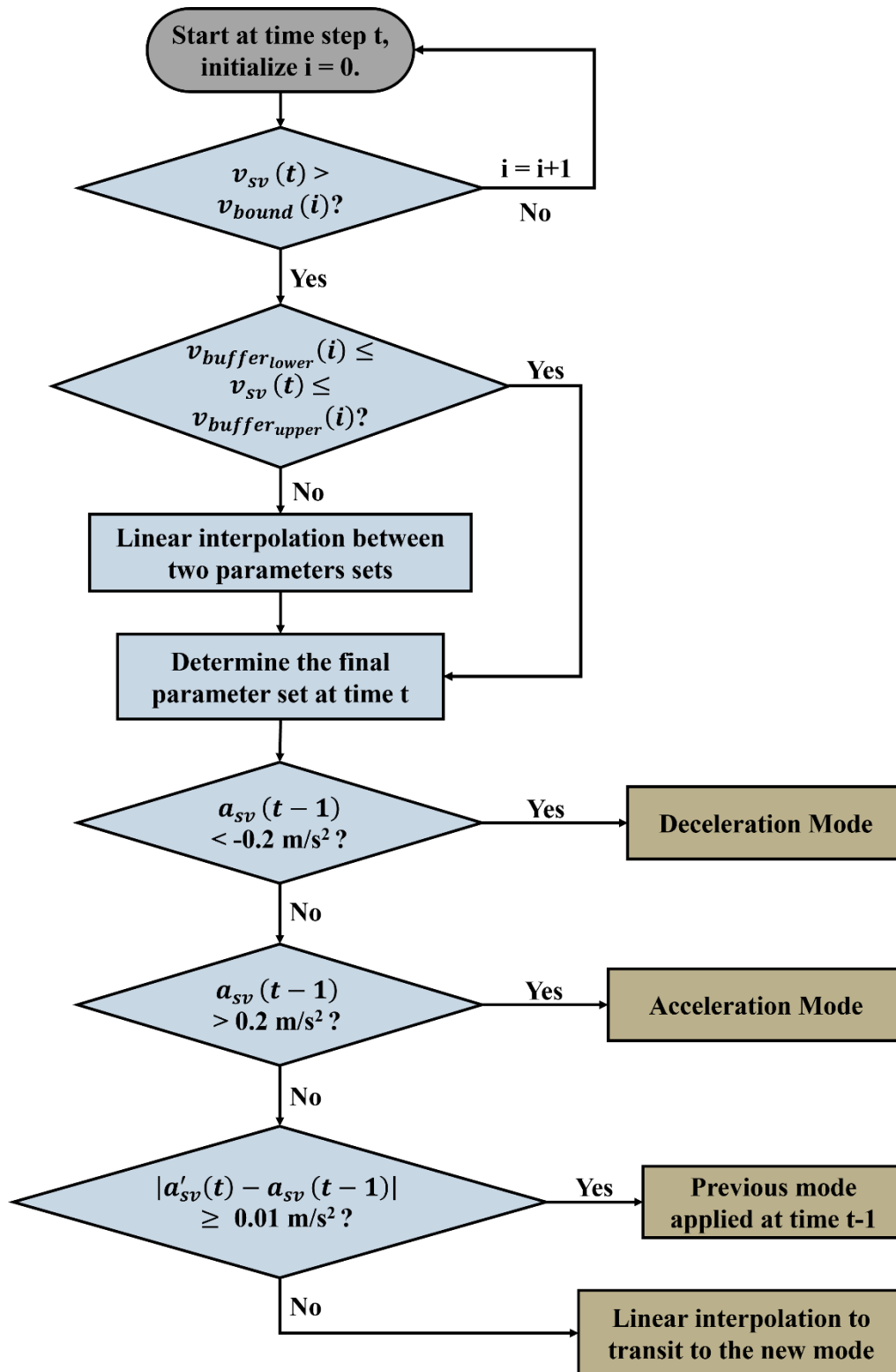
Figure 5.17. Flow chart of the ACC car-following model implementation in AIMSUN microSDK.

CHAPTER 6: SIMULATION RESULTS

Simulation experiments were conducted in the AIMSUN microscopic simulation (TSS, 2020) after the implementation of the new ACC car-following model framework for both ICE vehicles and EVs. Both an isolated freeway merge segment and the SR-99 northbound corridor were built in the simulation to investigate the effect of different car-following models on traffic mobility (Lu et al, 2017; Hao et al, 2018; Kan et al, 2019).
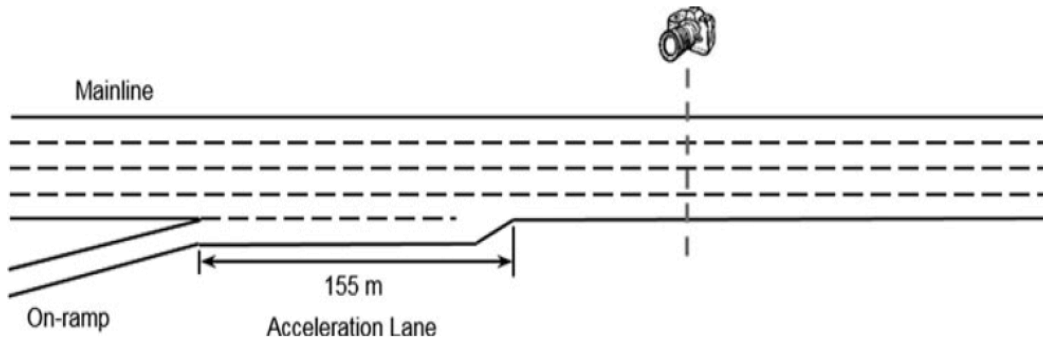
(a) Multilane freeway merge section
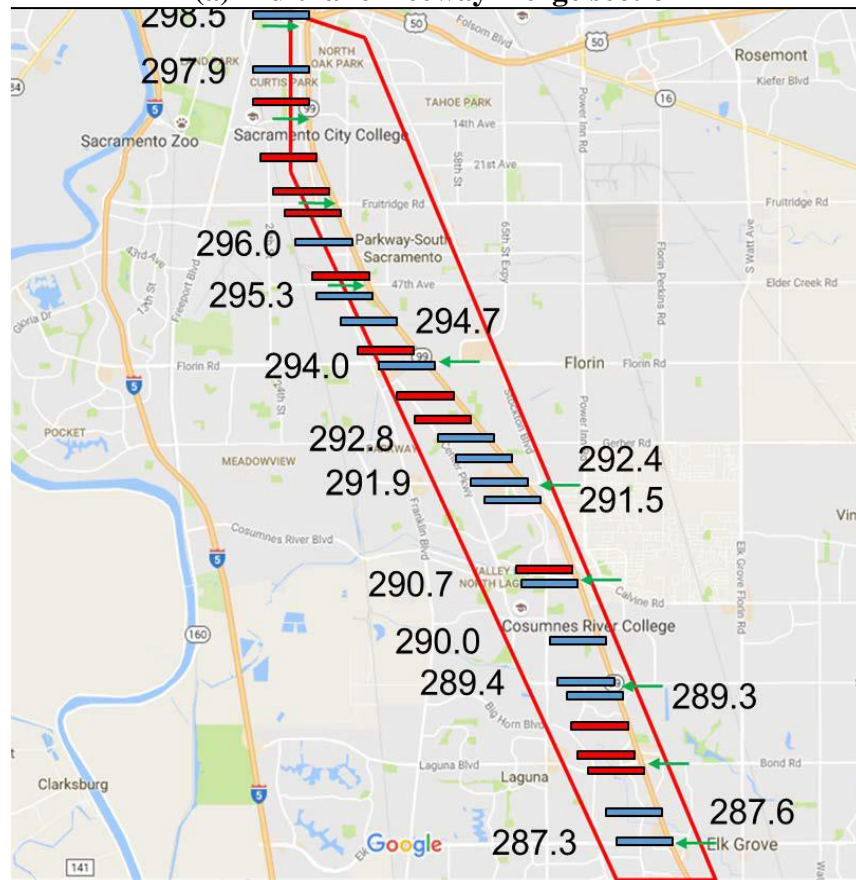
(b) SR-99 corridor
Figure 6.1. Microscopic simulation networks (Kan et al, 2019).

6.1 Freeway Bottleneck

The new models were tested on an isolated freeway merge bottleneck as this scenario is simple for us to analyze the difference between different models and powertrains. We used 100% ACC-equipped ICE vehicles with SCG model as baseline and tested two additional scenarios with 100% ACC-equipped ICE vehicles and EVs using ASVG model and SCG model with recalibrated parameters respectively. No human-driven vehicles were simulated in this study to exclude the potential interaction impacts between human-driven vehicles and ACC-controlled vehicles, which remains unknown. The summary mobility performance of these 3 scenarios has been compared and listed in Table 6.1.

We can see that if there was no vehicle coming from the on-ramp, which means that no lateral disturbance exists, the EV's recalibrated SCG model generated the highest discharge flow and longest total travel distance among the three scenarios, though the difference was subtle. Under free-flow condition without lateral disturbance, both SCG model and the new ASVG model can generate a similar traffic flow if the powertrain stays the same. Electric vehicles can show around 6% higher capacity due to their slightly shorter desired headway under stable traffic conditions, which has been tested in the field.

However, when 600 veh/hr comes from the on-ramp, which led to frequent lateral movements, while the SCG model showed 2% capacity drop, which was defined as the phenomenon that high demand from on-ramp merge would trigger flow breakdown, form a bottleneck, and reduce the maximum sustained flow it discharges (Cassidy and Bertini, 1999; Cassidy and Rudjanakanoknad, 2005), and 5% total travel distance decrease for ICE vehicles compared to the zero on-ramp demand case, the ASVG model for the ICE vehicles indicated a much larger difference. Over 10% capacity drop and 15% total travel distance decrease were observed. The results may look surprising at first glance, but they can be explained in a reasonable way if we look at the congested ACC car-following behaviors for ICE vehicles observed in real-world: these ACC vehicles can maintain a very short safety gap if the travel speed is stable (i.e. zero on-ramp demand case), while the gap will increase by a large amount if the vehicles experience a large speed fluctuation (i.e. high on-ramp demand case). The SCG model rapidly recovered the initial headway after speed fluctuations and therefore severely overestimated the capacity when frequent lateral movements occurred. This new ASVG model can sensitively capture the headway variation patterns, characterized by various system reaction and acceleration power. On the other hand, the recalibrated SCG model can make sure that EVs with ACC will yield minimal capacity drop under congested scenarios with major speed fluctuations and lateral disturbance.

Table 6.1. Mobility performance comparison between 100% ICE vehicle with ACC and 100% EV with ACC using SCG model and ASVG model at freeway merge bottleneck.

Scenarios	Freeway Bottleneck (zero on-ramp demand)			Freeway Bottleneck (600 veh/hr on-ramp demand)		
Models	ACC ICE (SCG)	ACC ICE (ASVG)	ACC EV (SCG)	ACC ICE (SCG)	ACC ICE (ASVG)	ACC EV (SCG)
Discharge Flow (veh/hr)	5996	5992	6365.66	5891.79	5271.72	6223.74
Total Travel Distance (km)	26318.72	26283.13	26643.68	24918.55	22385.73	26457.07

6.2 SR-99 Corridor

Simulations on the isolated merge bottleneck environment tested the main differences in the ACC car-following behaviors between SCG model and the new ASVG model and proved that the new model can accurately capture the ACC gap variation patterns under congested scenarios for ICE vehicles. Further simulations were run on a large-scale SR-99 corridor to mimic the real-world traffic on a typical day during peak hours, which has been calibrated using real-world traffic data (Kan et al, 2019). Besides, different market penetration rates (i.e., MPRs) between ICE vehicles with ACC and EVs with ACC have been simulated.

The simulation summary of their mobility performance has been listed in Table 6.2. This time, we also included the queue spillback speed and the average headway downstream the main bottleneck. Not surprisingly, as the MPR for EVs increases, the discharge flow, total travel distance, and the average headway downstream the bottleneck increase in a consistent way. From 100% ICE ACC-equipped vehicles to 100% electric ACC-equipped vehicles, the discharge flow and the total travel distance increased by 21.9% and 22.0% respectively, while the average headway downstream the major bottleneck decreased by 18.1%. The only measure that did not show a monotonical trend as MPR for EV with ACC increased is the queue spillback speed: it reached its highest value when the MPR was 50% for both powertrain vehicles; while it still maintained a normal decreasing trend before and after this 50% MPR was reached. The interaction between ICE vehicle and EV may need further investigation and could be modeled differently once additional filed tests are conducted in the future.

To better understand this phenomenon, second-by-second individual trajectories of ACC-equipped vehicles with both ICE and electric powertrains have been collected in the simulation and visualized via time-space diagram shown as Figure 6.2, where the individual trajectory of each vehicle has been sorted by the time and space. Color represents the current vehicle speed, while red represents the bottleneck and green represents the free-flow region. It is very clear to see that as MPR for ICE vehicles increased, especially after it reached 60% (i.e., Figure 6.2 (a), (b) and (c)), there existed a 'buffer region' with light congestion that separated the major bottleneck into two small sub-bottlenecks, which resulted from the slow ACC response under ICE powertrain and

left the queue spillback speed underestimated as it only considered the upstream sub-bottleneck instead of both.

Lastly, sensitivity analysis was conducted along two dimensions which were market penetration rate (MPR) and on-ramp demand. Figure 6.3 showed the changes of discharge flow and total travel distance across the different MPRs and on-ramp demands. As discussed above, in Figure 6.3(a), with a fixed on-ramp demand that led to heavy congestion, a monotonical trend of the traffic performance in terms of MPRs were expected: the higher the EV MPRs are, the larger discharge flow and longer total travel distance can be observed. Figure 6.3(b), on the other hand, fixed the MPRs for both powertrain vehicles at 100%, and investigated the impacts of on-ramp demand on traffic flow. Solid lines represent 100% ICE vehicles while the dashed lines represent 100% EVs. It is clear that for ICE vehicles, the capacity started to drop when the on-ramp demand was below 300 veh/hr, and 17% decrease occurred when the on-ramp demand reached 900 veh/hr. For EVs, no obvious decrease in both discharge flow and total travel distance was observed when on-ramp demand was 300 veh/hr, and they started to drop after the on-ramp demand reached 600 veh/hr. The largest drop for EVs was roughly 8%.

Table 6.2. Mobility performance comparison under different market penetrations (MPRs) between ICE vehicle and EV with ACC using new models on SR-99 corridor.

Scenarios	SR-99 Network						
MPRs	100% ICE with ACC	80% ICE + 20% EV	60% ICE + 40% EV	50% ICE + 50% EV	40% ICE + 60% EV	20% ICE + 80% EV	100% EV with ACC
Discharge Flow (veh/hr)	5335	5539	5836	5940	6078	6400	6503
Total Travel Distance (km)	22091.65	22223.13	23333.61	23723.60	24225.9	25464.91	26951.25
Queue Spillback Speed (m/s)	3.58	4.37	5.16	5.38	4.52	4.73	5.11
Average Headway Downstream Bottleneck (s)	2.70	2.60	2.47	2.42	2.37	2.25	2.21
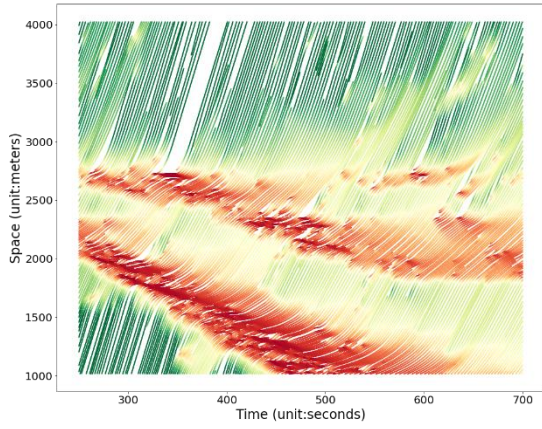
(a) 100% ICE
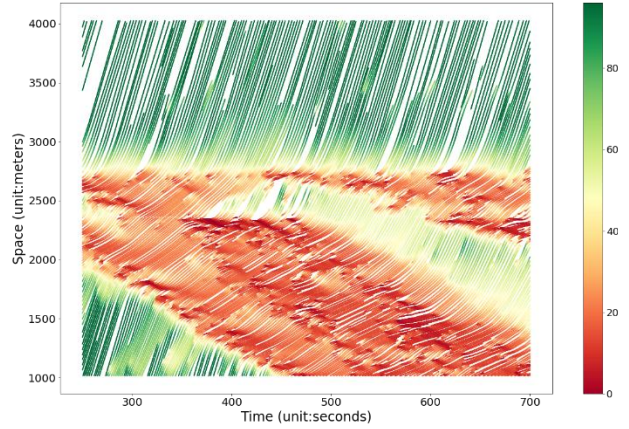
(b) 80% ICE + 20% EV
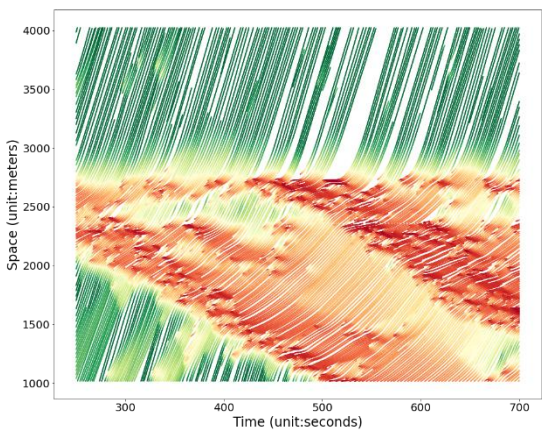
(c) 60% ICE+ 40% EV
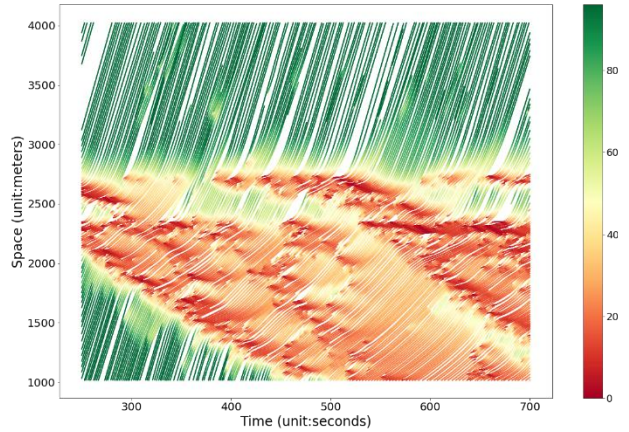
(d) 50% ICE + 50% EV
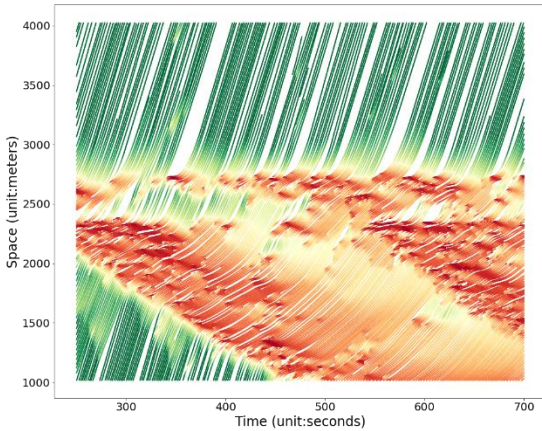
(e) 40% ICE+ 60% EV
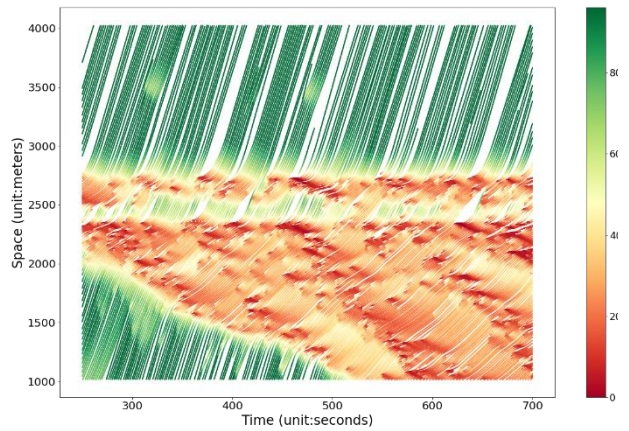
(f) 20% ICE+ 80% EV
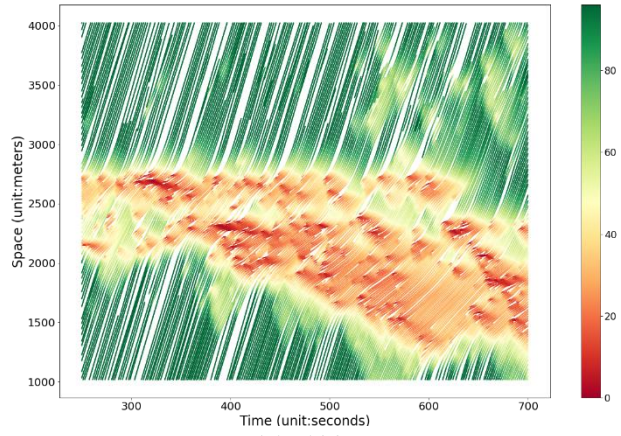
(g) 100% EV

Figure 6.2. Time-space diagram of various MPRs on SR-99 corridor.
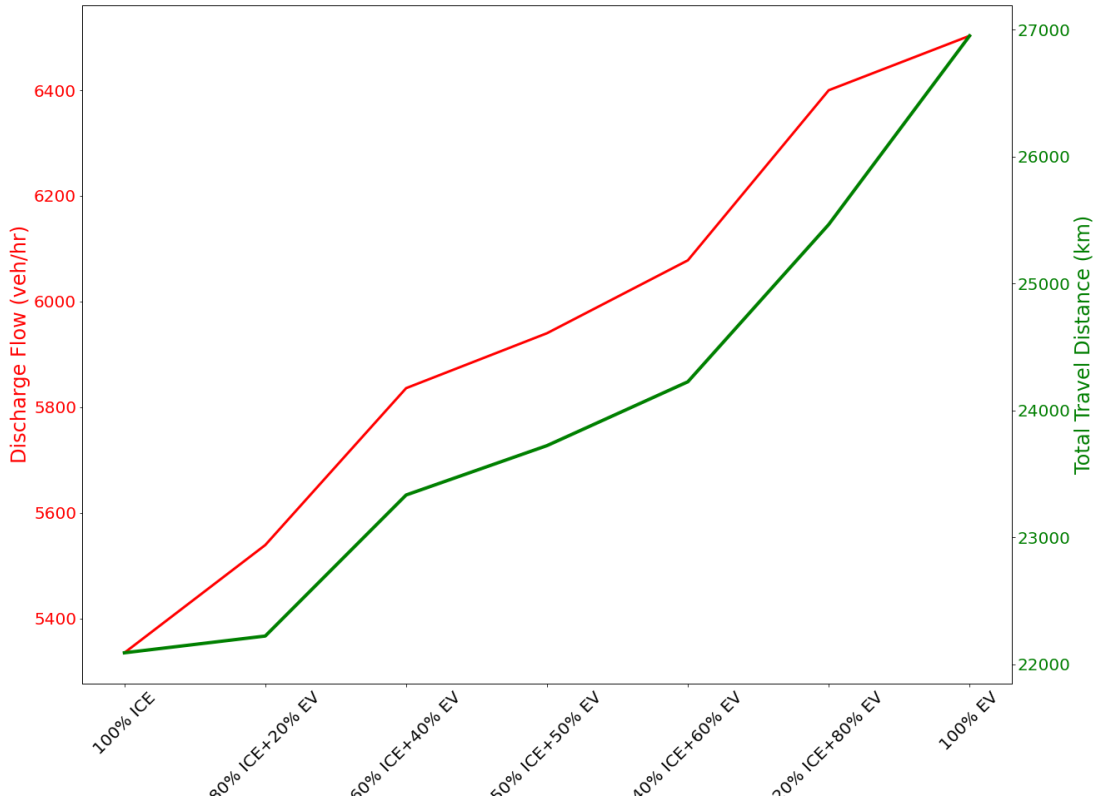
(a) Various MPRs between ICE vehicle and EV
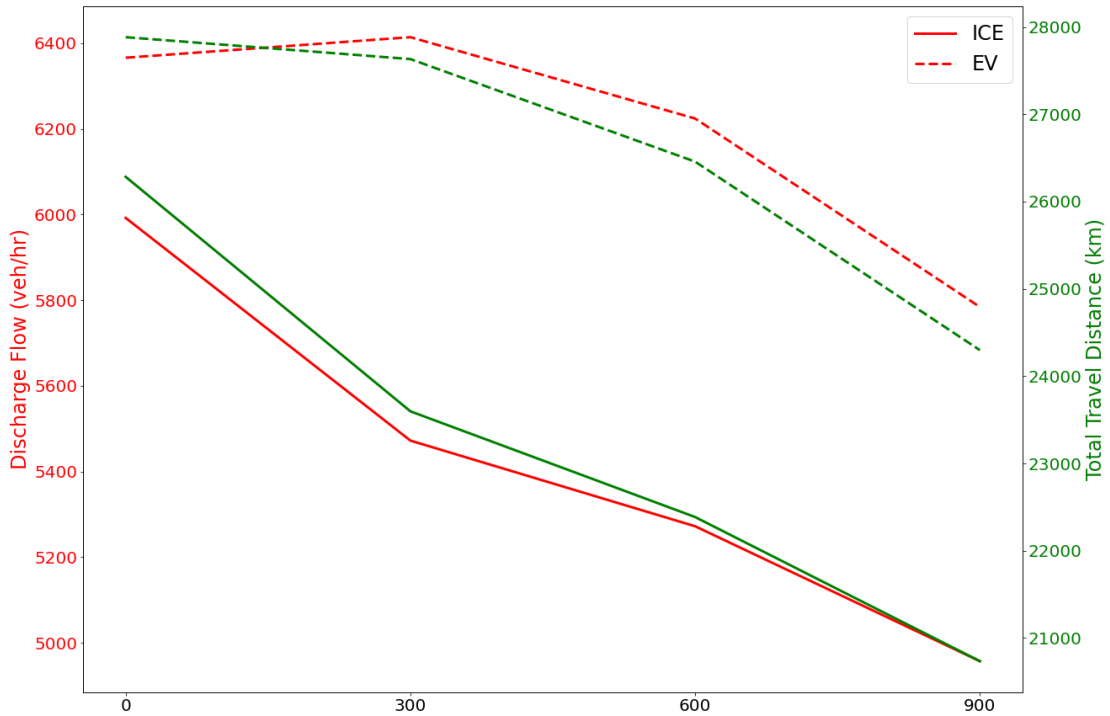
(b) Various on-ramp demands (unit: veh/hr)
Figure 6.3. Sensitivity analysis under mixed traffic flow.

CHAPTER 7: CONSLUSIONS

7.1 Summary of the Findings

Automated Vehicles (AVs) have been highly anticipated as they promise to potentially reduce congestion by improving capacity. While fully automated vehicles may take decades to reach a mass market adoption, vehicles equipped with the full-speed range Adaptive Cruise Control (ACC) are now widely available on mainstream vehicles today, thus understanding their car following behaviors becomes crucial to modeling traffic flow at the microscopic level. In this study, a series of carefully designed car-following experiments were conducted and trajectories of ACC-equipped vehicles under both internal combustion engine and electric motor were collected, named MicroSIMACC dataset.

Field experiments demonstrate that ACC-equipped ICE vehicles cannot deliver on the promise that vehicle automation could improve capacity, in fact, the opposite is true. Furthermore, the dataset reveal several important characteristics of ACC: (1) ACC-equipped ICE vehicles share similar headways and gaps as human driven vehicles under steady-state and free-flow conditions; (2) when the desired speed is the same as the initial free-flow speed, the increase in headway is amplified as speed changes become more severe, for example when approaching back of queue and accelerating again during queue discharge; (3) setting the desired speed 8 km/hr (5 mph) or more higher than the leading vehicle's desired speed (i.e., free-flow speed) will lead to a "catch-up" process, where the following vehicle exceeds the free-flow speed and shorten the gap with the leading vehicle; (4) the difference between the stabilized gap after lane change and the stabilized gap before lane change heavily depends on the difference between the target-lane and the lane-change speed. Smaller difference in target lane and lane-change speed leads to smaller stabilized gap after lane change. Long and medium gap setting always come with a positive gap difference, which means the stabilized gap increases after the lane change, while short gap setting can ensure a gap decrease after the lane change, especially on freeways.

On the contrary, ACC equipped EVs can achieve minimum headways as short as 1.23 seconds at constant speeds in steady-state conditions. This could potentially lead to an improved capacity as high as 2,931 veh/hr/lane. Moreover, deviations from the steady-state conditions do not affect the minimum headway, as shown by an extensive set of field experiment with a wide range of speed fluctuations to simulate approaching back of the queue and queue discharge at and near disturbances and bottlenecks that may arise from ingress and egress at freeway on and off-ramps, turning movements, etc. Furthermore, EVs equipped with ACC could potentially not amplify speed changes further upstream, which could imply better stability of the traffic stream and less abrupt queue propagation. Overall, ACC-equipped EVs could outperform ICE vehicles with ACC, in terms of the potential capacity and congestion reduction benefits. Interestingly, this only applies to the tested EVs from some manufacturers, whereas the tested EVs from other manufacturers such as Tesla deliver car following dynamics akin to an ICE vehicle with ACC. As the Autopilot technology evolves and software updates, further investigation is required on the car following dynamics.

The MicroSIMACC dataset were then utilized to help develop full-speed range car-following models for both internal combustion engine vehicle (ICE vehicle) and electric vehicle (EV) equipped with ACC, which could successfully capture the variable gaps under large speed oscillation and heterogeneous car-following behaviors across different speed levels, gap settings, and powertrains.

A new asymmetric variable gap model (ASVG) for ICE vehicles and the conventional symmetric constant gap model (SCG) for EVs were established to simulate the longitudinal car-following behaviors under congested single-lane scenarios. Both models were calibrated in piecewise linear format to account for the variability at different speed levels. Catch-up behaviors under heterogeneous desired speeds for ICE vehicles were investigated and captured by a recalibrated SCG model. Besides, an asymmetric constant gap model (ASCG) model with a reduced time gap was developed to deal with the receiving lane-change car-following (RCF) behaviors under cut-in scenarios, where more gentle ACC response when decelerating was found. The new RCF model successfully captured the initial minimum safety gap relaxation adopted by the ACC controller.

This study further clarified the logistics on how to implement and incorporate the new models with other models in microscopic simulation and provided novel insights about the impact of increasing market penetration of ACC with different powertrains via sensitivity analysis. The simulation results indicated that the higher the market penetration rates of EV are, the larger discharge flow and longer total travel distance can be achieved on a freeway corridor. From 100% ICE ACC-equipped vehicles to 100% electric ACC-equipped vehicles, the discharge flow and the total travel distance increased by 21.9% and 22.0% respectively, while the average headway downstream the major bottleneck decreased by 18.1%. These results further confirmed our filed observations that EVs with ACC adopted shorter headways and accelerated more swiftly to maintain shorter headways when speeds fluctuate than ICE vehicles with ACC.

7.2 Future Work

It is acknowledged that the experiments conducted in this study were simplified in a controlled environment, where different speed oscillation amplitude were tested separately. Besides, the inputs of the leading vehicle (i.e., acceleration and deceleration) were generated by ACC controller through the whole experiment, indicating a lack of different combinations of acceleration and deceleration. Future work should collect larger samples of naturalistic data with a combination of the traffic waves with different frequencies and amplitude so that new findings from this study can be validated, and the differences in ACC car following behavior among different manufacturers can be further clarified.

Besides, naturalistic ACC data can be used to capture the influence of human factors, for example, how drivers activate and use ACC on freeway (e.g., time period, location) as ACC is not always activated in the real world. As a result, the negative impacts of ACC on traffic flow simulated in this study may be overestimated, especially for ICE vehicles.

Moreover, further efforts could be undertaken to explore the interactions between ICE vehicles and EVs paired with ACC via additional field data, which could possibly lead to more accurate car-following models and thus provide more reliable traffic flow estimates in the simulation. Lastly, this study provided a model improvement guideline to deal with the variable gaps and other new car-following characteristics observed in the ACC car-following behaviors based on the OVRV model, additional efforts could be made to explore the potential of applying similar strategies on other conventional one-stage models such as the IDM model.

REFERENCES

Alkim, T.P., Bootsma, G. and Hoogendoorn, S.P., 2007, June. Field operational test" the assisted driver". In 2007 IEEE Intelligent Vehicles Symposium (pp. 1198-1203). IEEE.

Cassidy, M.J. and Bertini, R.L., 1999. Some traffic features at freeway bottlenecks. Transportation Research Part B: Methodological, 33(1), pp.25-42.

Cassidy, M.J. and Rudjanakanoknad, J., 2005. Increasing the capacity of an isolated merge by metering its on-ramp. Transportation Research Part B: Methodological, 39(10), pp.896-913.

Chon Kan, P., Lapardhaja, S. and Kan, X., 2021. Field experiments of commercially available automated vehicles on freeways. In Transportation Research Board 100th Annual Meeting.

Chon Kan, P., Imran, M., Murshed, M. and Kan, X., 2022. Field Experiment on the Impact of Automated Vehicles on Arterial Capacity–Case Study of Adaptive Cruise Control (ACC). In Transportation Research Board 101st Annual Meeting.

Cohen, S., 2004. Application of relaxation procedure for lane changing in microscopic simulation models. Transportation research record, 1883(1), pp.50-58.

Fiori, C., Arcidiacono, V., Fontaras, G., Makridis, M., Mattas, K., Marzano, V., Thiel, C. and Ciuffo, B., 2019. The effect of electrified mobility on the relationship between traffic conditions and energy consumption. Transportation Research Part D: Transport and Environment, 67, pp.275-290.

Gloudemans, D., Wang, Y., Ji, J., Zachar, G., Barbour, W., Hall, E., Cebelak, M., Smith, L. and Work, D.B., 2023. I-24 MOTION: An instrument for freeway traffic science. Transportation Research Part C: Emerging Technologies, 155, p.104311.

Gunter, G., Gloudemans, D., Stern, R.E., McQuade, S., Bhadani, R., Bunting, M., Delle Monache, M.L., Lysecky, R., Seibold, B., Sprinkle, J. and Piccoli, B., 2020. Are commercially implemented adaptive cruise control systems string stable?. IEEE Transactions on Intelligent Transportation Systems, 22(11), pp.6992-7003.

Gunter, G., Janssen, C., Barbour, W., Stern, R.E. and Work, D.B., 2019. Model-based string stability of adaptive cruise control systems using field data. IEEE Transactions on Intelligent Vehicles, 5(1), pp.90-99.

He, Y., Montanino, M., Mattas, K., Punzo, V. and Ciuffo, B., 2022. Physics-augmented models to simulate commercial adaptive cruise control (ACC) systems. Transportation Research Part C: Emerging Technologies, 139, p.103692.

James, R.M., Melson, C., Hu, J. and Bared, J., 2018. Characterizing the impact of production adaptive cruise control on traffic flow: An investigation. Transportmetrica B: Transport Dynamics.

Kan, X.D., Xiao, L., Liu, H., Wang, M., Schakel, W.J., Lu, X.Y., Van Arem, B., Shladover, S.E. and Ferlis, R.A., 2019. Cross-comparison and calibration of two microscopic traffic simulation

models for complex freeway corridors with dedicated lanes. Journal of Advanced Transportation, 2019.

Kesting, A., Treiber, M. and Helbing, D., 2010. Enhanced intelligent driver model to access the impact of driving strategies on traffic capacity. Philosophical Transactions of the Royal Society A: Mathematical, Physical and Engineering Sciences, 368(1928), pp.4585-4605.

Kesting, A., Treiber, M., Schönhof, M. and Helbing, D., 2007. Extending adaptive cruise control to adaptive driving strategies. Transportation Research Record, 2000(1), pp.16-24.

Kesting, A., Treiber, M., Schönhof, M. and Helbing, D., 2008. Adaptive cruise control design for active congestion avoidance. Transportation Research Part C: Emerging Technologies, 16(6), pp.668-683.

Lapardhaja, S., Gong, Y., Murshed, M.T. and Kan, X.D., 2021. Impact of Commercially Available Automated Vehicles on Freeway Bottleneck Capacity. In Transportation Research Board 100th Annual Meeting.

Lapardhaja, S., Yagantekin, K.U., Yang, M., Majumder, T.A., Kan, X. and Badhrudeen, M., 2023. Unlocking potential capacity benefits of electric vehicles (EVs) with adaptive cruise control (ACC). Transportmetrica B: Transport Dynamics, 11(1), pp.1894-1911.

Laval, J.A. and Leclercq, L., 2008. Microscopic modeling of the relaxation phenomenon using a macroscopic lane-changing model. Transportation Research Part B: Methodological, 42(6), pp.511-522.

Li, T., Chen, D., Zhou, H., Laval, J. and Xie, Y., 2021. Car-following behavior characteristics of adaptive cruise control vehicles based on empirical experiments. Transportation research part B: methodological, 147, pp.67-91.

Li, T., Chen, D., Zhou, H., Xie, Y. and Laval, J., 2022. Fundamental diagrams of commercial adaptive cruise control: Worldwide experimental evidence. Transportation research part C: emerging technologies, 134, p.103458.

Liu, H., Kan, X., Shladover, S.E., Lu, X.Y. and Ferlis, R.E., 2018a. Impact of cooperative adaptive cruise control on multilane freeway merge capacity. Journal of Intelligent Transportation Systems, 22(3), pp.263-275.

Liu, H., Kan, X.D., Shladover, S.E., Lu, X.Y. and Ferlis, R.E., 2018b. Modeling impacts of cooperative adaptive cruise control on mixed traffic flow in multi-lane freeway facilities. Transportation Research Part C: Emerging Technologies, 95, pp.261-279.

Lu, X.Y., Kan, X., Shladover, S.E., Wei, D. and Ferlis, R.A., 2017. An enhanced microscopic traffic simulation model for application to connected automated vehicles. In Transportation Research Board 96th Annual Meeting.

Makridis, M., Mattas, K., Anesiadou, A. and Ciuffo, B., 2021. OpenACC. An open database of car-following experiments to study the properties of commercial ACC systems. Transportation research part C: emerging technologies, 125, p.103047.

Makridis, M., Mattas, K. and Ciuffo, B., 2019. Response time and time headway of an adaptive cruise control. An empirical characterization and potential impacts on road capacity. IEEE transactions on intelligent transportation systems, 21(4), pp.1677-1686.

Makridis, M., Mattas, K., Ciuffo, B., Re, F., Kriston, A., Minarini, F. and Rognelund, G., 2020. Empirical study on the properties of adaptive cruise control systems and their impact on traffic flow and string stability. Transportation research record, 2674(4), pp.471-484.

Mattas, K., Makridis, M., Hallac, P., Raposo, M.A., Thiel, C., Toledo, T. and Ciuffo, B., 2018. Simulating deployment of connectivity and automation on the Antwerp ring road. IET Intelligent Transport Systems, 12(9), pp.1036-1044.

Milanés, V. and Shladover, S.E., 2014. Modeling cooperative and autonomous adaptive cruise control dynamic responses using experimental data. Transportation Research Part C: Emerging Technologies, 48, pp.285-300.

Nowakowski, C., O'Connell, J., Shladover, S.E. and Cody, D., 2010, September. Cooperative adaptive cruise control: Driver acceptance of following gap settings less than one second. In Proceedings of the human factors and ergonomics society annual meeting (Vol. 54, No. 24, pp. 2033-2037). Sage CA: Los Angeles, CA: SAGE Publications.

Shang, M., Rosenblad, B. and Stern, R., 2022. A novel asymmetric car following model for driver-assist enabled vehicle dynamics. IEEE Transactions on Intelligent Transportation Systems, 23(9), pp.15696-15706.

Shang, M. and Stern, R.E., 2021. Impacts of commercially available adaptive cruise control vehicles on highway stability and throughput. Transportation research part C: emerging technologies, 122, p.102897.

Shi, X. and Li, X., 2021a. Constructing a fundamental diagram for traffic flow with automated vehicles: Methodology and demonstration. Transportation Research Part B: Methodological, 150, pp.279-292.

Shi, X. and Li, X., 2021b. Empirical study on car-following characteristics of commercial automated vehicles with different headway settings. Transportation research part C: emerging technologies, 128, p.103134.

Shladover, S.E., Su, D. and Lu, X.Y., 2012. Impacts of cooperative adaptive cruise control on freeway traffic flow. Transportation Research Record, 2324(1), pp.63-70.

Treiber, M., Hennecke, A. and Helbing, D., 2000. Congested traffic states in empirical observations and microscopic simulations. Physical review E, 62(2), p.1805.

TSS|Aimsun. http://www.aimsun.com/. Accessed on November 16, 2020.

VanderWerf, J., Shladover, S., Kourjanskaia, N., Miller, M. and Krishnan, H., 2001. Modeling effects of driver control assistance systems on traffic. Transportation Research Record, 1748(1), pp.167-174.

Vander Werf, J., Shladover, S.E., Miller, M.A. and Kourjanskaia, N., 2002. Effects of adaptive cruise control systems on highway traffic flow capacity. Transportation Research Record, 1800(1), pp.78-84.

Yang, M., Chon Kan, P., Lapardhaja, S., Gong, Y., Imran, M.A., Murshed, M.T., Yagentekin, K., Khan, M.M., Kan, X., and Lee, C. 2024. MicroSimACC: An Open Database for Field Experiments on the Potential Capacity Impact of Commercial Adaptive Cruise Control (ACC). Transportmetrica Part A: Transport Science (Accepted).

Yang, M., Kan, X.D. and Yagantekin, K.U., 2023. Modeling Car-Following Behaviors of Adaptive Cruise Control–Equipped Vehicles Under Heterogeneous Desired Speeds (No. TRBAM-23-04056).

Yang, M., Lapardhaja, S., Kan-Munoz, P.C., Kan, X.D., Liu, H. and Lu, X.Y., 2022. Modeling CAV car following on freeways and arterials–case study of adaptive cruise control (ACC) equipped vehicles (No. TRBAM-22-02452).

Yang, M., Rawoof, M.B.M., Kan, X.D., Yagantekin, K.U. and Lu, X.Y., 2024. Modeling Commercial Adaptive Cruise Control (ACC) on Multi-Lane Facilities by Incorporating Receiving-Lane-Change Car-Following (No. TRBAM-24-04607).

Zheng, Z., Ahn, S., Chen, D. and Laval, J., 2013. The effects of lane-changing on the immediate follower: Anticipation, relaxation, and change in driver characteristics. Transportation research part C: emerging technologies, 26, pp.367-379.

Zhou, H., Zhou, A., Laval, J., Liu, Y. and Peeta, S., 2022. Incorporating driver relaxation into factory adaptive cruise control to reduce lane-change disruptions. Transportation research record, 2676(9), pp.13-27.

**Table A.1: RMSE comparison among SCG model, ASCG model, and ASVG model: ICE
vehicle, 55 mph (88 km/hr), 45 mph (72 km/hr), and 35 mph (56 km/hr) free-flow speed.**

Free-flow speed	Congested Speed	Gap Setting	SCG Model	ASCG Model	ASVG Model
55	0	L	0.77	0.414	**0.343**
	0	M	0.841	0.526	**0.393**
	0	S	0.925	0.893	**0.478**
	15	L	0.743	0.412	**0.352**
	15	M	0.845	0.644	**0.468**
	15	S	0.84	0.713	**0.641**
	25	L	0.872	0.663	**0.369**
	25	M	0.923	0.612	**0.416**
	25	S	0.831	0.558	**0.463**
	35	L	0.735	0.505	**0.392**
	35	M	0.842	0.467	**0.385**
	35	S	0.75	0.323	**0.3**
	45	L	0.445	0.36	**0.328**
	45	M	0.582	0.396	**0.3**
	45	S	0.505	**0.215**	0.23
45	0	L	0.754	**0.229**	0.238
	0	M	0.821	**0.339**	0.359
	0	S	0.902	0.683	**0.492**
	15	L	0.694	**0.251**	0.26
	15	M	0.815	0.43	**0.425**
	15	S	0.796	0.586	**0.472**
	25	L	0.592	0.405	**0.333**
	25	M	0.609	0.396	**0.329**
	25	S	0.518	0.468	**0.337**
	35	L	0.318	**0.224**	0.242
	35	M	0.362	0.279	**0.265**
	35	S	0.361	0.344	**0.262**
35	0	L	0.709	0.481	**0.414**
	0	M	0.767	0.353	**0.352**
	0	S	0.7	0.459	**0.427**
	15	L	0.539	0.294	**0.271**
	15	M	0.656	0.249	**0.226**
	15	S	0.728	0.424	**0.4**
	25	L	0.374	0.229	**0.224**
	25	M	0.365	0.185	**0.179**
	25	S	0.404	0.261	**0.229**

Table A.2: RMSE comparison among SCG model, ASCG model, and ASVG model: EV, 55 mph (88 km/hr), 45 mph (72 km/hr), and 35 mph (56 km/hr) free-flow speed.

Free-flow speed	Congested Speed	Gap Setting	SCG Model	ASCG Model	ASVG Model
55	0	X	**0.312**	0.505	0.366
	0	L	**0.399**	0.436	0.401
	0	M	**0.398**	0.438	0.401
	0	S	**0.312**	0.427	0.427
	15	X	**0.3**	0.682	0.396
	15	L	0.339	0.557	**0.313**
	15	M	**0.338**	0.428	0.396
	15	S	**0.3**	0.539	0.513
	25	X	**0.33**	0.708	0.368
	25	L	0.326	0.614	**0.324**
	25	M	**0.327**	0.569	0.362
	25	S	**0.333**	0.525	0.368
	35	X	**0.39**	0.771	0.533
	35	L	0.393	0.746	**0.356**
	35	M	**0.394**	0.604	0.418
	35	S	**0.392**	0.656	0.516
	45	X	0.313	0.321	**0.306**
	45	L	0.326	0.78	**0.29**
	45	M	**0.357**	0.541	0.847
	45	S	**0.327**	0.495	0.402
45	0	X	**0.268**	0.411	0.329
	0	L	**0.287**	0.369	0.329
	0	M	**0.287**	0.363	0.305
	0	S	**0.268**	0.414	0.386
	15	X	**0.239**	0.39	0.321
	15	L	**0.288**	0.66	0.315
	15	M	**0.287**	0.597	0.34
	15	S	**0.24**	0.488	0.351
	25	X	**0.223**	0.316	0.327
	25	L	**0.297**	0.46	0.332
	25	M	**0.331**	0.484	0.355
	25	S	**0.238**	0.516	0.419
	35	X	**0.187**	0.231	0.249
	35	L	**0.227**	0.269	0.343
	35	M	**0.288**	0.293	0.364
	35	S	**0.215**	0.544	0.375
35	0	X	**0.274**	0.384	0.351
	0	L	**0.27**	0.412	0.282
	0	M	**0.27**	0.346	0.343
	0	S	**0.274**	0.38	0.38
	15	X	**0.263**	0.544	0.27
	15	L	**0.28**	0.705	0.287
	15	M	0.279	0.513	**0.267**
	15	S	**0.262**	0.438	0.356

25	X	**0.216**	0.355	0.227
25	L	0.24	0.391	**0.221**
25	M	**0.258**	0.365	0.279
25	S	**0.221**	0.484	0.284

Table A.3: Calibrated parameters of ICE vehicle under 55 mph (88 km/hr), 45 mph (72 km/hr), and 35 mph (56 km/hr) free-flow speed.

Free-flow Speed (mph)	Congested Speed (mph)	Gap Setting			Model Version
		Short	**Medium**	**Long**	
55	45	$\tau = 0.4$ $K_{1\_2} = 0.036$ $K_{2\_2} = 0.208$ $K_{2\_3} = 0.240$	$\tau = 1.4$ $K_{1\_2} = 0.012$ $K_{2\_2} = 0.103$ $K_{2\_3} = 0.211$	$\tau = 2.0$ $K_{1\_2} = 0.008$ $K_{2\_2} = 0.000$ $K_{2\_3} = 0.179$	Version 2
	35	$\tau = 0.0$ $K_{1\_1} = 0.051$ $K_{2\_1} = 0.415$ $K_{2\_3} = 0.298$	$\tau = 0.2$ $K_{1\_1} = 0.020$ $K_{2\_2} = 0.270$ $K_{2\_3} = 0.205$	$\tau = 0.4$ $K_{1\_1} = 0.009$ $K_{2\_1} = 0.220$ $K_{2\_3} = 0.165$	Version 1
	25	$\tau = 0.0$ $K_{1\_1} = 0.049$ $K_{2\_1} = 0.420$ $K_{2\_3} = 0.363$	$\tau = 0.0$ $K_{1\_1} = 0.023$ $K_{2\_1} = 0.315$ $K_{2\_3} = 0.248$	$\tau = 0.0$ $K_{1\_1} = 0.011$ $K_{2\_1} = 0.212$ $K_{2\_3} = 0.177$	Version 1
	15	$\tau = 0.0$ $K_{1\_1} = 0.030$ $K_{2\_1} = 0.421$ $K_{2\_3} = 0.381$	$\tau = 0.0$ $K_{1\_1} = 0.016$ $K_{2\_1} = 0.331$ $K_{2\_3} = 0.277$	$\tau = 0.0$ $K_{1\_1} = 0.009$ $K_{2\_1} = 0.293$ $K_{2\_3} = 0.230$	Version 1
	0	$\tau = 0.0$ $K_{1\_1} = 0.029$ $K_{2\_1} = 0.553$ $K_{2\_3} = 0.439$	$\tau = 0.0$ $K_{1\_1} = 0.014$ $K_{2\_1} = 0.398$ $K_{2\_3} = 0.317$	$\tau = 0.0$ $K_{1\_1} = 0.009$ $K_{2\_1} = 0.320$ $K_{2\_3} = 0.267$	Version 1
45	35	$\tau = 1.0$ $K_{1\_2} = 0.025$ $K_{2\_2} = 0.000$ $K_{2\_3} = 0.390$	$\tau = 1.6$ $K_{1\_2} = 0.016$ $K_{2\_2} = 0.000$ $K_{2\_3} = 0.304$	$\tau = 1.6$ $K_{1\_2} = 0.013$ $K_{2\_2} = 0.050$ $K_{2\_3} = 0.255$	Version 2
	25	$\tau = 0.0$ $K_{1\_1} = 0.027$ $K_{2\_1} = 0.359$ $K_{2\_3} = 0.337$	$\tau = 0.0$ $K_{1\_1} = 0.018$ $K_{2\_1} = 0.371$ $K_{2\_3} = 0.253$	$\tau = 0.2$ $K_{1\_1} = 0.009$ $K_{2\_1} = 0.303$ $K_{2\_3} = 0.220$	Version 1
	15	$\tau = 0.0$ $K_{1\_1} = 0.022$ $K_{2\_1} = 0.759$ $K_{2\_3} = 0.331$	$\tau = 0.8$ $K_{1\_1} = 0.033$ $K_{2\_1} = 0.826$ $K_{2\_3} = 0.312$	$\tau = 1.0$ $K_{1\_1} = 0.014$ $K_{2\_1} = 0.615$ $K_{2\_3} = 0.274$	Version 1
	0	$\tau = 0.0$ $K_{1\_1} = 0.036$ $K_{2\_1} = 0.812$ $K_{2\_3} = 0.353$	$\tau = 0.8$ $K_{1\_1} = 0.033$ $K_{2\_1} = 0.888$ $K_{2\_3} = 0.369$	$\tau = 1.2$ $K_{1\_1} = 0.023$ $K_{2\_1} = 0.785$ $K_{2\_3} = 0.362$	Version 1
35	25	$\tau = 0.4$ $K_{1\_2} = 0.000$ $K_{2\_2} = 0.745$	$\tau = 0.8$ $K_{1\_2} = 0.000$ $K_{2\_2} = 0.595$	$\tau = 0.6$ $K_{1\_2} = 0.000$ $K_{2\_2} = 0.453$	Version 2

		$K_{2\_3} = 0.338$	$K_{2\_3} = 0.267$	$K_{2\_3} = 0.227$	
	15	$\tau = 0.0$ $K_{1\_2} = 0.000$ $K_{2\_2} = 0.770$ $K_{2\_3} = 0.327$	$\tau = 1.0$ $K_{1\_2} = 0.000$ $K_{2\_2} = 0.911$ $K_{2\_3} = 0.339$	$\tau = 0.4$ $K_{1\_2} = 0.000$ $K_{2\_2} = 0.481$ $K_{2\_3} = 0.273$	Version 2
	0	$\tau = 0.4$ $K_{1\_1} = 0.003$ $K_{2\_1} = 0.824$ $K_{2\_3} = 0.396$	$\tau = 0.4$ $K_{1\_1} = 0.013$ $K_{2\_1} = 0.870$ $K_{2\_3} = 0.362$	$\tau = 0.4$ $K_{1\_1} = 0.007$ $K_{2\_1} = 0.532$ $K_{2\_3} = 0.289$	Version 1

Table A.4: Calibrated parameters of EV under 55 mph (88 km/hr), 45 mph (72 km/hr), and 35 mph (56 km/hr) free-flow speed.

Free-flow Speed (mph)	Congested Speed (mph)	Gap Setting			
		Short	Medium	Long	Extra Long
55	45	$K_1 =0.045$ $K_2 =0.353$	$K_1 =0.038$ $K_2 =0.333$	$K_1 =0.042$ $K_2 =0.375$	$K_1 =0.014$ $K_2 =0.4$
	35	$K_1 =0.061$ $K_2 =0.409$	$K_1 =0.042$ $K_2 =0.489$	$K_1 =0.026$ $K_2 =0.509$	$K_1 =0.01$ $K_2 =0.441$
	25	$K_1 =0.057$ $K_2 =0.547$	$K_1 =0.034$ $K_2 =0.627$	$K_1 =0.019$ $K_2 =0.618$	$K_1 =0.006$ $K_2 =0.49$
	15	$K_1 =0.039$ $K_2 =0.633$	$K_1 =0.016$ $K_2 =0.69$	$K_1 =0.009$ $K_2 =0.658$	$K_1 = 0$ $K_2 =0.53$
	0	$K_1 =0.02$ $K_2 =0.961$	$K_1 =0.011$ $K_2 =0.816$	$K_1 =0.005$ $K_2 =0.702$	$K_1 = 0$ $K_2 =0.546$
45	35	$K_1 =0.047$ $K_2 =0.447$	$K_1 =0.053$ $K_2 =0.42$	$K_1 =0.06$ $K_2 =0.441$	$K_1 =0.03$ $K_2 =0.403$
	25	$K_1 =0.085$ $K_2 =0.493$	$K_1 =0.062$ $K_2 =0.554$	$K_1 =0.051$ $K_2 =0.537$	$K_1 =0.021$ $K_2 =0.482$
	15	$K_1 =0.04$ $K_2 =0.761$	$K_1 =0.02$ $K_2 =0.748$	$K_1 =0.007$ $K_2 =0.703$	$K_1 =0$ $K_2 =0.553$
	0	$K_1 =0.017$ $K_2 =0.936$	$K_1 =0$ $K_2 =0.945$	$K_1 =0$ $K_2 =0.773$	$K_1 = 0$ $K_2 =0.579$
35	25	$K_1 =0.079$ $K_2 =0.489$	$K_1 =0.078$ $K_2 =0.498$	$K_1 =0.046$ $K_2 =0.524$	$K_1 =0.013$ $K_2 =0.528$
	15	$K_1 =0.099$ $K_2 =0.565$	$K_1 =0.016$ $K_2 =0.757$	$K_1 =0.006$ $K_2 =0.698$	$K_1 = 0$ $K_2 =0.598$
	0	$K_1 =0.022$ $K_2 =0.881$	$K_1 =0$ $K_2 =0.918$	$K_1 =0$ $K_2 =0.822$	$K_1 = 0$ $K_2 =0.601$